

Study of Flow Characteristics of Reservoir Rock Using Digital Rock Physics

BY

Ali Adel Ali Mahmoud

A Thesis Presented to the
DEANSHIP OF GRADUATE STUDIES

KING FAHD UNIVERSITY OF PETROLEUM & MINERALS

DHAHRAN, SAUDI ARABIA

In Partial Fulfillment of the
Requirements for the Degree of

MASTER OF SCIENCE

In

PETROLEUM ENGINEERING

December 2019

KING FAHD UNIVERSITY OF PETROLEUM & MINERALS

DHAHRAN- 31261, SAUDI ARABIA

DEANSHIP OF GRADUATE STUDIES

This thesis, written by **Ali Adel Ali Mahmoud** under the direction of his thesis advisor and approved by his thesis committee, has been presented and accepted by the Dean of Graduate Studies, in partial fulfillment of the requirements for the degree of **MASTER OF SCIENCE IN PETROLEUM ENGINEERING**.



Dr. Dhafer Al Shehri
(Department Chairman)

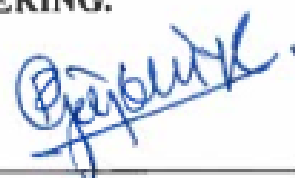


Dr. Salam A. Zummo
(Dean of Graduate Studies)



19/12/19

Date



Dr. Rahul N. Gajbhiye
(Advisor)



Dr. Mohamed A. Mahmoud
(Member)



Dr. Salaheldin Elkatatny
(Member)

© Ali Adel Ali Mahmoud

2019

I humbly and wholeheartedly dedicate this thesis to
*my beloved **parents**, for their endless support throughout my entire life,*
*my **brother** and **sister**, who I hope I will be part of their future success too,*
*my **friends**, who were the source of joy during this fruitful journey.*

ACKNOWLEDGMENT

*I am deeply indebted to my thesis advisor **Dr. Rahul Gajbhiye** for his constant support, guidance, encouragement and constructive criticism throughout the course of this research. I will always revere his patience, expert guidance and ability to solve intricate problems. The respect he offered me as a student and the opportunities provided in growing as a researcher will not be forgotten.*

*I would also like to thank my committee members **Dr. Mohamed Mahmoud** and **Dr. Salaheldin Elkatatny** for their suggestions, cooperation and for providing many valuable comments that improved the contents of this thesis. Their commitment to the success of this work and scientific expertise were invaluable in this accomplishment.*

*A sincere thank you to **Dr. Jack Dvorkin** for the work he made possible and to **Dr. Jun Li** for his large efforts and his assistance in permeability simulations. I would like to acknowledge **Mr. Syed Rizwanullah Hussaini** for carrying out the micro CT scans. I would also like to gratefully acknowledge the support of the Center for Integrative Petroleum Research (CIPR) their contribution to this scientific effort.*

*Finally, I would like to thank the Petroleum Engineering Department at King Fahd University of Petroleum & Minerals (**KFUPM**) for providing this great opportunity to pursue my master's degree.*

TABLE OF CONTENTS

ACKNOWLEDGMENT.....	v
TABLE OF CONTENTS.....	vi
LIST OF TABLES	x
LIST OF FIGURES	xi
LIST OF ABBREVIATIONS.....	xvi
ABSTRACT.....	xviii
ملخص الرسالة.....	xx
Chapter 1 INTRODUCTION.....	1
1.1 Problem Statement	13
1.2 Research Motivation.....	14
1.3 Thesis Objectives	15
1.4 Methodology	15
Chapter 2 LITERATURE REVIEW.....	18
2.1 Properties of Porous Media	21
2.1.1 Porosity	21
2.1.2 Single Phase Permeability.....	22
2.1.3 Two- Phase Capillary Pressure in Porous Media.....	24
2.1.4 Relative Permeability.....	26
2.2 Mercury Intrusion Porosimetry	28

2.3	Imaging Techniques	30
2.3.1	Thin Section Analysis	31
2.3.2	X-Ray Computed Tomography.....	32
2.3.3	X-Ray Micro Computed Tomography.....	37
2.3.4	Scanning Electron Microscopy	41
2.3.5	X-Ray Diffraction	43
2.3.6	X-Ray Fluorescence.....	44
2.4	Image Analysis	45
2.4.1	Image Preparation	45
2.4.2	Image Noise and Artifacts	46
2.4.3	Image Filtration.....	46
2.4.4	Image Segmentation.....	47
2.5	Rock Properties Estimation from Imaging Techniques	48
2.6	Representative Elementary Volume	56
2.7	Direct Pore-level Modelling.....	57
2.8	Pore Network Modelling	60
2.9	Pore-Scale Relative Permeability Modelling	64
Chapter 3 EXPERIMENTAL METHODOLOGY		66
3.1	Porosity and Permeability measurements.....	68
3.1.1	Procedure	69
3.2	X-ray Diffraction.....	71

3.2.1	CT Imaging	72
3.3	Micro-CT Imaging	73
3.4	QEMSCAN	76
3.5	Permeability Simulations	80
Chapter 4 RESULTS AND DISCUSSION		81
4.1	Porosity and Permeability measurements.....	81
4.2	X-Ray Diffraction.....	85
4.2.1	Sandstone Samples Mineralogy	85
4.2.2	Carbonate Samples Mineralogy	90
4.3	CT Imaging.....	94
4.3.1	Sandstone Samples.....	94
4.3.2	Carbonate Samples.....	97
4.4	Micro-CT Imaging	99
4.4.1	Sandstone micro-CT images	101
4.4.2	Carbonate Micro-CT images.....	107
4.5	QEMSCAN	112
4.6	Permeability Simulations	115
Chapter 5 CONCLUSION		119
5.1	Future work	121
APPENDICES		123
REFERENCES		142

Vitae.....	161
------------	-----

LIST OF TABLES

Table 4-1: Dimensions of core plugs used in this study	82
Table 4-2: Measured porosity and permeability of core plugs at 500 psi confining pressure	83
Table 4-3: Mineral composition of sandstone samples.....	86
Table 4-4: Mineral composition of carbonate samples.....	91
Table 4-5: Porosity from laboratory measurement compared with the estimated porosity using PerGeos software for sandstones	106
Table 4-6: Porosity from laboratory measurement compared with the estimated porosity using PerGeos software for carbonates.....	111
Table 4-7: QEMSCAN results	114
Table 4-8: Permeability from laboratory measurement compared with the estimated porosity using LBM simulations for sandstones	115
Table 4-9: Permeability from laboratory measurement compared with the estimated porosity using LBM simulations for carbonates	116

LIST OF FIGURES

Figure 1-1: Rock and flow properties computed directly from 3D images of the rock microstructure [1]	7
Figure 1-2: The applied Digital Core Analysis workflow	17
Figure 2-1: Diagram of droplet of water on a glass surface [32]	25
Figure 2-2: Relationship between the saturation of each wetting and non-wetting phase and the relative permeability of the fluid, along with predictive models computed using network modeling [34]	27
Figure 2-3: Scales and resolution in DRA. Decreasing sample size and increasing image resolution towards right, from the cm scale to the sub-micrometer scale	30
Figure 2-4: Micro-CT scanner applications (a to d) textural heterogeneity study in carbonate rocks [66]	40
Figure 2-5: Micro-CT scanner applications: Multiscale analysis of rock images [67]	41
Figure 2-6: Illustration of sub-micron porosity in carbonate samples. Images shows slices from the same region of the sample imaged at (c) low and(d) higher resolution [81] ..	51
Figure 2-7: Maximal balls method for pore network extraction. The initial increasing spheres model of [85] and the model of [87] extended to compute throats.....	52
Figure 2-8: Results of different techniques used to incorporate in a multi-scale imaging and modeling workflow. (a) Dry tomogram at 2.5-micron resolution (b) Registered SEM (c) Porosity map from wet/dry difference(d) Registered automated [89] ..	54
Figure 3-1: Sandstone samples used for this study	67
Figure 3-2: Reservoir Carbonate Samples used for this study.....	67
Figure 3-3: Automated Porosimeter Permeameter	70

Figure 3-4: X-Ray diffractometer	71
Figure 3-5: Toshiba Alexion TSX-032A medical X-ray CT scanner	73
Figure 3-6: Zeiss VersaXRM-500 X-ray micro-CT scanner	75
Figure 3-7: HeliScan micro CT.....	76
Figure 3-8: QEMSCAN - FEI 650F	78
Figure 3-9: Steps in generating 2D QEMSCAN maps	78
Figure 3-10: A generated QEMSCAN map.....	79
Figure 4-1: Measured porosity and permeability of the samples under examination. Left: compared with other sandstone datasets. Right: carbonate samples compared to outcrop carbonate data	84
Figure 4-2: Mineral composition of Berea Puff.....	87
Figure 4-3: Mineral composition of Crab Orchid	87
Figure 4-4: Mineral composition of Bandera Grey.....	88
Figure 4-5: Mineral composition of Bandera Brown.....	88
Figure 4-6: Mineral composition of Colton	89
Figure 4-7: Mineral composition of Berea Grey.....	89
Figure 4-8: Mineral composition of 9137-1.....	91
Figure 4-9: Mineral composition of 9058-3.....	92
Figure 4-10: Mineral composition of 9134-4.....	92
Figure 4-11: Mineral composition of 9135-5.....	93
Figure 4-12: Mineral composition of 9137-7.....	93
Figure 4-13: Mineral composition of 9136-8.....	94

Figure 4-14: CT images for sandstone samples 1) Berea Puff 2) Crab Orchid 3) Bandera Grey 4) Bandera Brown 5) Colton 6) Berea Grey.....	96
Figure 4-15: CT images for carbonate samples 1) 9137-1 2) 9058-3 3) 9134-4 4) 9135-5 5) 9137-7 6) 9136-8.....	98
Figure 4-16: The Cubic Porosity Segmentation Workflow	101
Figure 4-17: Bandera Grey sub-plug image scanned at 4 microns resolution using helical X-ray micro-CT	102
Figure 4-18: Bandera Grey sub-plug before and after applying non-local means filter	103
Figure 4-19: Bandera Grey sub-plug after the segmentation process.....	104
Figure 4-20: Bandera Grey sub-plug after applying axis connectivity.....	105
Figure 4-21: 9137-7 sub-plug image scanned at 4 microns resolution using X-ray microCT	107
Figure 4-22: 9137-7 sub-plug before and after applying non-local means filter.....	108
Figure 4-23: 9137-7 sub-plug after the segmentation process.....	109
Figure 4-24: 9137-7 sub-plug after applying axis connectivity.....	110
Figure 4-25: 2D QEMSCAN map for Bandera Brown sample	113
Figure 4-26: 2D QEMSCAN map for sample 9135-5	113
Figure 4-27: Calculated permeability vs lab permeability for all samples used in this study	117
Figure A1: Berea Puff sub-plug image scanned at 4 microns resolution	123
Figure A2: Berea Puff sub-plug before and after applying non-local means filter.....	124
Figure A3: Berea Puff sub-plug after the segmentation process	124
Figure A4: Berea Puff sub-plug after applying axis connectivity	125
Figure A5: Crab Orchid sub-plug image scanned at 4 microns resolution.....	125
Figure A6: Crab Orchid sub-plug before and after applying non-local means filter.....	126

Figure A7: Crab Orchid sub-plug after the segmentation process.....	126
Figure A8: Crab Orchid sub-plug after applying axis connectivity.....	127
Figure A9: Bandera Brown sub-plug image scanned at 4 microns resolution	127
Figure A10: Bandera Brown sub-plug before and after applying non-local means filter	128
Figure A11: Bandera Brown sub-plug after the segmentation process	128
Figure A12: Bandera Brown sub-plug after applying axis connectivity	129
Figure A13: Colton sub-plug image scanned at 4 microns resolution.....	130
Figure A14: Colton sub-plug before and after applying non-local means filter.....	130
Figure A15: Colton sub-plug after the segmentation process.....	131
Figure A16: Colton sub-plug after applying axis connectivity.....	131
Figure A17: Berea Grey sub-plug image scanned at 4 microns resolution using helical X-ray Micro-CT	132
Figure A18: Berea Grey sub-plug before and after applying non-local means filter	132
Figure A19: Berea Grey sub-plug after the segmentation process	133
Figure A20: Berea Grey sub-plug after applying axis connectivity	133
Figure B1: 9137-1 sub-plug image scanned at 4 microns resolution.....	134
Figure B2: 9137-1 sub-plug before and after applying non-local means filter.....	134
Figure B3: 9137-1 sub-plug after the segmentation process	135
Figure B4: 9137-1 sub-plug after applying axis connectivity	135
Figure B5: 9058-3 sub-plug image scanned at 4 microns resolution.....	136
Figure B6: 9058-3 sub-plug before and after applying non-local means filter.....	136
Figure B7: 9058-3 sub-plug after the segmentation process	137

Figure B8: 9058-3 sub-plug after applying axis connectivity	137
Figure B9: 9135-5 sub-plug image scanned at 4 microns resolution.....	138
Figure B10: 9135-5 sub-plug before and after applying non-local means filter.....	138
Figure B11: 9135-5 sub-plug after the segmentation process	139
Figure B12: 9135-5 sub-plug after applying axis connectivity	139
Figure B13: 9136-8 sub-plug image scanned at 4 microns resolution.....	140
Figure B14: 9136-8 sub-plug before and after applying non-local means filter.....	140
Figure B15: 9136-8 sub-plug after the segmentation process	141
Figure B16: 9136-8 sub-plug after applying axis connectivity	141

LIST OF ABBREVIATIONS

μm	:	Micrometer
3D	:	Three Dimension
in	:	Inch
mD	:	Millidarcy
mm	:	Millimeter
K_{ro}	:	Oil relative permeability
K_{rw}	:	Water relative permeability
ΔP_{grav}	:	gravitational forces
ρ	:	density (g/cc)
g	:	gravitational acceleration = 9.8 m/s^2
k	:	Permeability (md)
CT	:	Computed Tomography
XRM	:	X-ray microscopy

API	:	American Petroleum Institute
QEMSCAN	:	Quantitative Evaluation of Minerals by Scanning Electron Microscopy
SEM	:	Scanning Electron Microscopy
XRD	:	X Ray Diffraction
XRF	:	X Ray Fluorescence
FIBSEM	:	Focused Ion Beam Scanning Electron Microscopy

ABSTRACT

Full Name Ali Adel Ali Mahmoud

Thesis Title STUDY OF FLOW CHARACTERISTICS OF RESERVOIR ROCK USING
DIGITAL ROCK PHYSICS

Major Field Petroleum Engineering

Date of Degree December 2019

Understanding the petrophysical properties of reservoir rocks is crucial for hydrocarbon exploration and production. Reservoir rock is one of the main sources used to derive petrophysical properties by laboratory measurements. The evolution of Digital Rock Physics (DRP) in recent years has added vital improvement in core characterization and in providing high quality advanced Special Core Analysis (SCAL) measurements. DRP is able to estimate petrophysical properties in sandstone reservoirs by means of digital models. For carbonates, it is difficult to capture the full range of the pore structure with a single imaging technique due to pore sizes over broad range nm to cm.

This research aims to study the flow characteristics of rocks using DRP. Six sandstone outcrops samples were chosen for this study in order to cover different lithology types. In addition, six carbonate samples from Middle East reservoir were selected. A multiscale imaging approach

using X-ray computer tomography CT, 3D X-ray microtomographic CT and X-ray Diffraction (XRD) was carried out. After laboratory measurements, the whole sample was scanned using X-ray CT with 1 mm resolution. A sub-plug is then extracted for high resolution scanning. X-ray micro-CT is used to scan the sub-plug at a resolution of 4 μm . At this scale, pore connectivity is revealed from top to bottom. PerGeos software is used to visualize, analyze and process the 3D images. Then the connected porosity of the segmented pores is estimated. Lattice- Boltzmann method (LBM) is used to simulate fluid flow.

From this study, it was shown that the suggested DRP techniques could be a reliable complement for routine laboratory experiments. Results from conventional laboratory work with image based simulations showed a good agreement. In addition, the most important factors, which influenced the results, were image resolution, representative sample size and proper simulation set-up.

ملخص الرسالة

الاسم بالكامل: على عادل على محمود
عنوان الرسالة: دراسة خصائص تدفق صخور المكامن باستخدام فيزياء الصخور
الرقمية
التخصص: هندسة البترول
تاريخ الدرجة العلمية: ديسمبر 2019

إن فهم الخواص البتروفيزيائية لصخور المكامن أمر أساسي لاستكشاف وإنتاج الهيدروكربونات. صخور المكامن هي أحد المصادر الرئيسية المستخدمة لاستخلاص الخصائص البتروفيزيائية عن طريق القياسات المختبرية. أضاف تطور فيزياء الصخور الرقمية (DRP) في السنوات الأخيرة تحسيناً حيوياً في التوصيف الأساسي وفي توفير قياسات التحليل الأساسي المتطور (SCAL) المتقدمة عالية الجودة. DRP قادر على تقدير الخواص البتروفيزيائية في خزانات الحجر الرملي عن طريق النماذج الرقمية. بالنسبة للكربونات ، من الصعب التقاط المجموعة الكاملة من بنية المسام باستخدام تقنية تصوير واحدة بسبب أحجام المسام على مدى عريض من نانومتر إلى سنتيمتر.

تهدف هذه الدراسة إلى توصيف المكونات الأساسية من الحجر الرملي والكربونات بدقة باستخدام DRP. تم اختيار ستة عينات من الحجر الرملي لهذه الدراسة من أجل تغطية أنواع مختلفة من الحجر. بالإضافة إلى ذلك ، تم اختيار ستة عينات كربونات من خزان الشرق الأوسط. سوف نطبق نهج التصوير متعدد المقاييس باستخدام التصوير المقطعي بالأشعة السينية للتصوير المقطعي المحوسب ، التصوير المقطعي المحوسب بالأشعة السينية ثلاثية الأبعاد والأشعة السينية (XRD). بعد القياسات المختبرية ، نقوم بمسح العينة بأكملها باستخدام الأشعة السينية المقطعية بدقة 1 مم. ثم نقوم باستخراج قابس فرعي لإجراء مسح ضوئي عالي الدقة. يتم استخدام الأشعة السينية ، CT الصغيرة لمسح المكونات الفرعية بدقة 4 ميكرون. في

هذا المقياس ، يتم الكشف عن اتصال المسام من أعلى إلى أسفل. نقوم بتصوير وتحليل ومعالجة الصور ثلاثية الأبعاد باستخدام برنامج PerGeos. ثم نقدر مسامية متصلة المسام مجزأة. نحن نستخدم طريقة Lattice-بولتزمان (LBM) لمحاكاة تدفق السوائل.

من هذه الدراسة ، تبين أن تقنيات DRP المقترحة يمكن أن تكون مكملة موثوقة للتجارب المخبرية الروتينية. وأظهرت النتائج من العمل المختبري التقليدي مع عمليات المحاكاة القائمة على الصور وجود اتفاق جيد. بالإضافة إلى ذلك ، فإن أهم العوامل التي أثرت في النتائج ، كانت دقة الصورة وحجم العينة التمثيلي وإعداد المحاكاة المناسب.

Chapter 1

INTRODUCTION

The oil and gas industry is constantly shifting between remarkably prospering and tremendously unprofitable periods. Relying on this cycle and believing that a challenging year will be always followed by a successful one has been the reason to maintain the enthusiastic approach of the companies in the past two decades. Nevertheless, it is also a fact that the fast changing cycle has become slower, more and more unstable and that the two periods are no longer equivalent, in terms of either duration or outcomes. Becoming aware of this trend is causing deep changes in the way of thinking in the industry. Reduction of the costs is a natural and inescapable consequence. More than ever, the priority is to develop reliable technologies and methods or improve old ones, so that they can truly provide effective information and hence minimize and eventually eliminate the uncertainty prior to every important decision. This approach will be a benefit for the projects about to begin, but is focused mostly in improving the efficiency of the once already in course since the risks to start new projects are increasing due to less accessible reservoirs.

Information about the reservoir can be obtained at different scales from the reservoir scale down to the pore scale. Seismic mapping provides a three-dimensional picture of the reservoir at the reservoir scale and information about structural and textural variations. Most importantly, seismic maps can be used to identify traps and possible hydrocarbon resources. Well logs measure petrophysical properties at the meter scale, where physical properties such as radioactivity, resistivity, hydrogen index, and density are measured along the wellbore at varying depths. The information obtained from logs is subsequently converted to other properties such as fluid saturation, porosity, and permeability using empirical correlations. Core samples and core plugs provide millimeter scale information and smaller samples provide a nanometer scale or pore scale picture of the reservoir. For conventional reservoirs, routine and special core analysis methods provide mineralogy, porosity, pore size distribution, permeability, resistivity, saturation information, relative permeability, and capillary pressures.

Well log measurements are often performed through exploratory wells using measurement techniques to analyze larger scale changes in formation rock properties and to begin developing an understanding of the unique geometry and rock properties at certain locations within the field. The well log measurements can then be combined with seismic measurements to identify certain formation layers and potential areas of concerns within the reservoir. Similar regions from well logs can then be used to develop regions of similar characteristics used in selecting cores samples for laboratory measurements. Following

core and plug measurements; this data is then used to populate the predictive models with expected fluid flow properties for both the reservoir host and seal formations for better accuracy and injection operations optimization.

Reservoir characterization is one of the most important steps in exploration and development phases of any prospect. It combines the results of different analyses to reduce the risk and uncertainties and to enhance understanding of reservoirs. Obtaining information about the characteristics of a reservoir is vital for the petroleum industry to understand and assess the reservoir. The data for reservoir characterization is obtained from various sources such as well logging data, geophysical data, well test data, core data, etc. Cores are carefully studied in special laboratories at different conditions to determine different important experimental properties that characterize flow and storage capacity of the rock. In reservoir characterization, it is crucial to understand the mineralogy and the shape of the hydrocarbon bearing rocks. One crucial step unfortunately still associated to countless uncertainty is the characterization considered in a given field, namely its rocks and their properties. The rocks composing one petroleum system are source rocks (where the hydrocarbons are generated), reservoir rocks (where the hydrocarbons are accumulated after migration from the source rock), seal rocks (the ones acting as a cap and preventing the hydrocarbons from escaping) and overburden rocks (all the layers of rocks deposited above the seal). These rocks differ greatly from each other, conversely a full characterization is usually demanded only on the rock of interest, which conventionally is

the reservoir rock, therefore the source, seal and overburden rocks tends to be neglected from a characterization point of view. Reservoir rocks are generally sedimentary, in their great amount sandstones and carbonates. Porosity, pore size distribution and average pore diameter, as well as pore connectivity and formation factor are important parameters of any porous structure. Correctly estimated, they play a significant role in determining transport properties of reservoir rocks, since to have accurate predictions of absolute and relative permeability.

An exploration and production project has several phases, the first phase being called exploration when geological studies and geophysical methods determine the formations of the sedimentary basin with potential for hydrocarbon accumulation. Then a pioneer exploratory well is drilled and through mud gravel analysis, geophysical profiling measurements, formation production testing and core analysis confirm the accumulation of hydrocarbons in the target formations. If hydrocarbon accumulation is confirmed, the assessment phase is initiated by checking reservoir connectivity. Still during the evaluation, the reservoir is modeled using geophysical seismic data and data collected from all exploratory wells to determine the volume of the reservoir rock. With information on reservoir rock volume and petrophysical data from the characterization of reservoir rock samples such as porosity, it is possible to estimate the volume of hydrocarbons within the reservoir. The evaluation phase ends with the reservoir flow simulation. The simulation requires other sample characterization data, such as permeability, to determine the location

of development wells, as well as to calculate field production curves that determine whether the project is economically viable.

This demonstrates that the characterization of reservoir rocks becomes a fundamental component in a hydrocarbon exploration and production project, since the information obtained will inform critical project decisions. Traditional petrophysical analyzes have complex routines, such as cleaning and removing saturating fluid from within the core sample, which can take months. The proper characterization reservoir cap rocks requires numerous experimental techniques ranging from field scale formation interpretation all the way down to individual pore scale fluid flow behavior tests. Multiple scientific disciplines are involved in these processes and the development of experimental techniques continues to provide more accurate system predictions in shorter periods.

The properties that allow a full characterization of one rock can be distinguished in several types, namely mechanical (elastic constants, Poisson's ratio), physical (density, texture), chemical (chemical composition, reactivity), mineralogical (mineralogical composition, morphology), electrical (conductivity/resistivity), acoustic (compressional and shear waves velocity), magnetic (magnetic susceptibility, saturation magnetization). A reliable estimation of these properties has direct implications in the correct evaluation of the reserves of one reservoir, as well as in the plan building of drilling operations and production phases and in the proper understanding of the needs recovery. In other words, adequately characterized rocks are crucial in every stage from exploration until

abandonment of a field, therefore every effort in the investigation of rock properties related issues must be always of great significance.

Each type of the enumerated properties is essentially important for a specific application and when speaking of reservoir rocks characterization, the two most significant parameters are porosity and permeability. Porosity will define how much hydrocarbons can be entrapped in a certain reservoir, while permeability will dictate the ability to extract hydrocarbons. Porosity depends in a great matter on the way the rock was formed, nevertheless post-formation processes like dissolution or fracturing can contribute to change the primary porosity. Permeability depend on how much the pores are connected between each other to form paths where fluids can move and is in close association with porosity, yet the correlation is not necessarily linear because disconnected pores contribute to the total porosity but not to the fluid flow. Moreover, other variables like capillary pressure and type of fluid also influence the permeability.

Recent advances in numerical modeling and simulation methods in computer tomography CT imaging technologies brought a new technique termed as Digital Rock Physics (DRP) or Digital Core Analysis (DRA). This technique is aiming to enhance and complement conventional laboratory techniques for characterizing rock characteristics. It characterizes the rock samples by obtaining high-resolution images of the rock microstructures. Acquired images can be used to qualitatively describe the rock characteristics by obtaining some descriptive image parameters. This type of description is useful to inspect the internal

structure of rock sample and assess its heterogeneity. It assists many laboratory tests to select representative rock portion from whole plug or core-plug for performing measurements of rock properties of interest. In addition to qualitative analysis, images from CT scanner can be used to extract quantitative information about rock characteristics after some image analysis. Figure 1-1 shows the flow properties computed from 3D images of the rock microstructure.

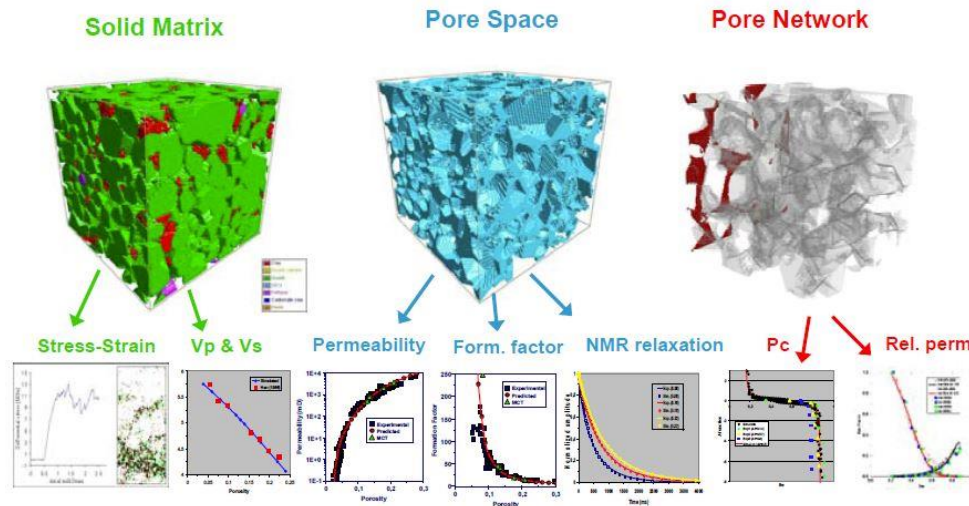


Figure 1-1: Rock and flow properties computed directly from 3D images of the rock microstructure [1]

DRP can be used to complement core analysis data or as an alternative when core data is inaccurate or unreliable [2]. In DRP, a two- or three-dimensional image of the reservoir rock is collected using X-ray CT at the whole core and core plug scale or SEM at the smaller scales. These images are used in advanced numerical simulators where properties

such as composition, porosity, pore size distribution, permeability, relative permeability, capillary pressure, electrical resistivity, and thermal conductivity can be predicted. As a result, some studies correlate different properties with one another at different scales [2].

Determined rock characteristics can be dynamic or static rock properties. Typical DRP workflow entails scanning rock sample with CT scanner at desired resolution, processing acquired raw images to eliminate images artifacts, extracting pore network by segmenting enhanced images into solid and pore phases and lastly estimating petrophysical properties from extracted pore network [3]–[10].

The use of DRP involves three steps:

- Digital imaging to create a digital representation of a rock in 2D and 3D at a scale and resolution that will resolve rock features such as pores, organics, and grains.
- Digital image processing to categorize pixels/voxels in 2D and 3D respectively, with similar properties.
- Digital rock analysis to digitally model the desired rock properties using the digital image of the rock.

DRP merges modern microscopic imaging techniques and advanced numerical simulations of the properties of the rock. Digital rock analysis is a technology under constant

development, and several studies have indicated that it offers significant value for delivering fast-track special core analysis [7], [11]–[14]. Digital rock modelling is an evolving technique for non-destructive description of the pore scale within rock sample. Analysis of the petrophysical properties, after the imaging techniques and visualization of the core sample gives a thorough understanding of the reservoir rock sample [15].

The principle of DRP is image and compute, image the pore space of natural rock and computationally simulate physical processes in the resulting digital object to arrive at porosity, permeability, electrical, and elastic properties. A conceptual challenge associated with this principle is that of spatial scale – while the pore-scale images produced by scanning are those of mm-sized rock fragments, the goal is to confidently use the results at a much larger scale, approximately meters or higher. This challenge arises from the fact that natural rock is heterogeneous at all scales and, hence, there is no guarantee that mm-scale properties are relevant to those at a much larger scale. Even such basic property as the total porosity may strongly vary within a mm-sized volume and certainly within an inch-sized plug.

One of the key challenges of digital rock analysis is capturing the whole range of pore sizes within one pore scale model. Capturing a representative elementary volume (REV) of a reservoir rock is essential to predict rock properties. The represented volume in a discretized 3D model is the result of the number of grid cells and the size of each grid cell. Higher resolution models will require increased number of grid cells to maintain the REV.

A multi-scale imaging and modeling approach will allow for a range of representative volumes, hence a range of resolutions according to the rock complexity. Integration of multiple 3D models, each model representing a finite range of the pore size distribution, allows for characterization of the complete pore system. Micro-porosity, in DRA often referred to as partial volume porosity, is affected by the resolution during image acquisition.

In some cases, the direct CT method may not be reliable, e.g. in carbonate reservoir studies due to their submicron structures and the similarity in X-ray absorption for calcite and dolomite [16]. There are several approaches to reconstruct 3D porous media from 2D thin section images. The practical importance of using pore-scale modeling is related to estimation of such macroscopic parameters as capillary pressure, absolute and relative permeabilities which are important data in every reservoir model. With the current development of computational methods in imaging, digital core analysis can become a good alternative of expensive laboratory experiments. Furthermore, it is possible to use the same digital model several times to simulate different displacement scenarios.

Rock physics numerical simulation based on digital core technology has become one of the important means of petrophysical research. The digital core model is the basis of digital core technology. Scholars have conducted extensive research and proposed various modeling methods. Digital core modeling is focused on the construction of core pore structure. Due to the large span of core pore size, it can be from nanometer to millimeter.

The single-resolution digital core model cannot fully describe the core pore characteristics. X-ray computed tomography CT is one of the most widely used techniques for digital core modeling, it is used to reconstruct digital 3D models of rock samples from which porosity and pore network are estimated. The tool is able to reproduce three-dimensional models of the internal structure of the imaged objects and differentiate, within the volume, between materials with different densities. The potential of this technique for the Oil and Gas industry was realized back in the early 90's, however only recently has been deeply explored, due to the computational advances. As one might already presume, applied to rocks characterization, micro-CT can be used to image the internal structures of rock samples, distinguishing between material and pores and most importantly, reproduce that structure in a digitized volume. Hence, with this tool the porosity of a sample can be determined accurately, with the additional advantage that the entire pore structure will be assessed and numerically described, including not only pore and grain sizes but also discrimination between connected and isolated void spaces and quantification of the grain/pore interface area. Porosity quantification is not the only outcome of such an approach, once having such a detailed quantification in a digital format enables one to input the numerical model in existing software and perform any kind of simulation, thereby estimating other rock parameters like permeability, capillary pressures, mechanical and acoustic properties. The difference between a micro-CT obtained digital volume and any other digital volume obtained by specifically designed software programs is that the former

is a real digital copy of the rock as it is obtained by direct reproduction of the sample and not a probabilistic structure, like is the case of simulation obtained rock volumes.

In sandstones, it is common to encounter homogeneous pore structures as the rock itself is composed of grains with approximately similar sizes, compacted in a regular manner. On the other hand, in carbonates there are sediments of great range of sizes, clustered by volumes of same grains size or different sizes mixed together. Due to this, enormous dissimilarity between grains, the porosity of carbonates is associated to structures a lot more complex than in the case of sandstones. To assess these complex structures it has always been a great challenge. The numerous existing laboratory measurements can provide an average value for the porosity of one rock, but is an excessive simplification to describe such a composite system with a single value. A far more sophisticated assessment is required to attend the industry demands, constructing realistic three-dimensional 3D models of the pore structure and describing numerically the pores size, the connection between pores, the grains size, fractures, channels and every feature responsible for porosity. The advances in computational power and the trends in software and programming make possible the multipart mathematical calculations associated to such numerical description, and the introduction of existing imaging tools is able to provide the three-dimensional realistic models.

For carbonates, it is difficult to capture the full range of the pore structure with a single imaging technique due to pore sizes over broad range nm to cm [17], [18]. Developing

relationships between the porosity and flow properties for carbonate reservoirs remains an area of active research, due mainly to the complexity of carbonate structures because of their dual porosity [18], [19]. Image registration techniques, which involves the use of multiple images at various resolutions to combine high-resolution data from scanning electron microscopy (SEM) with lower resolution micro CT data [20]. Image registration techniques, however, are dependent on computationally intensive algorithms [21] to combine the porosity data at disparate length scales. To overcome this challenge, most recently a methodology to determine the micro porosity directly from micro CT data of Indiana Limestone [22]. However, it has seen limited application to other carbonates. To determine the porosity of rocks from micro CT or SEM data, the greyscale images need to be converted to binary images (representing rock space and pore space) through a process called thresholding. The literature lacks a systematic thresholding technique applicable broadly to micro CT and SEM data of carbonates.

1.1 Problem Statement

There is a lack of methods in the industry to assess and quantify accurately the pore structure of core samples. This research aims to address this problem, and uses the advanced tools X-ray computer tomography CT, 3D X-ray microtomographic CT and X-ray Diffraction (XRD) to study the flow characteristics of rocks. These techniques are chosen due to their ability to compute 3D volumes of the imaged samples. Coupling the

Micro-CT slices with an image processing software has invaluable advantages. It permits creation of three-dimensional maps of fluid occupancy and estimation of the volume fraction of each phase using phase segmentation techniques. It can also be used to generate pore network models, illustrating connected porosity and pore size distribution. The data produced from these imaging and characterization techniques was utilized to understand the material phases, grain structure, and porous network. Based on the porous structure the flow characteristics of the rock was obtained using numerical simulation. Flow characteristics was validated using laboratory techniques.

1.2 Research Motivation

This study aims to extract necessary information by using advanced imaging techniques to build a reliable pore-scale model that can be used to predict important reservoir properties. In addition, it can be interesting to estimate how good the results obtained by proposed numerical solutions match with available experimental measurements. Advanced imaging techniques is used to reconstruct digital 3D models of rock samples from which porosity and pore network are estimated. Attempting to study the potential of these techniques for precise flow properties determination, the results are compared with laboratory measurements of through experimental methods.

1.3 Thesis Objectives

After a careful survey of the literature related to this topic, presented in the next chapter, several research gaps were identified. The thesis objectives are as follows:

1- To study flow characteristics of rock using DRP technology by:

- a) Obtaining digital images of rock using imaging techniques.
- b) Processing digital images to estimate the connected porosity using PerGeos software.
- c) Estimating absolute permeability of rocks using Lattice-Boltzmann Method (LBM).

2- Validating the flow characteristics of the rock by comparing simulated results with experimental results.

1.4 Methodology

The goal of this research is to prove that imaging techniques methods for estimating petrophysical properties of rock samples is a potential candidate to complement common laboratory methods due to its additional ability of providing a three-dimensional pore network. Laboratory measurements of porosity and permeability is performed on the same samples imaged by x-ray computed tomographic scanner. Core samples were imaged using

X-ray CT to quantify the heterogeneity of the samples and to give idea of the positions where a sub-plug is extracted from the core samples. PerGeos software is used to process, segment and analyze the 3D digital images obtained after scanning the sub-plugs and the connected porosity is estimated. Lattice-Boltzmann method (LBM) was used to estimate the permeability of the sub-plugs. Results obtained from numerical simulations were compared with laboratory measurements for validation. The aim for this work is to present a simplified workflow that can produce meaningful inputs for rock typing and reservoir characterization using a set of hardware and software tools. Figure 1-2 represents principal procedures of the study starting from imaging whole core-plugs to determination of rock properties.

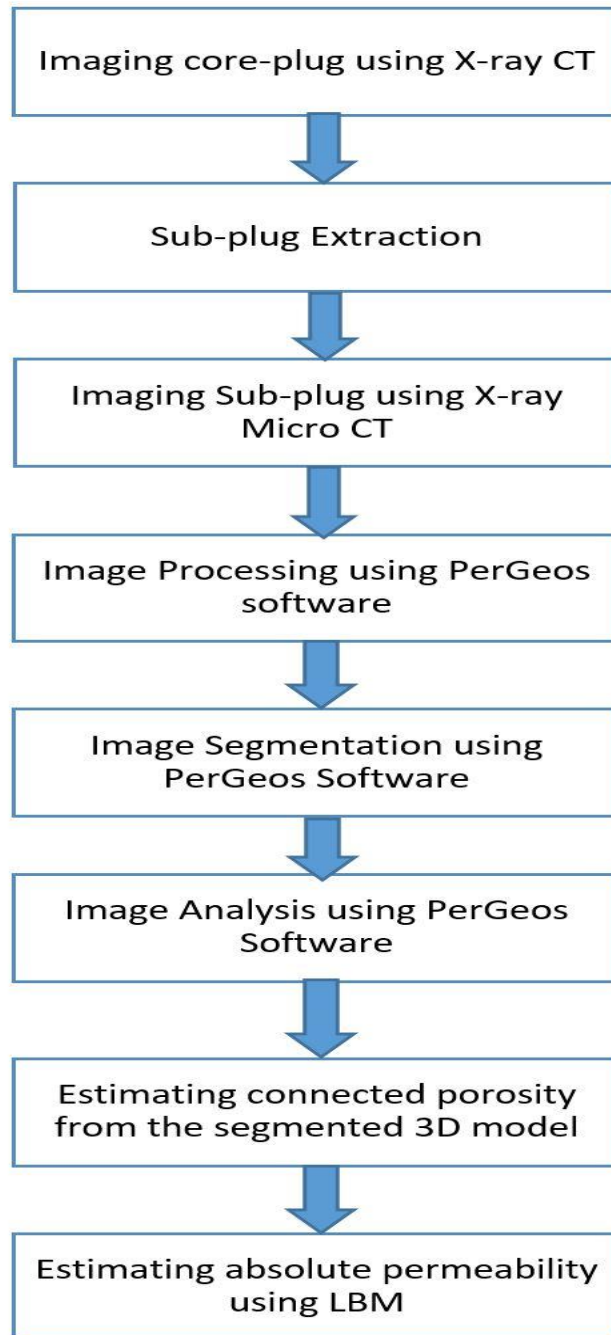


Figure 1-2: The applied Digital Core Analysis workflow

Chapter 2

LITERATURE REVIEW

To identify and quantify reserves in mature and green fields, reservoir characterization is important. The traditional tools for evaluating the characteristics of the reservoir are well logging and core analysis but parameters such as the capillary pressure functions, relative permeability and other macroscopic parameters required to model fluid-transport occurring in hydrocarbon production are obtained from experiments, which are often difficult to perform.

A new approach known as digital rock physics is emerging to better understand the rock's internal structure and to use this for rock characterization. DRP is a rather new technology combining computerized tomography (CT) and other X-ray scanning technologies to create high resolution, 3D images showing pore spaces and connections between pores. It offers non-destructive investigation methods to examine the inner workings of the samples. A suitable software program such as PerGeos can be used to build a three-dimensional image by stacking the individual slices one on top of the other. The process to recreate a virtual model is called reconstruction.

Combining digital rock methodology with computational fluid dynamics (CFD), leads to pore-scale simulation, which allows prediction of physical properties of rocks independent of classical rock analysis methods. On top of that, the numerical investigations are free from physical and chemical changes in core material occurring during experimental processes. Fluid transport modeling through porous media has been extensively studied in the past, however, the length scales involved and the complexity of pore structure make such studies mathematically and numerically challenging even up to the present day.

Reservoir characterization is essential for any oil company to model its hydrocarbon reservoirs and improve oil recovery. It is an integrating process, where static and dynamic reservoir rock properties are integrated to create a representative model of underground formation. Successful reservoir characterization requires an accurate and representative data measured at different scales and sources. Reservoir rocks or cores are one of the sources of data, which plays an essential role in the quantitative and qualitative description of a reservoir. Cores are cylindrical rock samples, which are extracted directly from the interested underground formation. Derived petrophysical properties from these rock samples represent characteristics of the underground formation. Normally, properties of cores are carefully studied in laboratories at different conditions. These properties include porosity, absolute and relative permeability, and capillary pressure. DRP has been a technology breakthrough for the Oil and Gas companies exploratory efforts [8]. Reservoir modeling and performance forecasting require a vast amount of information in order to

make educated decisions. Biased spatial sampling, insufficient amount of data and usually long periods for a comprehensive core analysis campaign can obscure and/or delay critical information to the decision makers. Digital rock characterization has a great potentiality to increase our ability to reduce reservoir uncertainty by increasing the amount of information from subsurface rock samples. Recent advances in imaging techniques, computational hardware and numerical simulation software have opened a possibility to obtain this information from realistic digital rock images. DRP has advanced in modern years depending on numerical simulation of physical experiments in pore space, and can be conducted on small rock fragments such as drill cuttings [23]. DRP has been used to obtain the transport properties, electrical properties and elastic properties of reservoir rocks [23]–[31]. Since its early development stage, this technology has been tested against the experimental protocols with very good statistical agreement [26]. However, this new technology is still complex, expensive and conducted by a reduced group of specialists.

The X-ray microtomography technique for reservoir rock characterization deepens the study of oil reservoirs and mineral deposits. With a simpler methodology for sample preparation and 3D imaging, Micro-CT enables key information such as porosity and permeability to be measured quickly and accurately, and is a non-destructive method. In this sense, Micro-CT characterization provides direct volumetric data acquisition, 3D quantitative analysis, shorter analysis time, etc.

High-resolution computed tomography enables the visualization and characterization of the internal structure of objects in three dimensions. As it is a technique of rapid acquisition of three-dimensional data and requires no more rigorous and delicate preparation (such as hydrocarbon-containing rock cleaning, impregnation, roughing, polishing, etc.), it is often used in qualitative and quantitative geological survey testing. In addition, the method provides numerical data, which can systematically lead to objective conclusions.

2.1 Properties of Porous Media

2.1.1 Porosity

Porosity is an intensive property of a porous medium. It relates the internal void space V_v to the bulk volume V_b that the porous medium has. This can also be determined knowing that the bulk volume of the porous structure is made up of both the void space and the space taken up by the solid structure V_s .

$$\phi = \frac{V_v}{V_b} = \frac{V_b - V_s}{V_b} \quad (2.1)$$

Mercury intrusion technique rely on having a fully connected pathway to a pore in order to be observed, whereas imaging and fluid movement detection techniques are capable of recording pores with no connectivity to the main pore space.

2.1.2 Single Phase Permeability

Single-phase permeability measurements are often one of the first characteristic parameters measured for any particular rock selected for scientific study. Henry Darcy initially proposed the concept of permeability in 1856 after experimenting on the flow rate of water through columns of sand. Through his experiments, he found that the flow rate of water varied linearly with the hydrostatic pressure caused by an upright column of water. These results were then used to form the general form of Darcy's Law:

$$q = -\frac{k}{\mu}(\Delta P - \rho g) \quad (2.2)$$

Where:

- q is the volumetric flux of fluid passing through the porous media.
- k is the absolute permeability.
- μ is the dynamic viscosity of the fluid.
- ρ is the density of the fluid.
- g is the gravitational vector.
- ΔP is the pressure difference.

Permeability varies widely across different core samples from extremely high permeability rocks and packed loose particle beds on the scale of a few Darcy's to extremely low

permeability rocks in the sub-nanodarcy scale. Correlations have been developed attempting to relate porosity to permeability in flow in porous samples, but the complexity of flow within the sample pore space caused by tortuosity, pore geometries, and other effects often lead to discrepancies. Even rocks with the same porosity are capable of showing permeability's that are orders of magnitude apart, often necessitating the development of correlation for unique rock types.

One traditional technique to measure the permeability of a rock sample is to place a fixed pressure gradient across the sample and then measure the flow rate of the fluid passing through the core. The permeability of the sample can then be found by using Darcy law following integration across the length of the core and neglecting gravitational effects found to be:

$$k = \frac{q\mu L}{(P_1 - P_2)} \quad (2.3)$$

Where:

- L is the length of the sample.
- P_1 and P_2 being the pressure upstream and downstream of the core, respectively.

2.1.3 Two- Phase Capillary Pressure in Porous Media

Whenever there is an interface between two different fluids, there exists a pressure difference between them caused by the tension of the separating surface. This pressure difference between the two phases, known as the capillary pressure, has been expressed as the Young-Laplace equation:

$$P_c = \sigma \left(\frac{1}{R_1} + \frac{1}{R_2} \right) \quad (2.4)$$

Where P_c is the capillary pressure, σ is the interfacial tension, and R_1 and R_2 are the principal radii of curvature for the interface. Since the Young-Laplace equation only considers the two fluids, an additional element is needed to take into account the effect of the solid surface itself in order to begin to understand the fundamentals of multiphase flow in porous media. Each of these interaction terms are given as σ_{so} for the interfacial tension between the solid and non-wetting phase (hydrocarbons or CO_2), σ_{sw} for the interfacial tension between the solid and wetting phase (water or brine), σ_{ow} for the interfacial tension between the wetting and non-wetting phases. The distinction between wetting and non-wetting phases stems from the attractive forces between the solid and each individual phase, where wetting phases have a higher attraction to the surface than non-wetting phases. Water being the wetting phase and the surrounding air the non-wetting phase as shown in Figure 2-1.

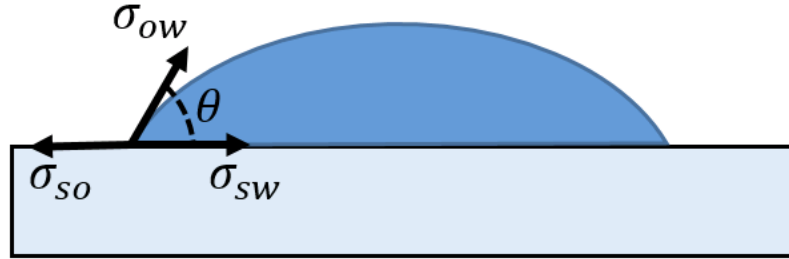


Figure 2-1: Diagram of droplet of water on a glass surface [32]

The edge of the drop hits the glass at a certain angle that corresponds to equilibrium all of these surface tension elements, that when a force balance is performed results in Young's equation:

$$\cos\theta = \frac{\sigma_{so} - \sigma_{sw}}{\sigma_{ow}} \quad (2.5)$$

This contact angle θ can then be used in extrapolation to multiphase fluid flow behavior. Taking this idea of contact angle and applying it to the analysis of a fluid interface inside of a narrow cylindrical capillary, the radii of curvature terms previously seen can be eliminated to something more easily determined as the radius of a cylinder r through which a fluid is flowing given as:

$$P_c = \frac{2\sigma \cos\theta}{r} \quad (2.6)$$

2.1.4 Relative Permeability

Relative permeability is a topic that has been studied in depth for several decades as it contains the major concepts behind the recovery of hydrocarbons from reservoirs. The permeability of individual phases has been found to vary throughout the production cycle of reservoirs and can be effected by numerous fluid and rock interactions. Relative permeability is defined as a modifying term in Darcy's law given as:

$$q_j = -\frac{Kk_{rj}}{\mu_g}(\nabla P - \rho_j g) \quad (2.7)$$

Where:

- K is the absolute permeability of the rock formation.
- K_{rj} is the relative permeability of fluid j , with the rest of the subscripted j terms being specific for fluid j only.

The relative permeability of an individual fluid varies from unity, being the highest amount of flow possible to zero, where only the other fluid is able to flow through the system. Relative permeability is typically referred to as a function of the saturation of

the material, with the zero relative permeability points for each given fluid being the irreducible saturations found within a porous structure. At any given point along these relative permeability curves, it is also possible to maintain fluid flow at points above irreducible saturation with the remaining non-flowing fluid left at residual saturation impeding the flow of the other fluid. Figure 2-2 shows a typical relative permeability graph for a water-wet system with the flow of oil and water taken from experiments by [33] and compared to a network model for fluid flow[33], [34].

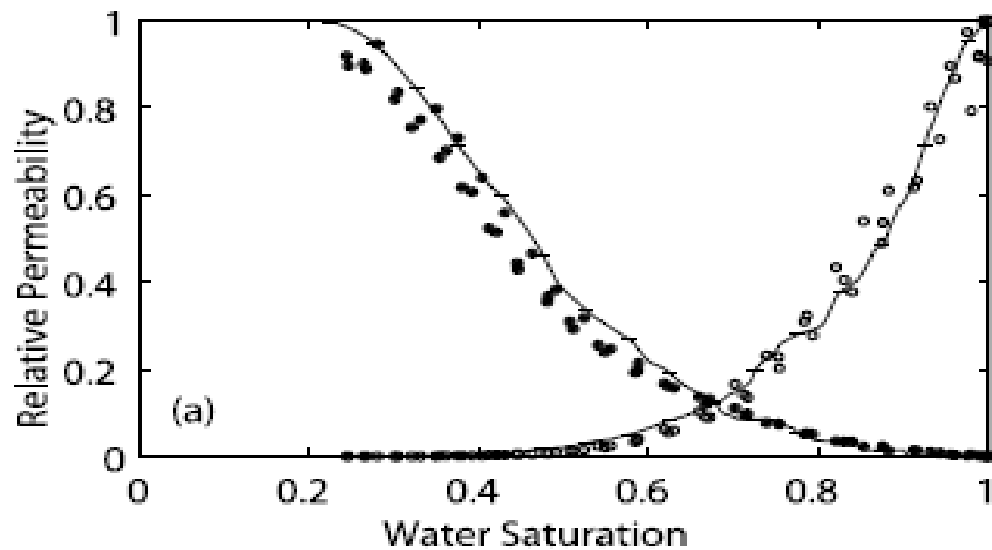


Figure 2-2: Relationship between the saturation of each wetting and non-wetting phase and the relative permeability of the fluid, along with predictive models computed using network modeling [34]

2.2 Mercury Intrusion Porosimetry

Two of the most common techniques in the oil and gas industry are Mercury Intrusion Porosimetry (MIP) and gas volume expansion for porosity. Mercury intrusion porosimetry can be used to investigate the specific characteristics of a rock samples pore network structure. In MIP, mercury is pressed into a dried sample saturated, in this case, with low-pressure air vacuum as the wetting phase. Pressures can often exceed several tens of thousands of psi and mercury can begin to enter pores on the nanometer scale. The use of mercury intrusion methods does require the destruction of the rock sample following analysis due to the toxicity of mercury that remains in the sample.

The mass of the sample is recorded before being loaded into the sample cup and the weight of the empty sample cup is recorded prior to being loaded. The sample is placed under a vacuum down to 50 μmHg mercury is allowed to fill the container to atmospheric pressure. The sample and sample cup are removed from the machine and their mass recorded again to find the mass of mercury that has entered the sample cup m_{hg} . The density of the mercury ρ_{hg} then used to find the volume of mercury that has been injected into the sample cup. This initial volume of mercury $V_{\text{hg},i}$ is taken to be the amount of mercury that fills all of the spaces surrounding the sample in the precisely measured empty volume of the sample cup V_o^{cup} or what can be shown to be the bulk volume V_b of the sample:

$$V_b = V_o^{cup} - V_{hg,i} = V_o^{cup} - \left(\frac{m_{hg}}{\rho_{hg}} \right) \quad (2.8)$$

The sample is then placed in the high-pressure hydraulic confining cylinder where an oil hydraulic fluid is used to press the mercury into the remaining pore space. The volume of mercury that enters the sample is recorded via conductance of the mercury down a metal-coated capillary tube. As pressure is increased incrementally, mercury enters smaller pores found in the samples pore network until the maximum pressure of the instrument is reached. The volume of mercury entering the pore space is recorded for each pressure increment after a predefined machine stability wait-time. This wait-time allows relaxation to occur within both the sample and machine components that may have occurred from temperature or sample structural changes.

The porosity of the sample is then computed knowing the final volume of mercury that entered the porous sample by assuming that this is the void space within the sample. This assumption is only partially correct, as there are several areas of ambiguity in recording such measurements. First, that this method has no way of detecting unconnected pores within the sample that may be present in other techniques such as X-ray imaging. If there is no throat leading to a pore, there is no way of the mercury entering the pore. MIP is defined to be an open porosity technique.

2.3 Imaging Techniques

Several methods exist that do allow for the characterization of porosity from direct measurements. Initially the study of thin sections allowed for the hand segmentation of samples, later to be developed into digitalization methods, and further advanced with more recent three-dimensional imaging techniques. Imaging of reservoir rock samples is performed at a range of scales and resolutions, as illustrated in Figure 2-3.

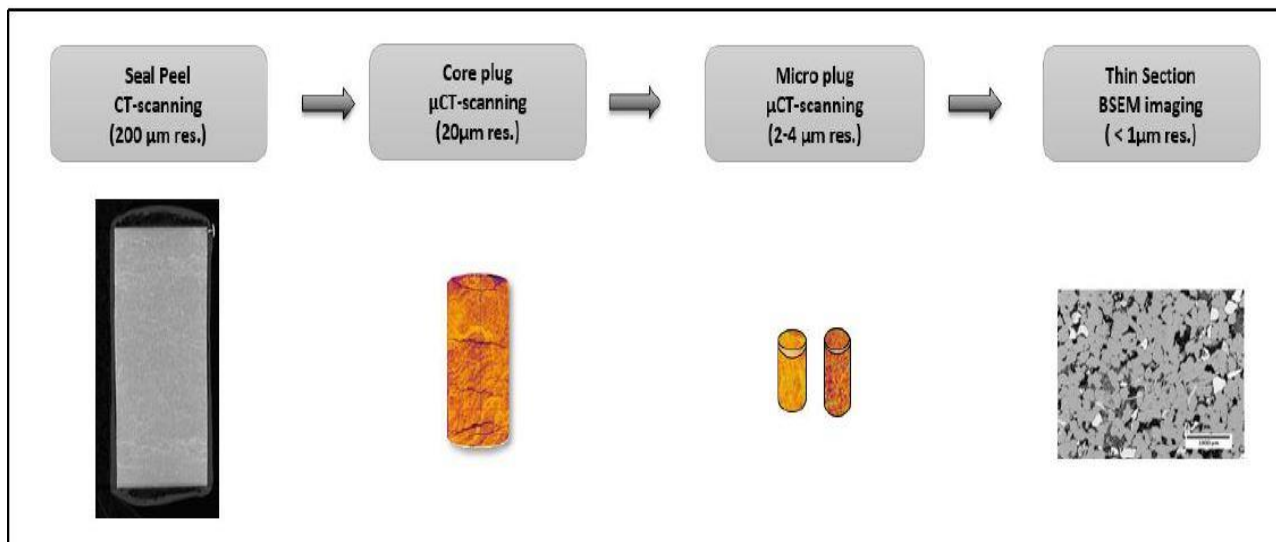


Figure 2-3: Scales and resolution in DRA. Decreasing sample size and increasing image resolution towards right, from the cm scale to the sub-micrometer scale

2.3.1 Thin Section Analysis

The first of these methods to be considered is the direct visualization of the pore space through thin sections of the rock sample. This is an extremely time intensive in the preparation of samples. This has partially improved with the advancement of digitalizing the thin section samples allowing for computational segmentation, rather than segmentation done by hand [35] Thin section examination is a standard technique of analysis under a petrographic microscope for almost all rock types, since it can provide a valuable information about mineralogical composition, textural and structural features of rocks and soils. The best resolution that can be achieved by petrographic microscopy is restricted by the wavelength of visible light, or so-called diffraction barrier, which is around 0.23 μm [36].

In thin sections, some grains may appear as dark brown or black due to their opacity. Opaque minerals do not allow any light to go through them even when thin slices (normally 30- μm thickness) had been cut. The most typical opaque minerals are oxides and sulphides, particularly iron oxides (hematite) and iron sulphides (pyrite). In these cases, it is important to highlight the pore space. Colored dye (e.g. blue epoxy vacuum impregnation) is used to assist in the determination of porosity and to stabilize the material.

2.3.2 X-Ray Computed Tomography

Medical X-ray computed tomography (CT) technology began gaining large success and implementation in the early 1970's, and soon after the geosciences began to utilize the technology to their own advantage [37]. Using the transmission of X-rays through a given sample, a series of images is collected as the source and detector rotate around the sample or the sample can be rotated on a movable stand within the X-ray beam of the source and detector. After collecting these images, complex mathematical operations allow for a full 3D reconstruction of the sample to be completed. Based on the principle of X-rays ability to be transmitted through various materials following Beer-Lambert law of transmittance [38], the external surface along with all interior features can be extracted. The technique gained further acclaim due to its ability to image interior features with no damage to the sample as most other techniques result in either irreversible changes to the rock sample's properties or complete destruction of the sample being required during or after analysis.

$$I = I_o e^{-\mu t} \quad (2.9)$$

Where:

- I is the absorbed energy.
- I_o is the incident energy.
- μ is the attenuation coefficient.
- t is the thickness of the sample.

From equation (2.9), the absorbed energy will increase in thicker objects and in locations of the object with higher attenuation coefficients. When speaking of rock samples the equation implies that the denser grains of the sample will attenuate more energy than less dense grains and void spaces of the rock will not attenuate any energy. Hence, a clear distinction between pores and material is observed in the projections, and different types of grains can be distinguished.

Since its introduction to the petrophysical research community, X-ray tomography has been used extensively for reservoir description and fluid flow visualization. The principles on which all future breakthroughs were made are expressed in a number of early papers that span each of these areas. One of the very first to demonstrate the usefulness of computer tomography in reservoir characterization by documenting the X-ray characteristics of mineral solids [39]. The physical principles of using x-ray imaging to study rock physics and developed an industry standard practice of measuring 3 phase fluid saturation using CT scanning through the use of dopants [40]. One of the most powerful applications of X-ray tomography is its use in providing quantitative descriptive data of analogue core samples. One of the earliest applications of this was imaging fluid invasion. The abilities of second, third and fourth generation CT scanners in measuring mud invasion in Berea sandstone [41]. The development of more advanced CT machines and the emergence of 3D reconstruction allowed fracture analysis of unique detail through mapping the internal features and fractures of a core segment [39]. Early efforts were made

to directly measure the porosity of homogeneous core samples using single scan techniques. Modern dual-scan CT machines for accurately measuring fracture and matrix porosity by scanning whole core samples from two wells, measuring their porosity, and correlating with pre-existing wireline density logs [42]. Building on this existing knowledge, many authors have since studied the capabilities of X-ray tomography in core characterization. The ability of CT technology was recorded to interpret data from acidizing trails and to visualize the creation of wormholes [43]. The usefulness of CT technology in measuring the porosity of shale formations was reported [44]. It was proved that the porosity measuring process has the accuracy to detect changes in porosity due to gas injection (CO_2 and H_2S) in carbonates [45], and verified the ability of CT technology to quantify the extent of skin damage in a core [46].

The visualization of fluid flow constitutes one of the most predominant uses of CT technology in the hydrocarbon industry. This requires the use of radiopaque tracers (dopant) to monitor the movement of fluids within a rock sample. The dopants provide sufficient information of the contrast between the different liquid phases inside the rock sample, and allow quantifying the distribution of fluid saturation inside the sample [38]. The use of computer tomography in special core analysis (SCAL), including investigating miscible displacement, measuring relative permeability, and determining core porosity [47]. Many authors built on the foundation set by these early researchers and have transformed computed tomography in to an indispensable tool for the industry.

The pore sizes of almost all rock samples are below the minimum voxel size resolution achievable with most medical grade X-ray scanners. To overcome this limitation, medical image analysis can use the change in CT number before and after saturation with different fluids, usually water and air, to determine the porosity of a given region within a core.

A CT number is a calculated reference scale based on the attenuation feedback from the X-ray detector, scaled so that water gives a CT number of zero and air is usually near -1000. Reference scans are thus needed for both the pure water signal and pure air signal recorded without the rock sample in place and the scale of CT number is computed [38]:

$$n_{CT,j} = K \frac{(\alpha_j - \alpha_r)}{\alpha_r} \quad (2.10)$$

Where:

- α_r is the attenuation of the reference phase.
- α_j is the attenuation of material j.
- K is a scaling constant.

The CT number values are determined for both water and air, and complete core scans are recorded for air and water saturated cores. The porosity of the core can then be determined by using values at 100% saturation for both of the different phases [38], [48].

$$\phi = \frac{n_{CT,ws} - n_{CT,as}}{n_{CT,w} - n_{CT,a}} \quad (2.11)$$

Where:

- w_s and a_s are for the water and air saturated sample, respectively.
- w and a are the pure reference values for the phases.

The detection of sample porosity in extremely tight porous samples has been achieved with doped brines [49] and gas [50] with increased X-ray contrast compared to water. The use of medical CT equipment can be used in a similar manner to porosity determination in the investigation of fluid flow behavior and saturation estimation in relative permeability studies [51]. Gas migration pathways through water saturated synthetic silt samples have also been successfully studied using medical CT scanning equipment [52].

X-ray computer tomography (CT) is a very valuable tool for characterizing the internal structure of different materials at different scales. Due to its practicality and non-destructive approach, the CT scan has been used in a wide range of research disciplines. It allows visualizing the pore network, and to perform qualitative and quantitative analysis of 3D object. CT scans have been widely used in the core analysis of sedimentary rocks. It is used to study grains density, porosity variation, fracture distribution, bedding characteristics and heterogeneity of long core samples [53]. However, such resolutions are not enough to fully capture the pore structure of sedimentary rocks. The advancement in technology has contributed to increase the resolution of the CT scan. As a result, micro-CT and nano-CT scans have been developed to improve image quality.

2.3.3 X-Ray Micro Computed Tomography

Advances in X-ray computerized tomography technique at the micrometer scale has also recently allowed for the direct visualization of a rock's pore space. With voxel capabilities down to a fraction of a μm , the direct imaging of larger pore spaces allows for the direct computation of both open and closed porosity based on connectivity [54]. Micro-computed tomography (micro CT) is a powerful tool for characterizing, in three dimensions, the internal structure of rock core samples through non-destructive examination. The collected data is used to extract a pore network model, which is a geometrical representation of the pore space as a series of pores connected by throats [55].

The technique is based on the principle of X-ray imaging, in which several radiographs of the object analyzed are recorded at different angles of rotation. Such images are used to compose a three dimensional representation through computational processing. The sample is positioned between the X-ray emission source and the detector and is then rotated to acquire projections at various positions. These projections are proportional to the amount of radiation reaching the detector, which varies according to the different X-ray attenuation coefficients of each material.

The pore network model provides the fundamental pore scale structure of the rocks, in terms of the pore size distribution, throat radius distribution, pore coordination number (representing the connectivity of the pores to one another), and the pore-to-pore distance. The invasion of a fluid through the material can then be simulated through invasion

percolation simulations to determine the rock's permeability. This information is crucial to the development of realistic characterizations of the pore geometry and saturation profiles that lead to improved system scale simulations. Micro CT and the extracted pore network models have been used widely for petroleum [6], [56] and geologic [57], [58] studies to characterize the pore geometry, permeability and porosity of sandstone [59] and oil-bearing carbonates [60].

The pore sizes found in many sealing formations are often still below this image resolution. The X-ray contrast between fluids can also be used to show specific fluid flow and saturation behavior within individual pores [61]. Limitations exist between the desired resolution of the recorded tomogram and total imaged volume requiring careful consideration for desired sample observations. Sub voxel resolution information can also be extracted similar to medical CT techniques determining the porosity of samples with pore size far below imaging limitations [54]. Investigations have also been carried out to characterize previously fractured systems to observe two-phase fluid flow behavior. Due to the larger physical size of system fractures, the exploration of micro-CT imaging capable of capturing fluid saturations and aperture size is possible [62]. Advances in nano-CT systems have recently been able to extract nanometer scale features from porous samples, but with a limitation on the recorded tomogram volume [63]. There are two main types of micro-CT devices that are used in imaging of geological materials. The desktop micro-CT scanner and synchrotron X-ray setup. The main differences between them are related to the

resolution limit and rotational angle for a sample 360 deg. for desktop and 180 deg. for synchrotron, due to having two parallel beams in the latter case [36], [64]. The intensity of X-rays reaching detector, among other factors, depends on the sample's thickness, composition and density. At the time when the rotational angle reaches 360 deg. (or 180 deg. for synchrotron), several hundreds of radiographs are registered and further transformed into a 3D volume by applying appropriate reconstruction algorithm. This data volume represents a 3D distribution of the linear attenuation coefficient values that can be viewed as gray scales. After that, it is necessary to apply filtering to smooth, reduce noise and improve the contrast between pores and grains of the obtained image [36]. Although most of the desktop scanners can typically provide a resolution between 2 and 5 microns, the best achievable image resolution is around 700 nm, and it has been obtained by using synchrotron micro-CT [36].

Micro CT 3D images are based on the X-ray attenuation of the scanned material, which is a function of both physical density and effective atomic number of the material the X-rays pass through [54] with the advantage that the 3D images are produced without damaging the samples [65]. Figure 2-4 and Figure 2-5 shows examples of Micro-CT scanner applications in carbonate rocks. These tools have demonstrated their ability to capture pore structures at micro and nano scales. The applications of the Computed Tomography in the hydrocarbon industry are mainly concentrated in the scanning of porous media without compromising its physical integrity or wettability. X-ray computed micro-tomographs can

image rock samples with a resolution of approximately $1\mu\text{m}$ per voxel and upwards. Acquisition of pore size information below this resolution will require other sources of imaging. Scanning electron microscopes (SEM) are widely used for reservoir rock analysis, and is especially valuable with the possibility to register high-resolution 2D images into the 3D volume generated from micro CT. The 2D images could be BSEM images for improved segmentation or QEM scan data for supporting mineralogical analyses. Investigation of pores down to the nano-scale will require additional imaging techniques, such as FIB-SEM imaging.

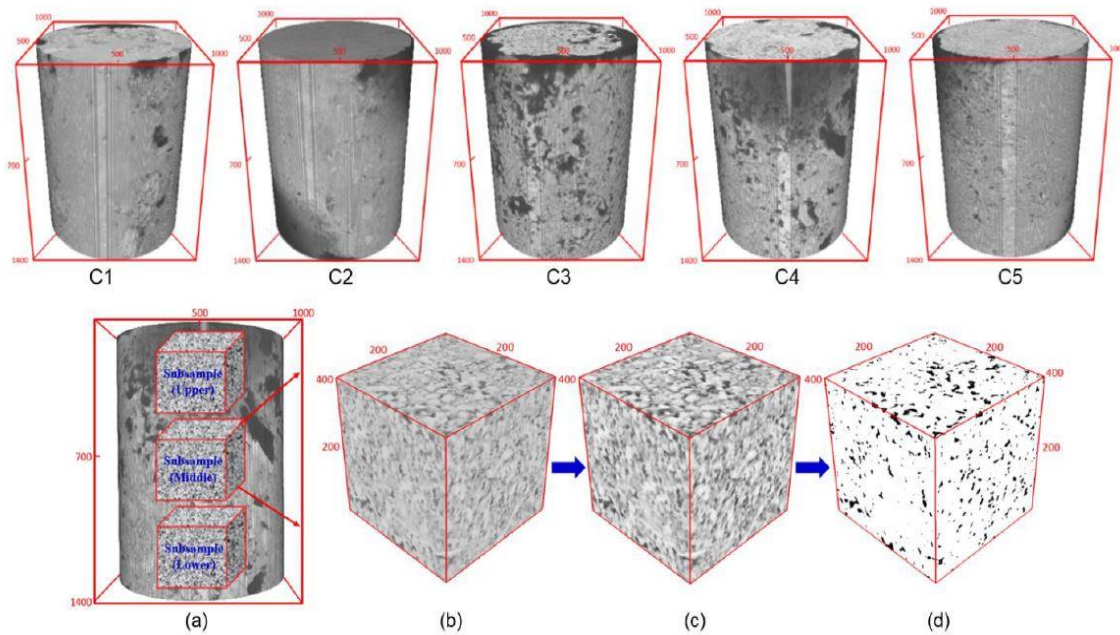


Figure 2-4: Micro-CT scanner applications (a to d) textural heterogeneity study in carbonate rocks [66]

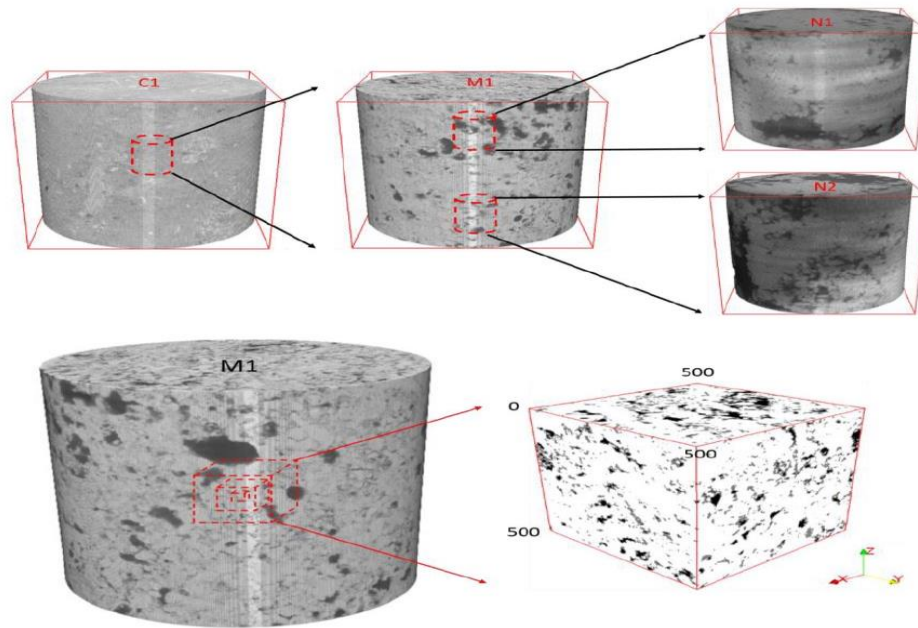


Figure 2-5: Micro-CT scanner applications: Multiscale analysis of rock images [67]

2.3.4 Scanning Electron Microscopy

Scanning electron microscopy (SEM) is another technique that has been developed for the imaging of pore spaces within extremely tight rock samples. SEM is capable of some of the highest level of magnification possible for pore space imaging. The SEM is used investigate the type of clay minerals present in the samples and to study the effect of these minerals on porosity and permeability changes. The use of SEM systems allowed for the imaging of individual clay platelets in different clay minerals [68]. SEM provides resolution down to several nanometers. Images are produced by scanning the sample with

a high-energy electron beam. SEM uses a high-energy electron beam to interact with a conductive specimen. The electron beam is decelerated by the specimen and can be visualized using secondary electrons emitted from the sample as in back scattered electrons, or using photons, as in electron dispersive spectroscopy. In SEM-electron dispersive spectroscopy, specific microscale features of the sample can be analyzed for their chemical composition. The most common SEM approach is to detect secondary electrons that are emitted by atoms excited by the electron beam due to their low energy. As a result, very high resolution can be achieved. An additional advancement of the technique came from the incorporation of a high precision milling beam capable of removing extremely small layers of material away from the sample surface. This is accomplished in most machines with a focused ion beam (FIB). The focused beam of ions is used to remove very precise amounts of material in several repeating layers alternating with SEM scanning of the surface. These series of images are then combined to build complete 3D reconstructions of the milled volumes similar to those recreated with CT techniques, although the sample is destroyed with the milling process. FIB-SEM imaging techniques can then be used in a similar manner to CT imaging techniques for the analysis of porosity and pore network of samples, only with a much smaller observed volume. While thin-section analysis, SEM and focused-ion-beam-SEM can provide two-dimensional images of the microstructure, micro CT is the only experimental technique that can provide high spatial resolution data in three-dimensions.

Further improving the imaging limitations beyond that of the micro-CT, SEM systems are capable of capturing features down to a few nanometers. These systems often contain several ways of measuring a sample response to the bombardment of electrons via an electron beam. SEM systems can directly image pores within seal formation samples at the nanometer scale. The SEM system can be further enhanced with a focused ion beam used to mill away sample material in a very controlled fashion. A focused ion beam – scanning electron microscope (FIB-SEM) can be used to collect a series of surface images in sequence as material is milled away to allow for the reconstruction of a 3D volume of the explored region at extremely high image resolutions. This technique can then be used to directly image even the tightest of pore spaces.

The use of FIB-SEM imaging in the analysis of shale pores has shown several unique pore shapes. Heterogeneities within the shale pore space are important in understanding fluid flow behaviors within samples, giving rise to the use of multi-scale imaging techniques in order to incorporate results on numerous imaging length scales [69].

2.3.5 X-Ray Diffraction

X-Ray Diffraction (XRD) is a versatile method used in characterizing crystalline materials and determine their structure. XRD is a non-destructive analytical method to analyze material properties like phase composition, structure, texture and many more of powder samples, solid samples or even liquid samples. Most minerals are crystalline and scatter X-

rays in a regular, characteristic way dependent on their crystal structure. XRD measures the intensities of a reflected area and from the results, obtained atomic-level spacing of the crystal can be calculated.

In 1913, Bragg described diffraction and interference of X-rays in a crystal as reflections at the atomic planes of the crystal lattice.

$$n\lambda = 2d\sin\theta \quad (2.12)$$

Where:

- n is an integer count of the number of incident waves.
- λ is the wavelength of the incident ray.
- d is the spacing between the atomic lattices.
- θ is the angle between the scattered waves and the incident wave.

2.3.6 X-Ray Fluorescence

X-ray fluorescence spectrometry works on the principle of ionization of elements resulting in the emission of electrons at energies correlated to the elemental composition in weight percent. The investigated material, in a powdered and pressed sample holder is subjected to a collimated X-ray beam that excites the orbital electrons, which are subsequently emitted. The emitted waves scatter and are counted by a detector. The frequency, at which the scattered waves influence the detector, as the sample passes through a 360 deg. rotation,

indicates the percentage by weight of the sample's chemical composition. X-ray fluorescence spectrometry provides a detailed elemental mineral composition of the bulk sample [70]. Quantitative analysis by XRF delivers very reproducible results, which can be reported as element concentrations, compound concentrations or other concentration related functions.

X-ray fluorescence spectrometry is reliant on Bragg's Law to deduce the overall frequency of the chemical composition. It relies on the diffraction of a collimated X-ray beam off a sample. The approach relies on the angle of scattering off a sample due to Bragg's Law equation (2.12).

2.4 Image Analysis

Once any form of image is collected from a rock sample, image analysis becomes an extremely complex and delicate procedure to extract information from sample images because of the influence of humans on the data. A concept that initially seems straightforward, image analysis is notorious for the amounts of user influence on results.

2.4.1 Image Preparation

The first step to building a pore network model is to obtain a micro-CT scan image from a relevant sample. Micro-CT is an X-ray imaging technique in 3D with a very high resolution. Employing digital images for computational modeling ensures that the models

capture the pore morphology of the real materials, such as pore size distributions, pore-scale heterogeneity, and spatial correlations.

2.4.2 Image Noise and Artifacts

Image noise occurs from the transposing of physical phenomena into digitizations through, in the case of the micro-CT instrument, a scintillator and a charged-coupled device (CCD) camera to collect digital images. Image noise can come from a variety of sources, from the cable transferring the image from the CCD, to an error in the processor, to internal component's interference with each other forming electrical interference noise. The noise from each projection is processed along with the true signal in forming the tomographic slices of the imaged sample, complete with the combined noise of all the projections. Noise is a random occurrence within images, and in this way, the collection of a larger number of projections allows for a higher signal-to-noise ratio (SNR) to be reconstructed in the tomographic sections, as each projection's noise is inconsistent with the next.

2.4.3 Image Filtration

Image filtering may be employed to counteract the effects of image noise in both qualitative and quantitative analyses. The key parameter is to reduce the amount of noise that is found in pictures, while preserving all information contained in the image signal. The random distribution of noise throughout images makes this an extremely difficult problem to solve where complex patterns and extremely small features in images are often blurred due to

the denoising techniques. These filters include Gaussian smoothing, anisotropic filtering, and non-local means filters, along with others. Different algorithms have varying results, as one would expect. The very simple Gaussian-smoothing filter has the effect of blurring all features found within an image, whereas certain filters have been designed to be edge preserving. An anisotropic filter uses the same blurring technique as Gaussian smoothing, but with the designation of a grey value gradient threshold not to exceed, as found at the edge of different phases. A nonlocal means filter is extremely effective at feature and edge-preservation, but comes with the cost of being extremely computationally expensive.

2.4.4 Image Segmentation

The main approaches applied in image segmentation are simple thresholding based of the grey values of produced images, or watershed segmentation algorithms. Thresholding segmentation relies on the simple principle that a given material, located anywhere within an image, should have the same CT number. In this way, a simple user defined cut off point is designated between phases, and the grey values above and below this boundary are assigned to certain phases. At this point, the concept of noise becomes exceedingly important, as noise within a given material will assign certain erroneous pixels to the wrong phase. In light of this, image filtering is applied before segmentation in an attempt to avoid designating materials incorrectly. Watershed segmentation begins with the user selecting grey values for certain phases, but only small portions of each phase are selected where it is certain there is only one phase present. Then the gradient of grey values is computed

across all of the images, and the initially selected portions of the phases are allowed to growing a manner similar to water spreading in a hilly terrain. The predesignated phases then meet at the high gradient areas and the image is segmented along these various boarders into individual phases.

2.5 Rock Properties Estimation from Imaging Techniques

Dual-energy CT scanning method involves two X-ray beams with different energy levels pointed at the sample to be studied. These two effects have a known dependency on the atomic number and electron density. The qualitative evaluation of the CT images of rock samples provides information of the heterogeneity, lithological changes, fractures, etc., while the quantitative evaluation allows quantifying the apparent density and porosity, among other petrophysical properties [71].

The mineralogy and porosity of core plugs is correlated from ρ_b and Z_{eff} values [40], [72]. CT scan is valuable as it is a nondestructive technique to measure cores porosity, lithology characteristics, and oil and gas saturations within the cores. The expressions used to calculate ρ_b and Z_{eff} are shown in equations 2.12 and 2.13.

$$\rho_b = m \times CTN_{low} + p \times CTN_{high} + q \quad (2.13)$$

$$Z_{eff} = \left[\frac{r \times CTN_{low} + s \times CTN_{high} + t}{0.9342 \times \rho_b} \right] \quad (2.14)$$

Porosity and permeability of carbonate rocks were predicted using confocal laser scanning microscope (CSLM) as one of the tools. The authors introduced the Lattice Boltzmann method as an efficient model to solve the Navier-Stokes equations directly for flow in complex geometries, such as pore-scale images of real rock samples obtained from micro-CT and confocal microscopy imaging. The LB method describes the fluid system by interaction of fictitious particle groups, much bigger than the molecules of real fluids, but show the same behavior in density and velocity as the real fluid at the macroscopic scales reside on the lattice nodes, which reside on the lattice nodes. Water Saturation as a function of time was measured and preliminary results for the imbibition in carbonate rocks was obtained using CT scanner [73].

A procedure based on CT imaging to better understand porosity and permeability measurements at different depths in a core sample to a continuous measurement with depth. The authors investigated the relationship between porosity, permeability and CT number. As a result, a new exponential correlation was developed to express permeability as a function of porosity, two adjustment parameters and CT number [74].

Dual Energy CT imaging has been used in complex carbonate and sandstone reservoirs in the Middle East to characterize reservoir heterogeneity and optimize sample selection for special core analysis (SCAL) testing [2], [75]–[77]. DRP has contributed to the

computations of reservoir properties through image segmentation in 3D and direct simulation [2], [78]–[80].

Multi-resolution imaging of carbonate rock with CT, backscattered scanning electron microscopy (BSEM) and focused ion beam scanning electron microscopy (FIB-SEM) was combined to perform full-scale analysis of pore distribution. Better evidence on micro porosity and microstructure of the samples were obtained by merging μ -CT with SEM images [81].

It became evident that carbonate rocks are characterized by a significant percentage of porosity in sub-micron scale Figure 2-6, therefore approaches of coupling micro-CT with electron microscopy and focused ion beam electron microscopy. (techniques that image at the nano scale) were attempted [15],[82].

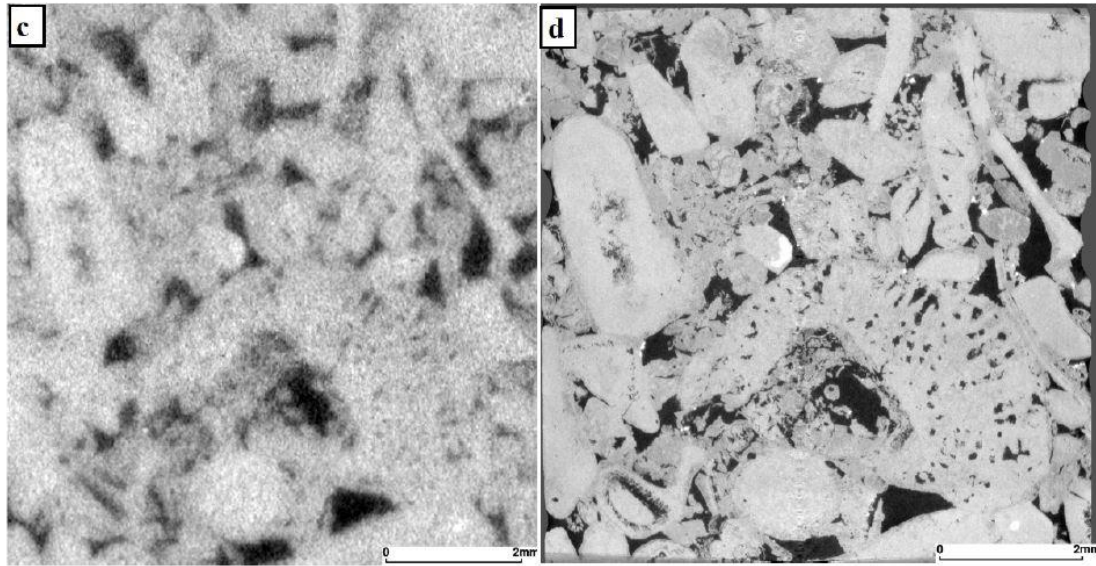


Figure 2-6: Illustration of sub-micron porosity in carbonate samples. Images shows slices from the same region of the sample imaged at (c) low and (d) higher resolutions [81]

The first work regarding quantification of porosity and generation of 3D pore networks from micro-CT images [83], a sophisticated software for micro-CT images analysis, where the pore network generation was based on skeletonization using the medial axis transform. The software was applied to tomographic images of Fontainebleau sandstones and had incorporated an indicator kriging segmentation. It performs well on relatively clean synchrotron images later validated methods with indicator kriging [84].

A different method was developed, called the method of maximal balls. In this approach, the porosity is estimated by fitting inside the voxels spheres of sequentially larger radii. The spheres could exit the voxel and continue growing until the sphere boundary touches a solid material [85].

Also, the method can be used to compute pore throats [86]. Figure 2-7 shows the two methods, but in both cases, the results needed post-processing to remove excess pores and throats.

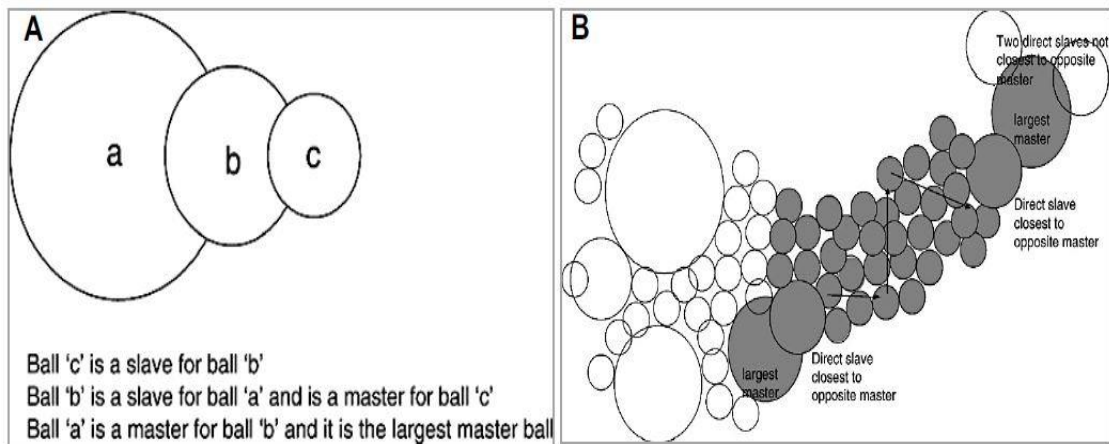


Figure 2-7: Maximal balls method for pore network extraction. The initial increasing spheres model of [85] and the model of [87] extended to compute throats

The skeletonization method was compared with the maximal balls method and showed that the network extracted is not so sensitive to the method used as it is to the geometrical shape assigned by each method for the pores. The big limitation of skeletonization methods is that, reducing the pore to a line skeleton is unable to detect structures like fractures [64].

An accurate pore network extraction also implies an accurate segmentation process. Segmentation is the discretization of the micro-CT images into void spaces and material, applying a threshold value by which the attenuation coefficients are categorized in black

void space or white material. It is not a linear and simple task because is made on 2D images, and each 2D projection might be suited by a different thresholding value.

Different imaging and segmentation methods and different numerical methods for calculation of elastic properties, single-phase fluid flow properties and electrical properties, were compared attempting to create benchmarks that future studies can rely on to comparison. In their evaluation, segmentation method is specific for each case and should be chosen according to the situation. Moreover, the numerical predictions of the studied properties are influenced by the segmentation method, as well as by the type of numerical method used to estimate the property and by the sample size and rock heterogeneity [28].

The effective porosity was estimated using a dry/wet technique. Samples were first imaged dry, then saturated with water, and imaged saturated. Subtracting the saturated micro-CT images and the dry micro-CT images, they obtained the effective porosity. Different subtracting algorithms were used, and corrected the misalignment between images with more than one correction methods. The results compared well with subsequent porosity measurements [88].

Carbonate samples were imaged in two resolutions, a high resolution $1.1\mu\text{m}$ per voxel acquisition and a low-resolution $42\mu\text{m}$ acquisition. Higher resolution images were used to extract the pore network of the carbonate sample and then up scaled the model to the less resolution $42\mu\text{m}$ acquisition. It was reported that increasing of the apparent porosity with

resolution, and that the estimated porosity from the micro-CT images is lower than the porosity measured in laboratory [86].

A multi-scale imaging-modeling workflow was proposed, where besides micro-CT imaging and 2D scattered electron microscopy (2D-SEM) imaging, the authors incorporate mineralogical identification at the 2D-SEM and micro-CT imaging Figure 2-8. The porosity from this workflow is close to the porosity determined in laboratory [89].

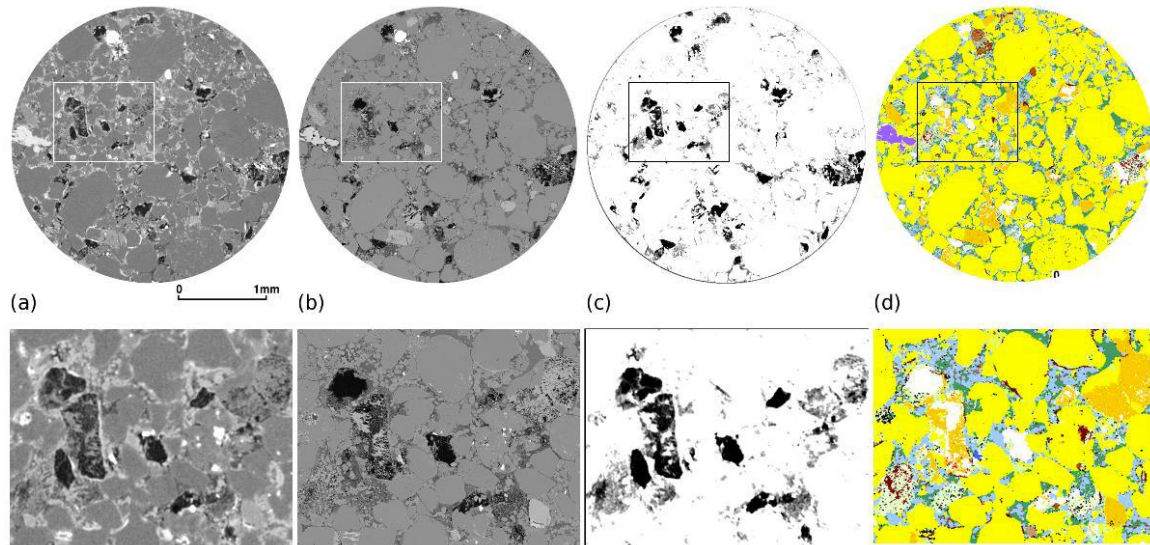


Figure 2-8: Results of different techniques used to incorporate in a multi-scale imaging and modeling workflow. (a) Dry tomogram at 2.5-micron resolution (b) Registered SEM (c) Porosity map from wet/dry difference (d) Registered automated [89]

Micro-CT images was used to estimate effective elastic properties. Then used the estimated properties to run numerical simulations of effective transport and effective mechanical properties. Lattice-Boltzmann flow simulation was used to predict the permeability and dynamic wave propagation simulations to estimate the rock moduli and the tortuosity. The sample imaged was a sandstone and was imaged by synchrotron-based X-ray tomography [90].

X-ray CT imaging was used to assess the anisotropy performing systematical and planar clustering of 3D X-ray attenuation values, coupled with an associated statistical analysis. It was shown that anisotropic orientation is identified by the variation of the voxel values [91].

Three-dimensional images of sandstones were extracted to validate an innovative extraction algorithm. The permeability values of the extracted network differed significantly from those calculated using the Lattice-Boltzmann methodology, indicating further refinements were required [60].

Multi-scale imaging technique was employed to acquire images of carbonate rocks at various resolutions. High-resolution images were used to compute petrophysical properties, e.g. porosity, absolute and relative permeability [80].

Measurements of carbonate samples were performed and ranged from small trims to whole core samples. Differences in permeability and cementation exponents measured on

different scales were observed. It was concluded that whole cores provide measurements that are more representative and decrease uncertainty in physical interpretation [92].

Three scales of petrophysical data were integrated using measurements and digital rock physics. The Darcy upscaling simulations were used to predict permeability of large-scale samples [93].

An upscaling approach was proposed for permeability and formation factor using multi-scale X-ray CT imaging techniques, image registration technique and digital rock physics. Relations between porosity and permeability/formation factor were derived from a randomly selected size at various locations within small-scale samples [94].

2.6 Representative Elementary Volume

The idea of a representative sample volume stems from the known heterogeneity of most geological formations on certain scales. Preferential pathways exist within core samples, and flow can be seen to travel in specific directions within a formation showing heterogeneous effects at the full scale. It is important to determine the representative size of sample needed to encapsulate any parameters. When the observed volume is below the representative volume, the analyzed variable will fluctuate wildly, then as the REV is approached, the fluctuations within the data subside and a repeatable value is found to exist with the porous structure. A homogeneous porous medium for a given parameter then goes

on to define as one where after the REV is exceeded the result of a specific analysis always returns the same value. If after the REV is exceeded, changes within the recorded parameter continue to fluctuate, the porous medium is considered heterogeneous for the given parameter throughout the formation.

2.7 Direct Pore-level Modelling

DRP has grown rapidly due to the advancement in imaging, computing technologies, and image processing techniques. For example, high spatial and temporal resolutions of 3D images of pore space to $<1\ \mu\text{m}$ and sub-second respectively have been employed to image pore-scale displacements and to measure real-time pore-scale properties. Advanced imaging scanners such as non-destructive and non-invasive X-ray micro computed tomography (μ -CT) have captured the high-resolution 3D images or Nano computed tomography for ultra-low permeability samples and synchrotron [86], [95]–[99]. In addition, other emerging technologies such as confocal microscopy, e.g., laser scanning fluorescence microscopy, and super-resolution fluorescence microscopy are conceivable in near future. Porosity and permeability are chosen as the first calibration points for digital rock analysis. Digitally derived porosity has been a subject for discussion due to partial volume effects from pores smaller than the model resolution. Imaging techniques, such as dry/wet imaging together with registration [89], are being continuously developed and improved to reduce the uncertainties related to quantification of pores. Generation of

micro-porosity maps is also used for spatial mapping of various micro-porosity classes within a rock sample. This information is of high importance for selection of relevant locations for higher resolution images, such as SEM or FIB-SEM. The connected network of larger pores mainly governs the permeability of a rock sample. This way the absolute permeability is less sensitive to model resolution compared to other parameters, as long as the main flow paths are well characterized. For rock samples where the main flow paths contain pore throats that require multi-scale imaging, the calibration to experimental data would be of increased importance to validate the integration methodology.

Rather than direct 3D imaging, the construction of complex core structure has also flourished by state-of-the-art techniques in stochastic or object-based reconstruction procedures. At first, one requires 2D petrographical thin section images extracted from scanning electron microporosity (SEM) generating submicron scale images. Then, by applying an optimization approach, the reconstruction techniques result in 3D representative rock samples by integrating images and obtained data for example porosity, grain size distribution, clay and cement content [5], [61], [87], [100], [101]. Nevertheless, even by providing a detailed analysis of 2D thin sections, reconstructing complex pore structures based on currently applied reconstruction methods are problematic. These complexities include, but not limited to, microporosity, clays, and long-range connectivity of pore space.

Finally, high-performance parallel computing such as multi-core Central Processing Unit (CPU) architecture and Graphics Processing Unit (GPU) have rendered data acquisition, processing, and visualizing of computationally intensive pore-scale data arising from pore-level images. In a study [78], the authors applied a domain decomposition method to simulate a matrix of $500 \times 500 \times 1000$ voxel (1 voxel of a tomogram or image represents volume element equivalent to a pixel in the 2D element) in parallel with 50 GPUs. They generated a 20483-voxel telegram with 128 CPUs in approximately 4 hours.

Providing the desired flow experiment, both the spatial and temporal saturation distribution are assessed through the digitized rock. Once a 3D voxel representation of the porous medium and its embedded fluids are constructed, one shall validate them against laboratory experiments in conventional and special core analysis or 2D micromodels [102].

In pore-scale modeling, the parameter estimation, e.g., multiphase relative permeability is accomplished based on a multiphase flow simulation in pore-level via either direct pore-level models or extracted 3D pore-network models. Direct pore-level modeling on the constructed 3D image is more fundamental and more computation demanding than pore-network in comparison with direct counterpart, pore-network models may not fully capture behavior of a heterogeneous system due to their principal simplifying and averaging assumptions.

2.8 Pore Network Modelling

Pore size distributions started to be used as constraints regular lattice patterns to match coordination numbers of the considered networks. However, in most cases, regular lattice networks are not able to catch the complex topology of the complex porous structures properly. When transition to network approach from the real pore microstructure occurs, some arbitrary considerations should be made as to where a pore ends and a constriction starts. It means that PNM is a non-unique representation of pore space, and for each network extraction method different assumptions should be made, which may complicate significantly a comparison of networks obtained by different extraction algorithms [36]. Typically, network extraction includes segmentation of continuous pore space into discrete network elements and defining the main geometrical properties of each element, e.g. hydraulic radius, the volumes and lengths of pores and throats, etc. [36]. There are several different approaches to classify PNM extraction; however, the most common one is to distinguish two classes: topology-central and morphology-central methods [36].

Pore network extraction and modeling is used in porous material research to simplify the structure of a sample void space into a form that can be analyzed in various ways [102], [103]. A pore network model consists of pores that represent the samples voids and the throats connecting the pores [55]. Pore network extraction techniques can be used to

characterize the porous structures imaged using micro CT to identify detailed geometric information regarding the pore space.

Methods based on the concept of the medial axis captures pore interconnection adequately, but may have some problems with pore identification, i.e. partitioning of the pore bodies. These methods are sensitive to small defects in the input pore space surface that may lead to significant pore over-segmentation, as faked brunches of the medial axis would be identified. Pre- and post-processing of the input images can help to avoid this problem [36], [64].

The concept of maximal ball algorithm begins with extraction of maximal balls, which are the largest inscribed spheres centered on each void voxel that just touch the grain or the boundary. After that, spheres located completely inside other spheres are removed, allowing decreasing the complexity of resulting set of maximal balls. It is possible to cluster them into families, where the common ancestor of each cluster denotes a pore. The main advantage of the maximal ball method deals with explicit manner of pore and throat distinction [89]. In general, the scheme works good for pore identification, but the construction of throats may become a challenge, since there can be several ways to connect pores by overlapping smaller spheres [64].

Correlations have been developed to offer a simple approach to the prediction of fluid flow behavior within porous media. These correlations have been developed on assumptions

about sample pore space arrangement and geometries, often stemming from an analysis of packed spheres. The Kozeny-Carman equation is a correlation widely used to predict the permeability of reservoir samples with relative success in samples with simple pore spaces. The use of the Kozeny-Carman equation has been showed to have limitations in dealing with ductile porous samples or samples with large clay contents due to the assumptions of the model. Ductile sample pore space results in variations within sample porosity and exposed surface area under varying fluid flow conditions not accounted for. Clays were determined to have immobile wetting layers impeding fluid flow causing deviations in the quantification of sample pore space used in the prediction of the equation.

Initially considering idealized systems, fluid flow modeling has evolved to be capable of utilizing geometry inputs directly from imaged real systems. Instead of using correlations or derived relationships between pore geometries and fluid flow behavior, these models determine fluid flow behavior by using numerical approximations of fluid flow equations bounded within the extracted pore space volume. This allows these models to overcome substantial challenges that are often problematic for volume-averaged approaches such as multiscale pore space systems and pore space heterogeneities. These models have developed with sufficient complexity to predict multiphase fluid flow properties of porous

systems including fractured systems, variations in fluid wettability, and fluid-fluid interactions within complex pore geometries [104].

Direct fluid flow modeling is highly favored using the lattice-Boltzmann method [105]. This method is based on modeling the motion and collisions of particles in a structured lattice. The behavior of particles using this technique can be shown to result in behavior similar to that of the Navier-Stokes equation. The main limitation of such models is the computational power required to observe fluid flow behavior on large simulation sizes. Coinciding with direct fluid flow simulations in porous media are models that use simplified structures of the pore network to decrease computational power required to model large systems. The first of these was designed to relate fluid flow behaviors to an interconnected network of electric resistors [106]. These models quickly grew in complexity capable of describing complex multiphase fluid flow phenomena with continued advancements today [102].

Recently, pore-network modeling has included detailed description of rock geometry and topology, general wettability and wettability alteration during the fluid displacement, and the underlying mechanism of multiphase flow in porous media, e.g., multiple displacement, coupled capillary and viscous flow, film flow [60], [107]–[110].

Pore network platform is a viable tool for building and understanding of the complicated multiphase flow in a complex rock structure. The pore-network models are useful in

deriving macroscale properties including multiphase relative permeability and in reproducing macroscopic results from laboratory experiments. Moreover, they are computationally efficient compared to other pore-level approaches. Consequently, there is a growing interest in pore-network modeling. Nevertheless, as will be discussed, the latter currently has limited applicability for modeling complex rock structure, fluid distribution, and fluid interface due to its inherent simplifying assumptions.

2.9 Pore-Scale Relative Permeability Modelling

Several researchers have calculated multiphase relative permeability calculations from pore-scale modeling or measurements [78], [109], [111]–[113]. A representative relative permeability can be obtained from a detailed analysis of pore scale pore structure, fluid distribution, fluid configuration, and fluid displacement. In addition, the relative permeability's need to be upscaled to a large scale. One solution is to tabulate each phase relative permeability in a three-dimensional table as input to the simulator. During a simulation, each grid-block has an associated phase relative permeability based on saturations. This methodology, however, is questionable because the fluid configuration and distribution together with grid wettability are not necessarily identical to those

conditions by which the pore-scale modeling was accomplished. As a result, this option cannot represent the physical behavior of fluid flow in porous media.

Alternatively, one may consider coupling dynamic pore-scale relative permeability with a reservoir simulator. This methodology referred to self-consistent three-phase modeling [111] represents the physical behavior of fluid displacement accurately as relative permeability is evaluated from pore-scale events. Initially, the network model computes relative permeability based on a fluid configuration within each grid-block; the saturation distribution, then, is re-evaluated using a conventional simulator. The saturation path is checked against the initial input values in the pore-network model. If the saturation paths are not identical, the overall pattern is recomputed until a user-defined tolerance is reached. This multi-scale and multi-physics modeling approach is promising and results in a more detailed representation of fluid flow at several spatial scales.

Chapter 3

EXPERIMENTAL METHODOLOGY

The final aspiration of this thesis is to prove that micro-CT method for estimating petrophysical properties of rock samples is a potential candidate to complement common laboratory methods due to its additional ability of providing a three-dimensional pore network.

Six sandstone outcrop samples were chosen for this study as shown in Figure 3-1 in order to cover different lithology types. In addition, six carbonate samples obtained from Middle East reservoir were chosen for this study as shown in Figure 3-2. The samples range from 2-3 inches length and 1-1.5 inches diameter. Sandstones were obtained from cylindrical rock cores, 15 to 20 cm in height.



Figure 3-1: Sandstone samples used for this study



Figure 3-2: Reservoir Carbonate Samples used for this study

In the first phase, laboratory measurements of porosity and permeability are performed on the all the core plugs.

After laboratory measurements, whole core sample is scanned using X-ray CT with 1 mm resolution. A sub-plug is extracted for high resolution scanning. X-ray micro-CT is used to

scan the sub-plug at a resolution of 4 μm . At this scale, pore connectivity is revealed from top to bottom. PerGeos software is used to visualize, analyze and process the 3D images. The connected porosity of the segmented pores is then estimated.

In the third phase, the Lattice-Boltzmann method (LBM) is used to simulate fluid flow and to estimate permeability. The results obtained from numerical simulations will be compared with laboratory measurements for validation.

3.1 Porosity and Permeability measurements

Before performing any laboratory measurements, it is necessary to make sure that the samples are clean and dry. Dry weight and dimensions of the samples are measured. Then the samples are wrapped by Teflon tape. At this stage, porosity and permeability measurements can be performed.

Gas Porosimeter is used to measure porosity of core plugs, which is common equipment used for measuring pore and grain volume of core plugs. Injection fluid in this device is helium gas, which has several advantages over other gases. It is nonreactive gas, which will not cause any chemical alteration of the rock. In addition, helium behaves like ideal gases at test conditions. Moreover, it has small molecules and high diffusivity, which allow penetrating small pores and measure porosity of low permeable rocks. Before any

measurements, the equipment should be calibrated in order to accurately measure porosity. After calibration, the porosity of core plugs is measured at 500 psi confining pressure.

For permeability determination, a steady state Gas Permeameter is used. It is commonly applied apparatus in the laboratory. Gas Permeameter is a simple and practical method for determining permeability. It is a displacement equipment, which uses a non-reactive fluid, helium, to flood through core-plug samples and monitor pressure drop across the sample. Permeability is then calculated from modified Darcy equation. The resulted permeability is gas permeability, which is different from true permeability. This is due to slippage effect and it should be corrected. The true liquid permeability is estimated from straight line intercept on a plot of determined gas permeability versus reciprocal mean pressure, which is an arithmetic average of inlet and outlet pressure.

The automated porosimeter and permeameter shown in Figure 3-3, was used to measure the porosity and permeability of core plugs (1" or 1.5" diameter) under different pressures. The pressures available range from 500 psi to 9950 psi.

3.1.1 Procedure

- Input the basic measurements of the cores. Mainly weight, length and diameter. The software will calculate the bulk volume of the sample.

- Place the core sample in the core holder. This is done by extending the arm of the holder from the top and then opening the holder from the bottom. The samples must be dry and wrapped by Teflon tape. Once the sample is placed, the core holder is tightened from both ends.
- The equipment will run and measure the porosity/permeability values all by itself at multiple conditions.
- Once the experiment is completed, save the data, release the confining pressure and take out the samples.

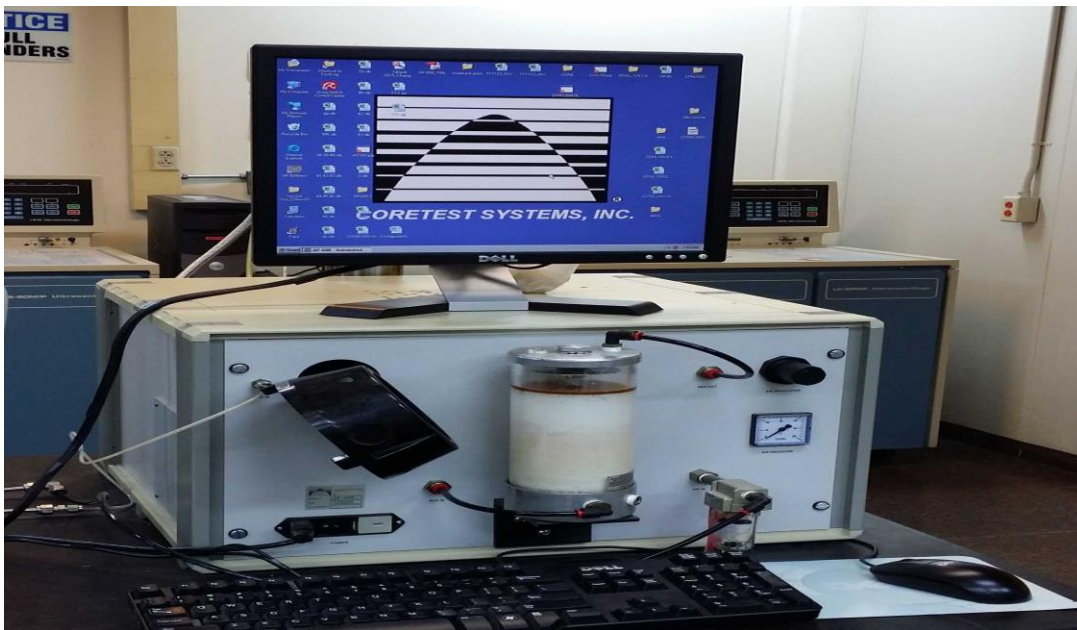


Figure 3-3: Automated Porosimeter Permeameter

3.2 X-ray Diffraction

XRD analysis was conducted to determine the crystalline constitution of core samples that reveal structural information. XRD evaluates the mineral composition present in the samples to determine the quantitative mineralogy of samples. Figure 3-4 shows the X-Ray diffraction system used to give qualitative and quantitative information of the samples.



Figure 3-4: X-Ray diffractometer

3.2.1 CT Imaging

The medical CT system is incapable of directly imaging the majority of the pore space found within porous samples, but can be used to show several important characteristics of an imaged sample. The medical CT has a large advantage over the micro-CT system with the overall size of the recorded volume capable of imaging complete cores up to 3” in diameter and large lengths. It is also possible to record individual image slices in places of interest in under a minute. These scans can be used in core-scale imaging techniques, or used to identify regions of interest for high-resolution imaging with extracted sample plugs. The Toshiba Alexion TSX-032A medical X-ray CT scanner (resolution > 1mm) is a multi-slice CT system with advanced 3D and post processing applications. Figure 3-5 was used to scan the core samples for the qualification of sample homogeneity. Voxel Calc. software was used to process the digital images.



Figure 3-5: Toshiba Alexion TSX-032A medical X-ray CT scanner

3.3 Micro-CT Imaging

The micro-CT system has the large advantage of being able to capture high-resolution images. This allows for the direct imaging of pore bodies and throats in larger pore system such as reservoir samples. The collection of these tomograms comes at the cost of extended collection times of over several hours and smaller total volumes compared to the medical system. The Zeiss VersaXRM-500 X-ray micro-CT scanner Figure 3-6 (resolution >

0.7 μ m) is a 3D X-ray microscopy equipment optimized for non-destructive tomography. The software used for image processing is PerGeos (FEI-ThermoFisher). It utilizes advanced artifact removal techniques, as well as filtering and analytical algorithms to render the images obtained from the micro- CT more meaningful. It has great visualization power for 2D and 3D images that makes the segmentation process easier and reliable. It was used to produce high-resolution images of the cutted rock samples for low permeable rocks. The HeliScan Figure 3-7 (resolution > 0.8 μ m) employs a helical scan trajectory and a patented iterative reconstruction algorithm to generate high resolution images of uniform intensity throughout the length of the sample. This is an equipment of choice for scanning tall samples without the need for stitching. It also has a provision for mounting and operating an in-situ cell for flow studies at reservoir conditions. It is designed to enable fast, artifact-free imaging of the samples.



Figure 3-6: Zeiss VersaXRM-500 X-ray micro-CT scanner



Figure 3-7: HeliScan micro CT

3.4 QEMSCAN

The QEMSCAN (Quantitative Evaluation of Minerals using Scanning Electron Microscopy) provides an automated, non-destructive quantitative SEM analysis of mineralogy and petrography. It can be used for advanced texture analysis (grain morphology). The QEMSCAN heavily depends on the Backscattered Electron (BSE) and Energy Dispersive (EDS) X-ray data to automate image analysis. The system uses a

combination of database and elemental chemistry at each point to identify the minerals. It also produces digital images at each point. The system is mainly operator independent, time efficient, generates reproducible and statistically valid results. The QEMSCAN uses Energy Dispersive X-Ray Spectroscopy (EDS) to produce 2D elemental maps of thin-sections, core chips or drill cuttings. The 2D SEMEDS elemental maps are post-treated using a dedicated Spectral Analysis Engine (SAE) developed by FEI allowing the automatic 2D quantification of mineralogy through the deconvolution of the mixed X-ray spectra of each analyzed pixel using up to three reference mineral spectra. The system works by mineralogical imaging a polished section through the sample so that mineralogical textures are preserved. For particulate samples, populations of particles can be classified based on their mineralogy and texture. Therefore, this method is particularly well suited to the analysis of samples where a wide range of particle types are present and which may exhibit a range of mineralogical, chemical and textural styles. This analysis was conducted on two samples Bandera Brown and sample 9135-5. Figure 3-8 shows the QEMSCAN used in this study. Figure 3-9 shows the steps used to generate 2D QEMSCAN maps. Figure 3-10 shows an example of a generated QEMSCAN map.



Figure 3-8: QEMSCAN - FEI 650F

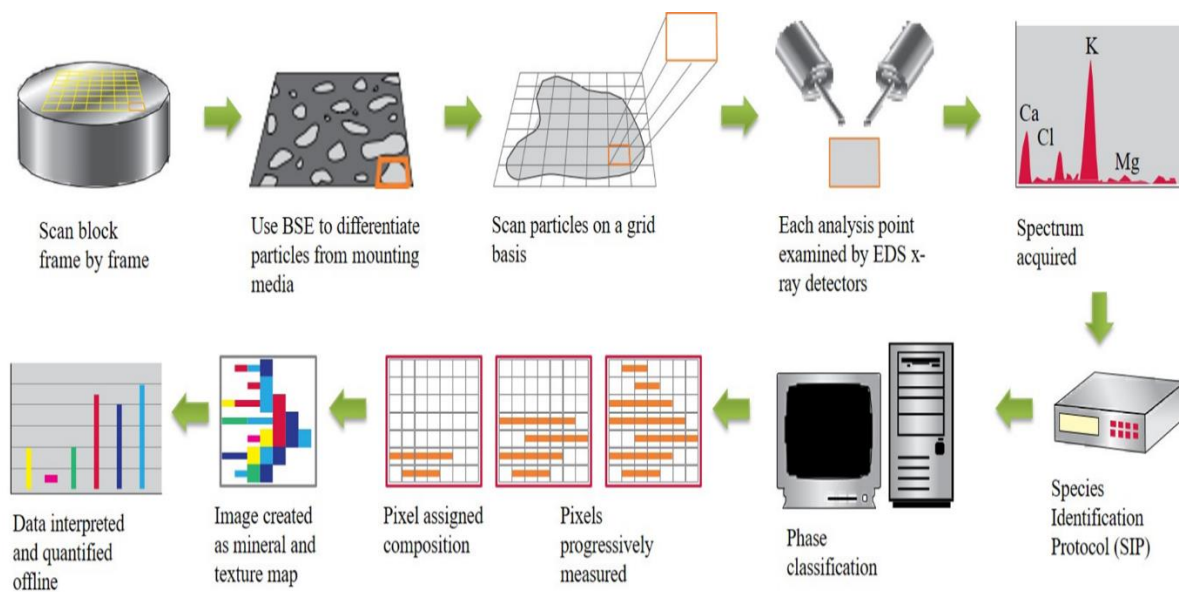


Figure 3-9: Steps in generating 2D QEMSCAN maps

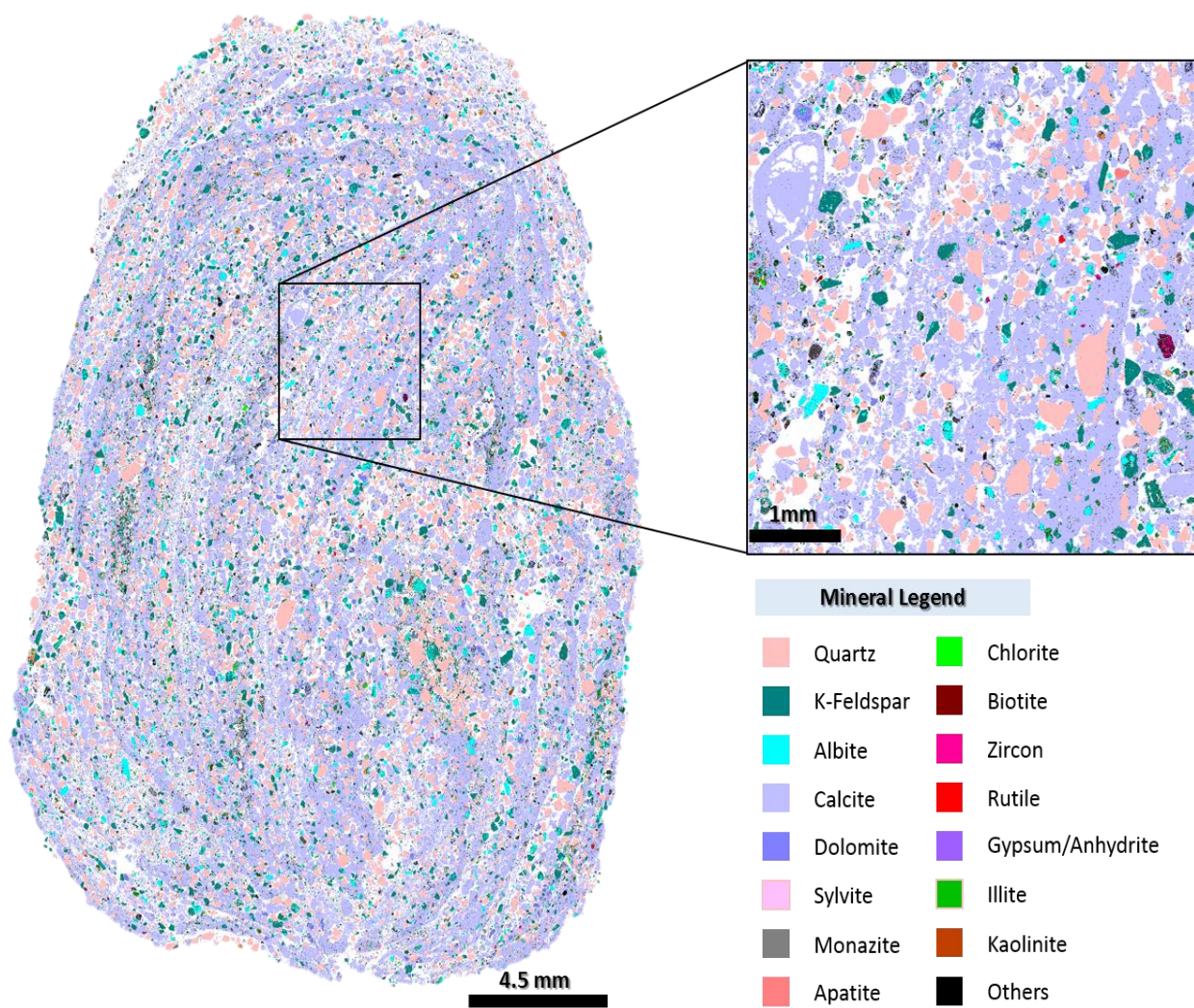


Figure 3-10: A generated QEMSCAN map

3.5 Permeability Simulations

Absolute permeability is a dynamic property. Hence, absolute permeability is calculated by simulating fluid flow through the connected pore network of 3D segmented rock model. The 3D pore topologies of carbonates are complex and directly solving physical equations in these topologies is very difficult. Therefore, Lattice Boltzmann Method (LBM) is used. LBM is an alternative approach for the conventional computational CFD method. This method mimics fluid flow system by interaction of small particles, which collide and stream when there is a pressure gradient. LBM can accurately simulate fluid flow in porous media [114]. The permeability is calculated when fluid flow simulation reaches steady state. It is derived from Darcy equation:

$$k = \frac{L Q \mu}{A \Delta P} \quad (3.1)$$

Where k is absolute permeability, L is length of the sample in direction of the flow, Q is flow rate, μ is fluid viscosity, A is cross sectional area and ΔP is applied pressure gradient.

Simulating fluid flow of whole sub-plug images requires high memory and takes longer simulation time, whereas taking smaller blocks from whole core images shows quick simulation run with less computational resources. The permeability of a 3D image is computed, the size of the sub-region is set as 600 x 600 x 600. The selected blocks are big enough to represent whole sample.

Chapter 4

RESULTS AND DISCUSSION

4.1 Porosity and Permeability measurements

The porosity and permeability of the core plugs were measured at 500 psi confining pressure using the AP-608 automated porosimeter and permeameter. Figure 4-1 shows the description and dimensions of core plugs used in this study. Results show that the sandstone core plugs porosity values are ranging from 11-22% with permeability values ranging from 0.28 mD up to 210.07 mD. Colton sandstone sample shows the lowest permeability and porosity among all sandstone sample whereas Bandera Grey show the highest permeable sample. The carbonates generally showed low permeability values ranging from 0.11 mD to 2.83 mD while the porosity values range from 7-14%. Figure 4-2 summarizes results of porosity and permeability of the core-plugs at 500 psi confining pressure.

Table 4-1: Dimensions of core plugs used in this study

Rock Type	Sample ID	Weight (gm)	Average Length (cm)	Average Diameter (cm)
Sandstone	Berea Puff	157.38	6.73	3.79
Sandstone	Crab Orchid	187.82	7.06	3.79
Sandstone	Bandera Grey	177.43	7.48	3.79
Sandstone	Bandera Brown	188.60	7.62	3.81
Sandstone	Colton	195.91	7.39	3.78
Sandstone	Berea Grey	80.15	7.31	2.56
Carbonate	9137-1	77.39	6.75	2.53
Carbonate	9058-3	88.45	7.15	2.54
Carbonate	9134-4	103.00	8.44	2.53
Carbonate	9135-5	97.45	8.45	2.53
Carbonate	9137-7	80.33	7.04	2.53
Carbonate	9136-8	57.21	4.82	2.52

Table 4-2: Measured porosity and permeability of core plugs at 500 psi confining pressure

Rock Type	Sample ID	Porosity (%)	Permeability (mD)
Sandstone	Berea Puff	22.04	182.87
Sandstone	Crab Orchid	10.94	13.51
Sandstone	Bandera Grey	20.23	210.07
Sandstone	Bandera Brown	18.42	5.03
Sandstone	Colton	11.34	0.28
Sandstone	Berea Grey	18.15	141.71
Carbonate	9137-1	13.25	0.73
Carbonate	9058-3	7.23	0.68
Carbonate	9134-4	9.04	0.11
Carbonate	9135-5	13.68	2.83
Carbonate	9137-7	14.23	0.80
Carbonate	9136-8	10.41	0.32

Figure 4-1 shows the porosity-permeability relation obtained for our core samples as compared to literature data for validation purposes. For the carbonate samples, the results show a similar behavior as the literature data and fall within the same range. For sandstone, however, the results show a different trend and does not fall within the same range. This can be attributed to the different mineralogy, particle size, and porosity distribution.

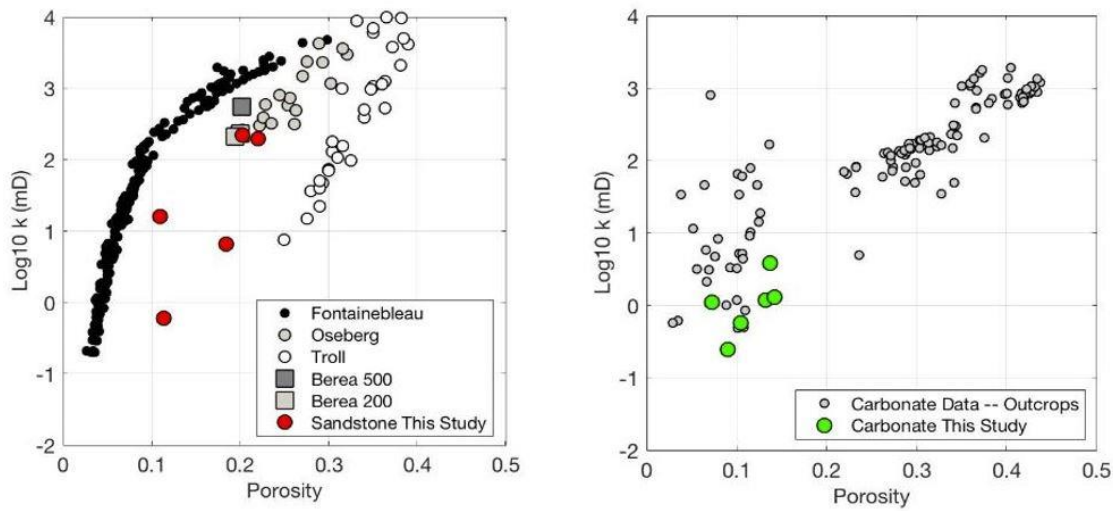


Figure 4-1: Measured porosity and permeability of the samples under examination. Left: compared with other sandstone datasets. Right: carbonate samples compared to outcrop carbonate data

4.2 X-Ray Diffraction

4.2.1 Sandstone Samples Mineralogy

Table 4-3 illustrates the mineral compositions of the different sandstone samples. Figure 4-2 to Figure 4-7 show the 2θ peaks for these samples along with the legends showing each mineral percentages forming the rock sample. Sandstone generally consists of high percentage of quartz and other minerals such as clay, whereas carbonate is generally formed by calcite and dolomite.

Colton sandstone shows the lowest quartz percentage among all other sandstone samples, however, the other sandstone samples showed minimum of 88.2% of quartz forming its lithology. Carb Orchid sample has the highest quartz percentage 98.1% and 1.9% of microcline; it could be considered as clean quartz sample due the high percentage of quartz. Microcline exists in all samples except Colton and Berea Buff. Albite exists in all samples except Berea Grey and Carb Orchid. Bandera Brown and Colton showed the highest percentage of clay minerals since the former has 9.4 % (combination of kaolinite and albite) and the latter showed 16.5% (combination of kaolinite and albite).

Table 4-3: Mineral composition of sandstone samples

Sample ID	Berea Puff	Carb Orchid	Bandera Grey	Bandera Brown	Colton	Berea Grey
Quartz [%]	94.5	98.1	89.1	88.2	55.4	91.8
Calcite [%]	-	-	-	-	11.4	-
Dolomite [%]	-	-	1.3	-	8.4	1.5
Muscovite [%]	3.2	-	-	-	3.8	2.2
Kaolinite [%]	-	-	2.5	1.7	4.1	-
Orthoclase [%]	-	-	-	-	4.6	-
Albite [%]	2.3	-	2.8	7.7	12.4	-
Microcline [%]	-	1.9	4.3	2.4	-	4.5

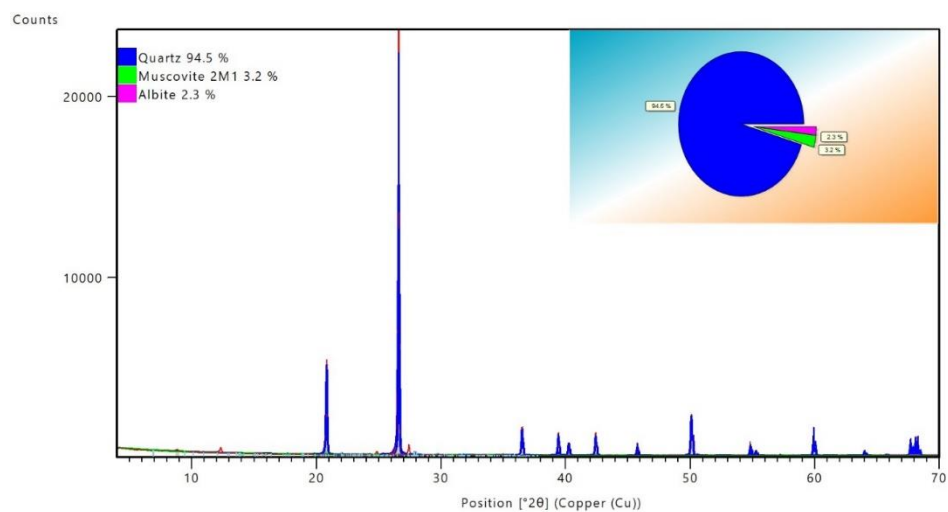


Figure 4-2: Mineral composition of Berea Puff

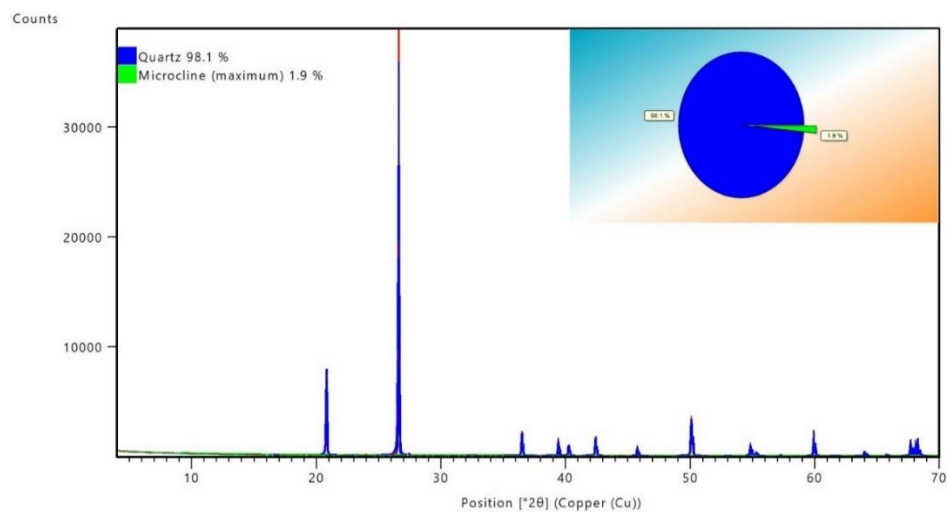


Figure 4-3: Mineral composition of Crab Orchid

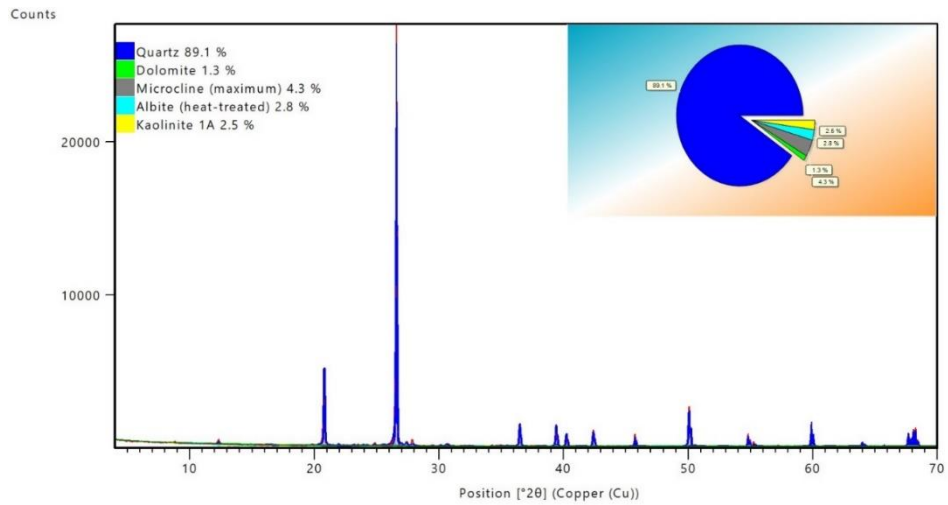


Figure 4-4: Mineral composition of Bandera Grey

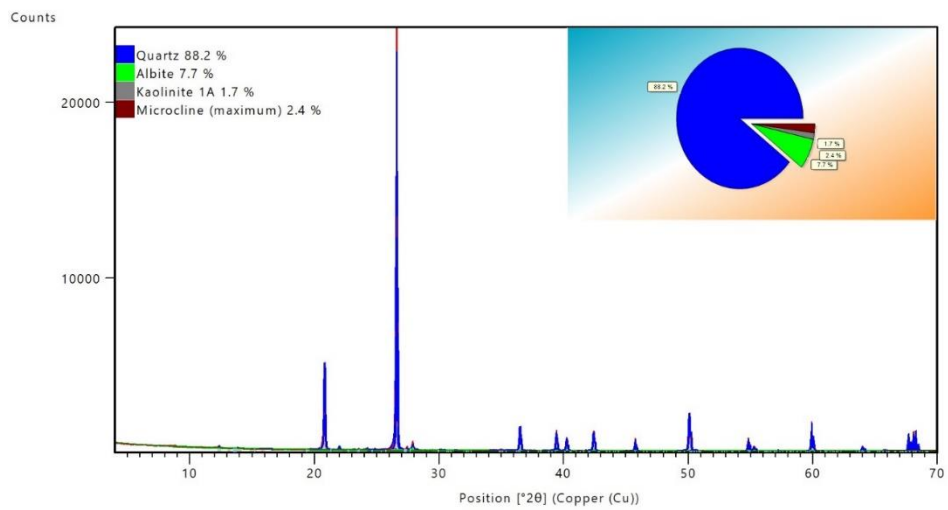


Figure 4-5: Mineral composition of Bandera Brown

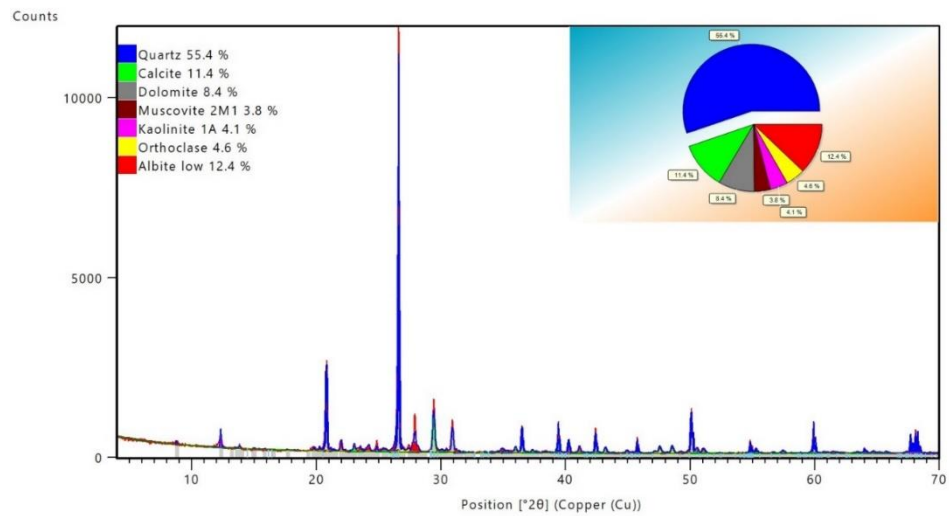


Figure 4-6: Mineral composition of Colton

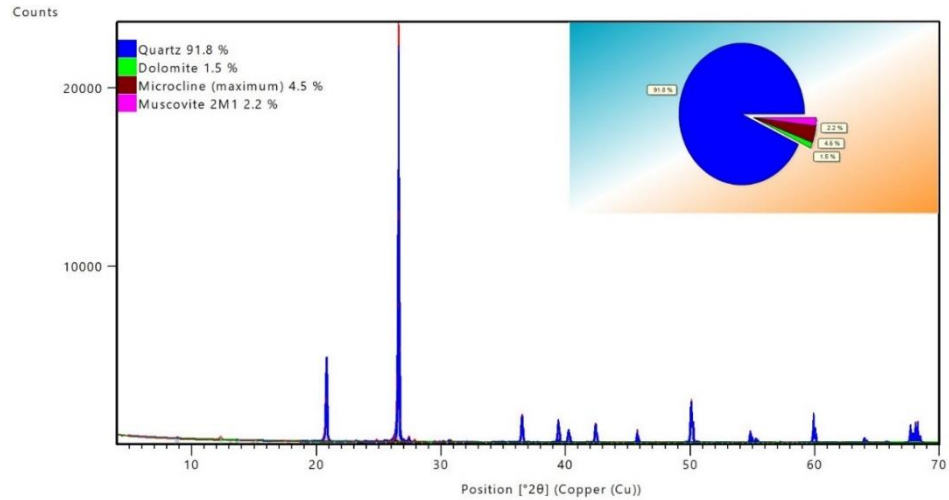


Figure 4-7: Mineral composition of Berea Grey

4.2.2 Carbonate Samples Mineralogy

Table 4-4 illustrates the mineral compositions of the different carbonate samples. Figure 4-8 to Figure 4-13 show the 2θ peaks for these samples along with the legends showing each mineral percentages forming the rock sample.

Sample 9058-3 consists of 100% calcite, which is an implication of the homogeneity of the sample. Sample 9134-4 has the lowest percentage of calcite 76%, dolomite 14%, quartz 2%, and pyrrhotite 8%; however, it has the highest percentage of dolomite among the other entire samples. The existence of dolomite is also observed in sample 9135-5 and sample 9136-8 showing 10% and 6% of dolomite respectively. Quartz also appears in low percentage in samples 9137-1, 9134-4, and 9137-7. Carbonate samples consists of lower number of minerals as compared to sandstone samples. However, carbonate samples might complicate the analysis due to the different pore system appearing in its body. XRD results supported out objective to study wide range of lithology types and mineral composition in order to end up with the full picture from this study.

Table 4-4: Mineral composition of carbonate samples

Sample ID	9137-1	9058-3	9134-4	9135-5	9137-7	9136-8
Calcite [%]	97	100	76	90	98	94
Dolomite [%]	-	-	14	10	-	6
Quartz [%]	3	-	2	-	2	-
Pyrrhotite [%]	-	-	8	-	-	-

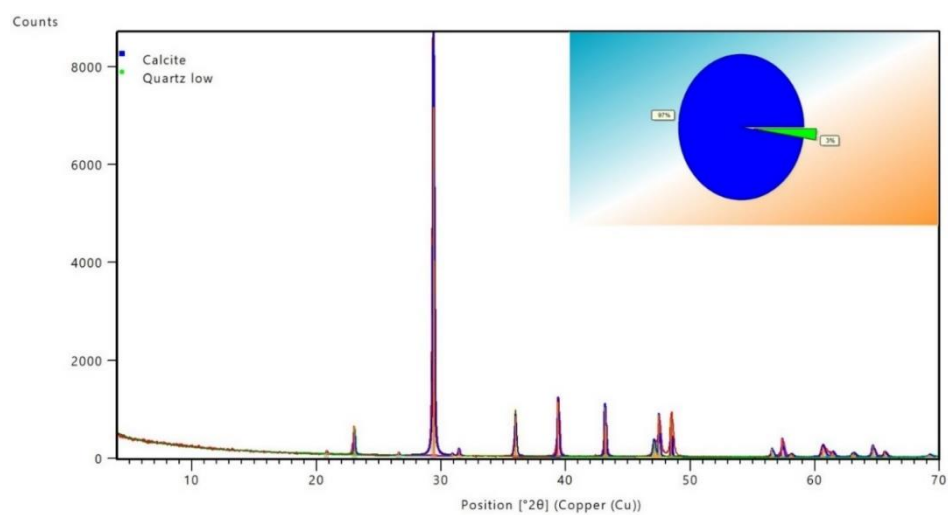


Figure 4-8: Mineral composition of 9137-1

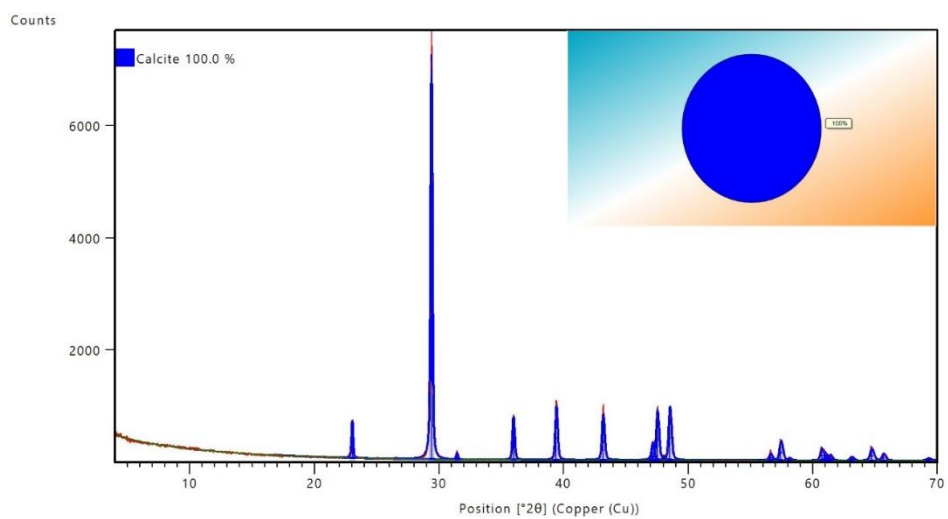


Figure 4-9: Mineral composition of 9058-3

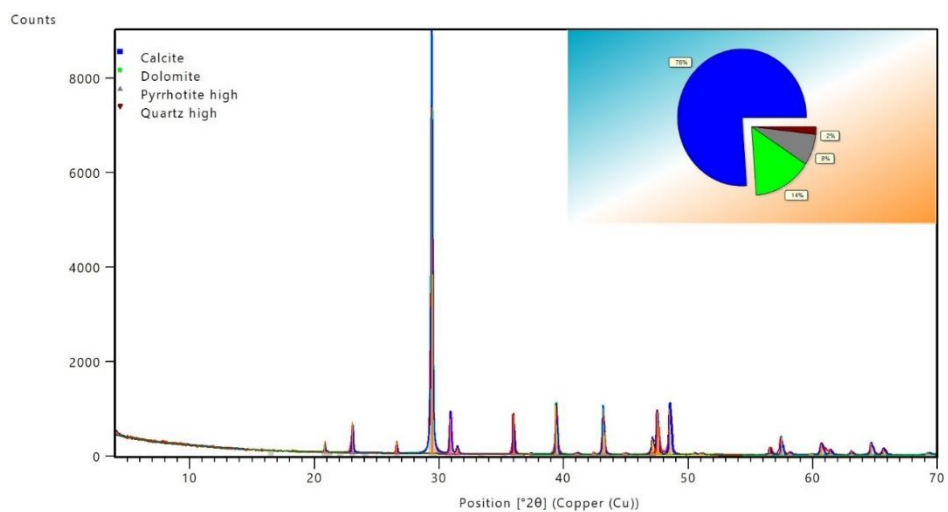


Figure 4-10: Mineral composition of 9134-4

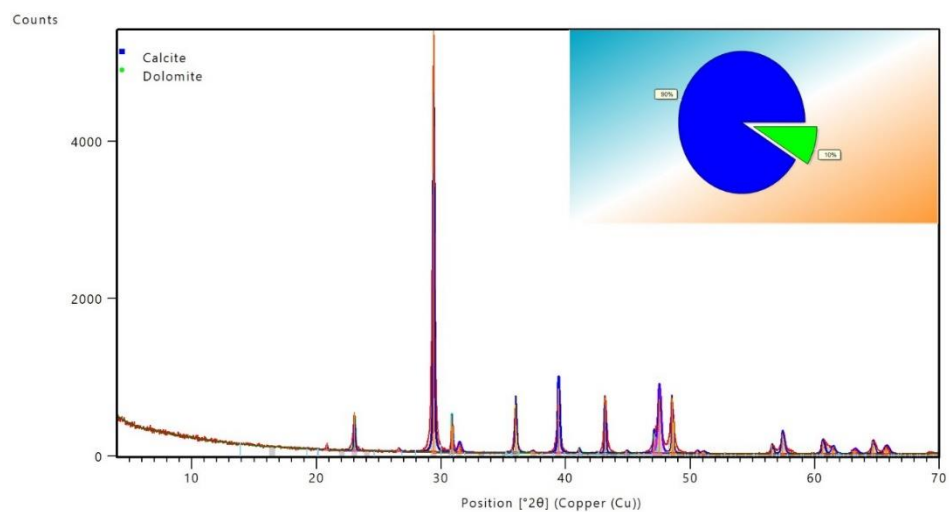


Figure 4-11: Mineral composition of 9135-5

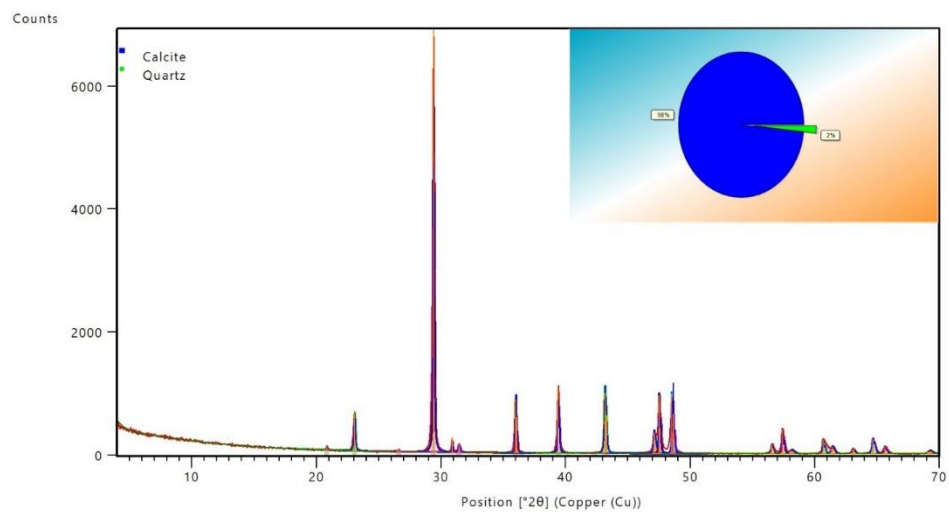


Figure 4-12: Mineral composition of 9137-7

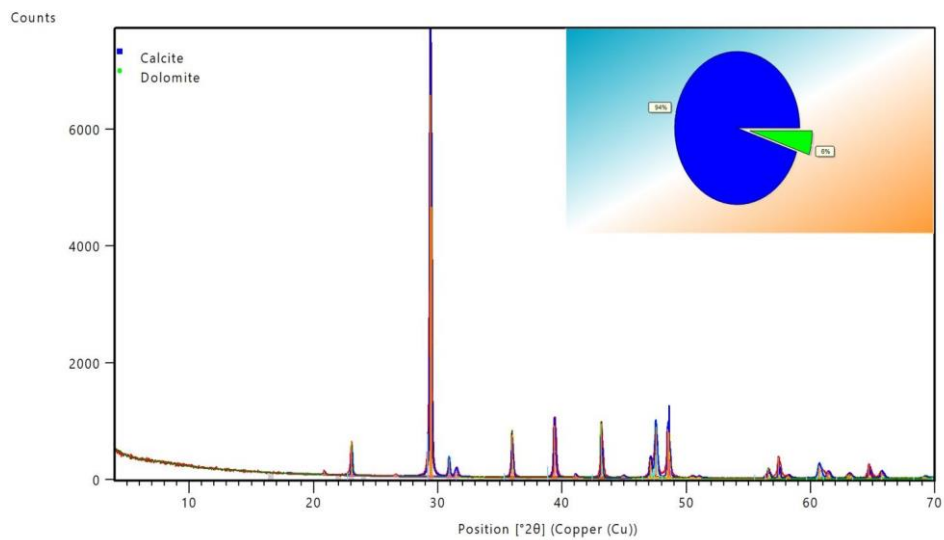


Figure 4-13: Mineral composition of 9136-8

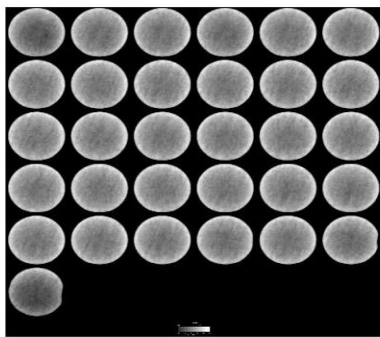
4.3 CT Imaging

CT imaging was conducted on all the samples to study the homogeneity in order to help in the selection of the position of the chip that will be studied using Micro-CT imaging. The resolution of the images was (>1 mm) and Voxel Calc. software was used to process the digital images

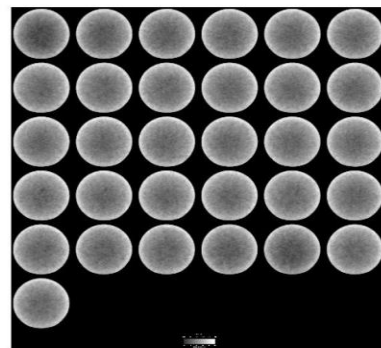
4.3.1 Sandstone Samples

Figure 4-14 shows the CT images for sandstone samples. All the sandstone samples showed high homogeneity. Berea Puff and Crab Orchid samples showed a very

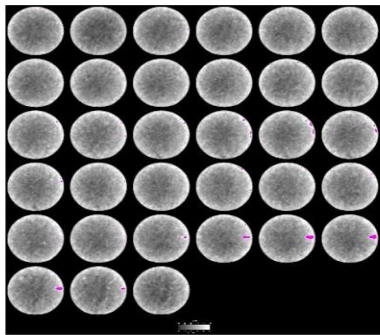
homogeneous structure. Bandera Grey and Bandera Brown showed regions of white colour, which confirms high percentage of dense minerals that is proved by XRD, which showed the existence of high percentage of clay minerals. Berea Grey is considered as laminated homogeneous sample, which means variation exists in the radial axis of the sample but not along the vertical length of the sample. By interpreting the previous CT images, it provides a clear understanding where to trim the samples for Micro CT scan.



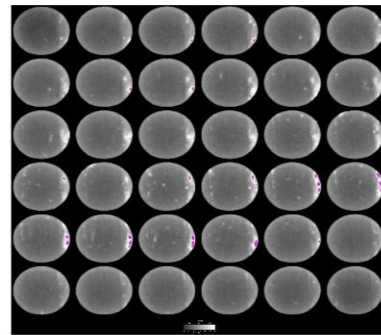
1)



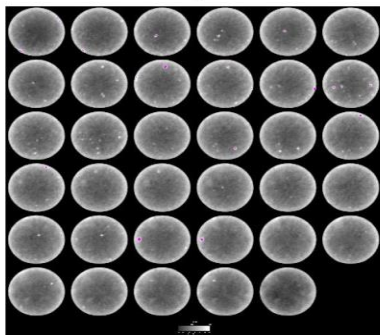
2)



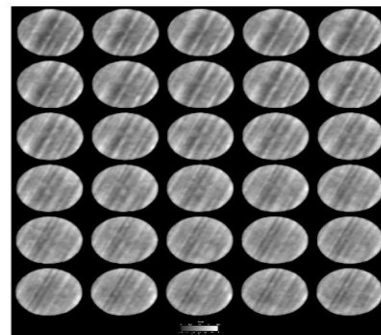
3)



4)



5)



6)

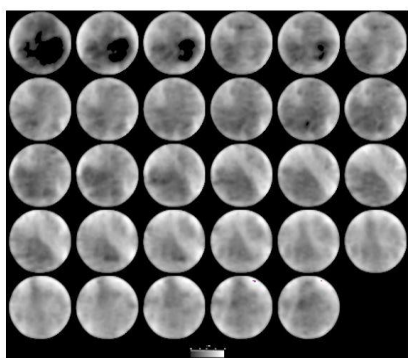


Figure 4-14: CT images for sandstone samples 1) Berea Puff 2) Crab Orchid 3) Bandera Grey 4) Bandera Brown

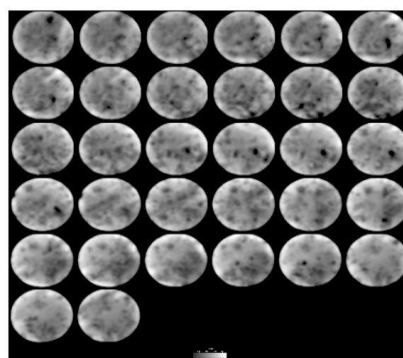
5) Colton 6) Berea Grey

4.3.2 Carbonate Samples

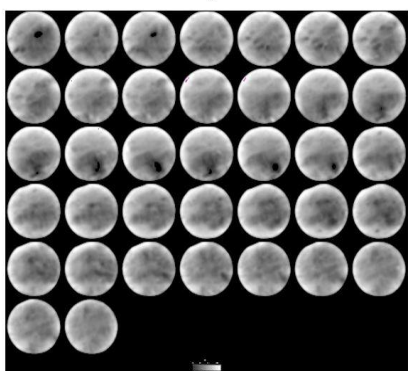
Figure 4-15 shows the CT images for carbonate samples. All the samples showed generally heterogeneity in their structure. Sample 9137-1 has a very low dense mineral from the top end of the sample, which can be shown from the first three slices of the images. It can be inferred from sample 9058-3 that it has dual porosity system (different pore sizes), hence, it was decided to trim from the top and bottom end of the sample for Micro CT scan. Sample 9137-7 showed a laminated layer from the bottom end of the sample. Sample 9136-8 showed the most homogeneous structure among the carbonate samples, however, it is considered as a heterogeneous sample. By interpreting the previous CT images, it provides a clear understanding from where to trim the samples for Micro CT scan.



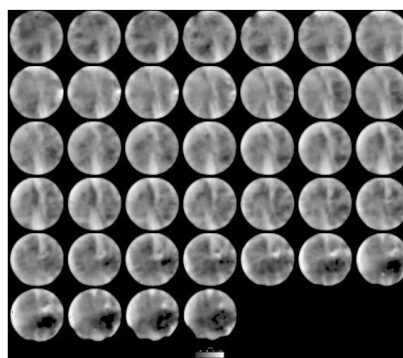
1)



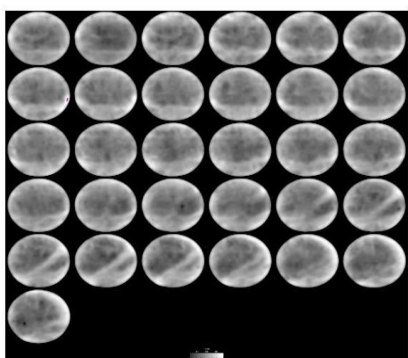
2)



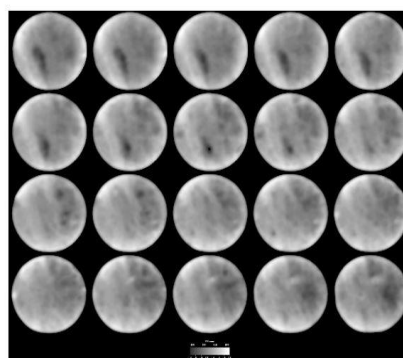
3)



4)



5)



6)

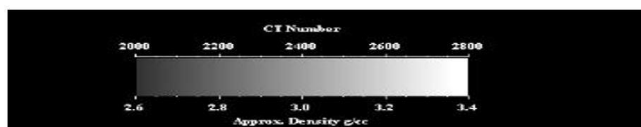


Figure 4-15: CT images for carbonate samples 1) 9137-1 2) 9058-3 3) 9134-4 4) 9135-5 5) 9137-7 6) 9136-8

4.4 Micro-CT Imaging

All sandstone samples and five carbonate samples were scanned using micro-CT and the images were processed using PerGeos software. PerGeos is a digital rock software tool for analyzing, processing, and performing simulations on 2D and 3D images of rock. It consists of built-in functions that help in interpreting digital rock images and quickly and easily obtaining meaningful data.

The image acquisition involves several key steps. First, the X-ray source and detector are brought close to the sample until the sample projection covers the entire detectors field of view. Then, projection of the sample is tested at different rotational angles, to ensure that it will fit inside detection area and will not collide to detector and source during scanning. After that, voltage and current of X-ray source are adjusted with regard to specimen being imaged. Next a calibration image are captured to remove some noises while reconstruction. Furthermore, some other parameters are selected like the rotation step and degree, exposure time, number of images to be acquired and number of averaging frames for one projection image. Once the adjustments are made, the image acquisition is started. After acquiring 2D sample projections, it is assembled into 3D image.

The first step is the pre-processing, the data obtained by micro-CT which includes extracting a sub volume from the rock to be analyzed then applying a non-local means filter

to remove noise from the volume using a non-local means approximation based on adaptive manifold.

The second step is the segmentation, a cubic porosity segmentation recipe that involves marking the pores with threshold by letting the boundary unassigned so that the empty spaces are filled by threshold. Top Hat is applied to enhance pore markers, which can be very light in order to avoid overlapping the high gradient regions. Then by marking the grains with threshold and lastly by adding final Top Hat to enhance the pores, the segmentation process is completed. Figure 4-16 shows the cubic porosity segmentation workflow used for the segmentation process.

The last step is the analysis; to compute the volume fraction and then apply the axis connectivity that generates a binary image containing all path-linking planes.

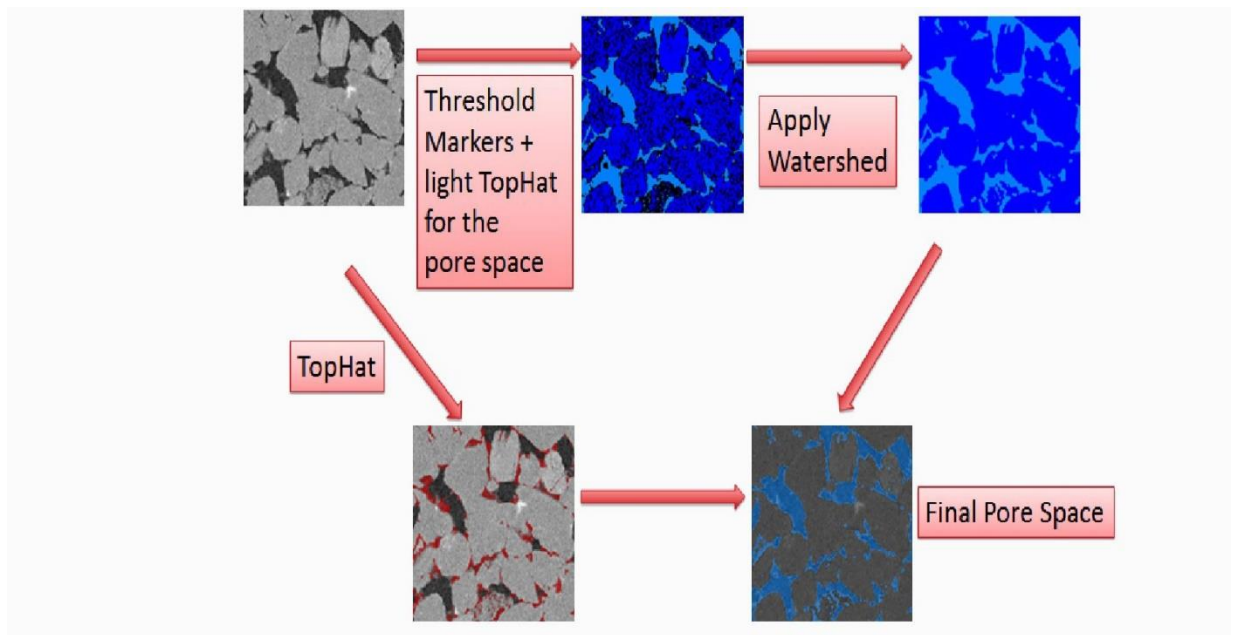


Figure 4-16: The Cubic Porosity Segmentation Workflow

4.4.1 Sandstone micro-CT images

A 1.5-inch length and 0.2 inch thick chip of the Bandera Grey sub-plug was scanned using micro-CT and the resulting 3D images were analyzed using PerGeos software. Figure 4-17 shows the micro CT image of the Bandera Grey sub-plug after scanning at a resolution of 4 microns.

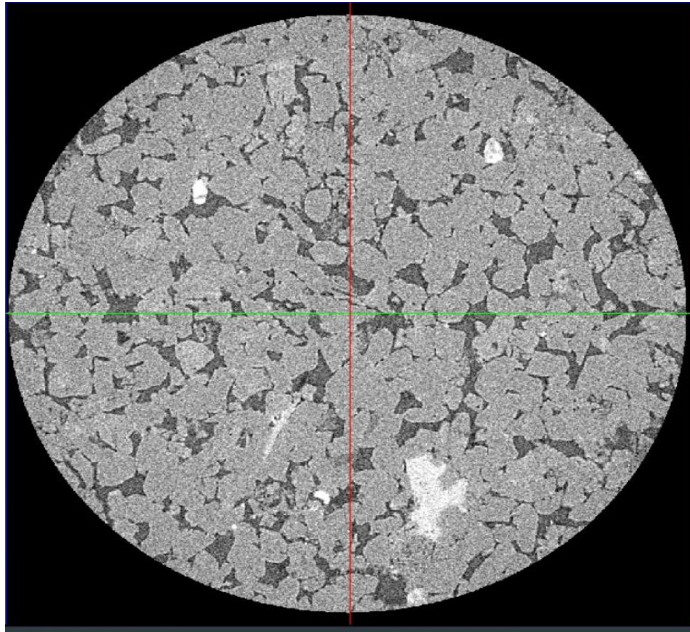


Figure 4-17: Bandera Grey sub-plug image scanned at 4 microns resolution using helical X-ray micro-CT

The scanning yields some artifacts, which will lead to inaccurate prediction of macroscopic properties. Artifacts should be removed before segmentation. For image processing, PerGeos software is used. The image enhancement takes several steps. First, a sub volume is extracted from the original 3D image with $600 \times 600 \times 600$ voxels. After analyzing the images several artifacts are detected. Non-Local means filter reduces noise and preserves edges between grains and pores. Figure 4-18 shows Bandera Grey sub-plug before and after applied filtering technique.

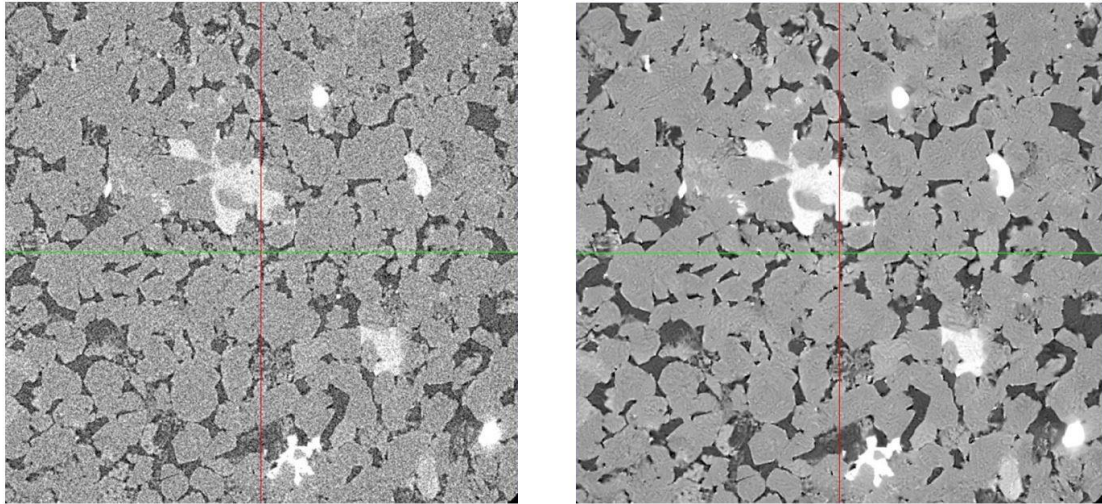


Figure 4-18: Bandera Grey sub-plug before and after applying non-local means filter

Image segmentation is an essential step of the workflow that should be carefully performed. It is a process, where greyscale images are discretized into pore and solid phases. The segmented image can then be used to determine macroscopic properties, porosity and permeability. After enhancing the quality of 3D image and analyzing the images a proper thresholding is set. Cubic porosity segmentation process is used to segment the 3D filtered images. The cubic porosity segmentation recipe involves marking the pores with threshold by letting the boundary unassigned so that the empty spaces are filled by threshold. Top Hat is applied to enhance pore markers, which can be very light in order to avoid overlapping the high gradient regions. Then by marking the grains with threshold and lastly by adding final Top Hat to enhance the pores, the segmentation process is completed. Figure A19 shows the Bandera Grey sample after the segmentation process.

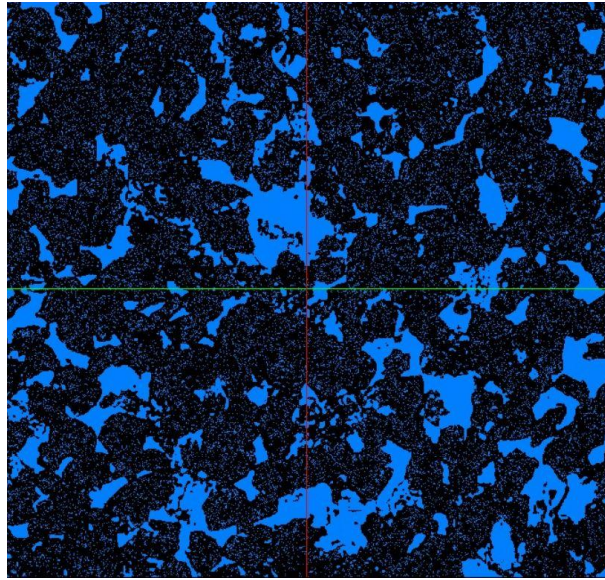


Figure 4-19: Bandera Grey sub-plug after the segmentation process

The last step is the analysis; by computing the volume fraction and then apply the axis connectivity that generates a binary image containing all path-linking planes. It was required to have binary images, since for digital images the porosity was suggested to be defined as the ratio of white or black pixels over the total number of them. Figure 4-20 shows the Bandera Grey sample after applying axis connectivity to estimate the connected porosity.

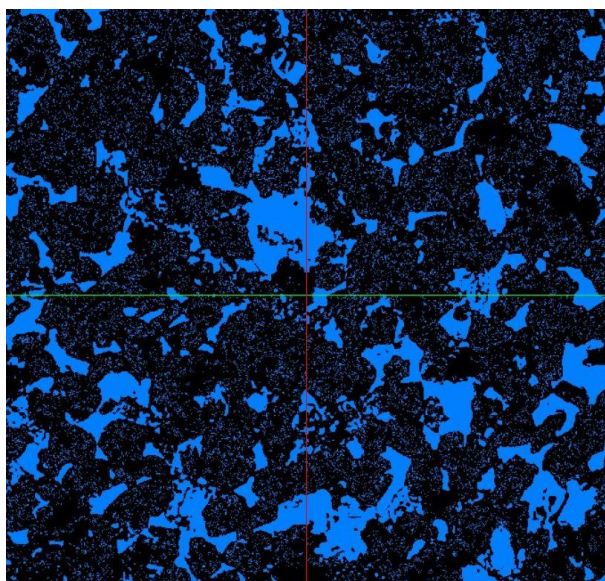


Figure 4-20: Bandera Grey sub-plug after applying axis connectivity

Table 4-6 shows the porosity obtained using lab measurements and PerGeos software after applying axis connectivity for sandstone sub-plugs. Other sandstone samples micro-CT figures can be found in **Error! Reference source not found..**

Table 4-5: Porosity from laboratory measurement compared with the estimated porosity using PerGeos software for sandstones

Sample	Lab Porosity (%)	Estimated Porosity (%)
Berea Puff	22.04	21.16
Crab Orchid	10.94	12.32
Bandera Grey	20.23	20.44
Bandera Brown	18.42	19.36
Colton	11.34	11.05
Berea Grey	18.15	16.90

4.4.2 Carbonate Micro-CT images

A 1.5-inch length and 0.2 inch thick chip of sample 9137-1 was scanned using micro-CT and the resulting 3D images were analyzed using PerGeos software. Figure 4-21 shows the 9137-7 sample after scanning at a resolution of 4 microns.

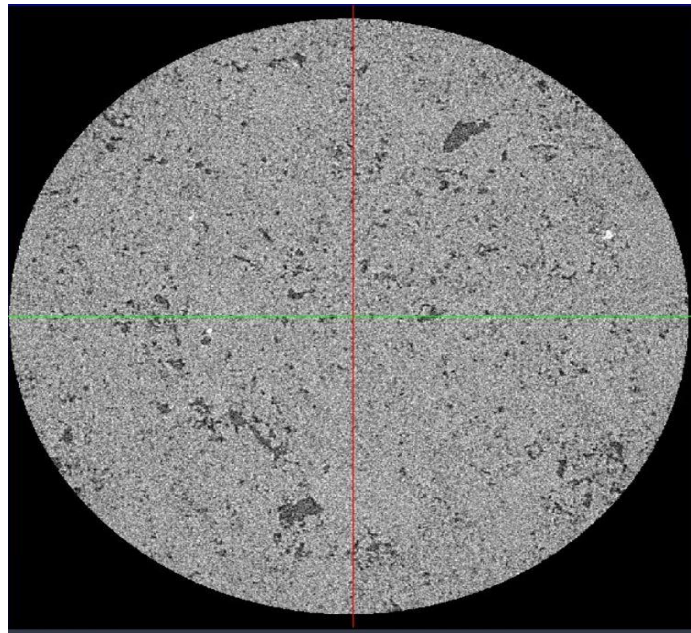


Figure 4-21: 9137-7 sub-plug image scanned at 4 microns resolution using X-ray micro-CT

The scanning yields some artifacts, which will lead to inaccurate prediction of macroscopic properties. Artifacts should be removed before segmentation. For image processing, PerGeos software is used. The image enhancement takes several steps. First, a sub volume is extracted from the original 3D image with 600 x 600 x 600 voxels. Then, by analyzing the images several artifacts were detected. Non-Local means filter reduces noise and

preserves edges between grains and pores. Figure 4-22 shows 9137-7 sub-plug before and after applied filtering technique. At this stage, processed image can be segmented.

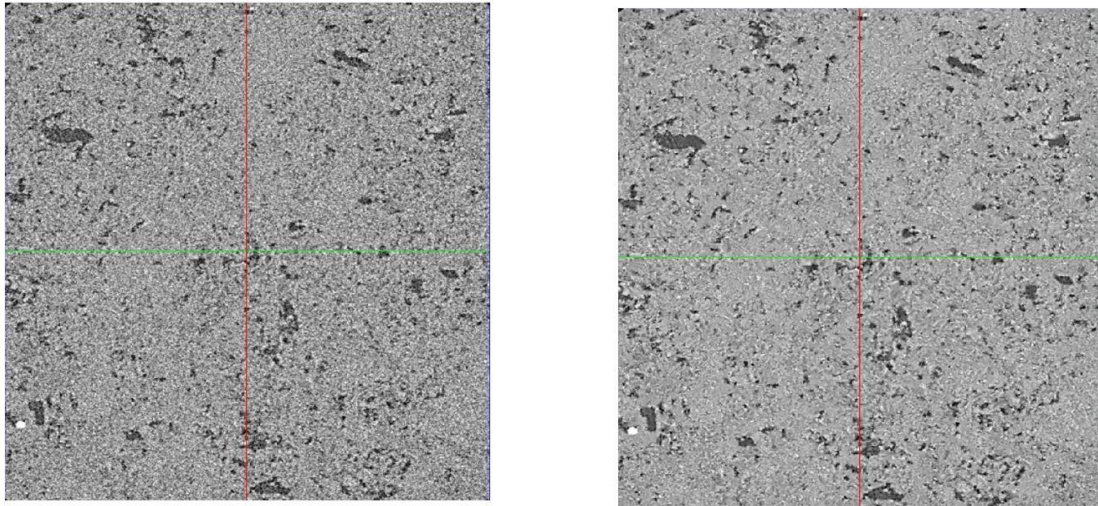


Figure 4-22: 9137-7 sub-plug before and after applying non-local means filter

Image segmentation is an essential step of the workflow that should be carefully performed. It is a process, where greyscale images are discretized into pore and solid phases. The segmented image can then be used to determine macroscopic properties, porosity and permeability. After enhancing the quality of 3D image, and analyzing the images a proper thresholding is set. Cubic porosity segmentation process is used to segment the 3D filtered images. The cubic porosity segmentation recipe involves marking the pores with threshold by letting the boundary unassigned so that the empty spaces are filled by threshold. Top Hat is applied to enhance pore markers, which can be very light in order to avoid overlapping the high gradient regions. Then by marking the grains with threshold and lastly

by adding final Top Hat to enhance the pores, the segmentation process is completed.

Figure 4-23 shows the 9137-7 sub-plug after the segmentation process.

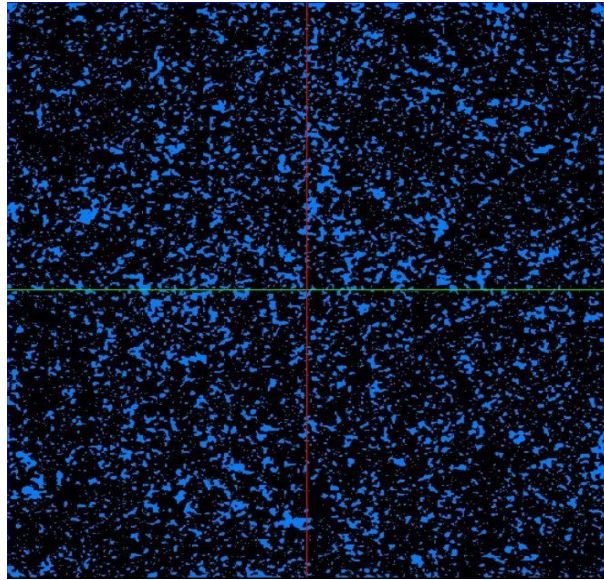


Figure 4-23: 9137-7 sub-plug after the segmentation process

The last step is the analysis; by compute the volume fraction and then apply the axis connectivity that generates a binary image containing all path-linking planes. It was required to have binary images, since for digital images the porosity was suggested to be defined as the ratio of white or black pixels over the total number of them Figure 4-24 shows 9137-7 sub-plug after applying axis connectivity to estimate the connected porosity.

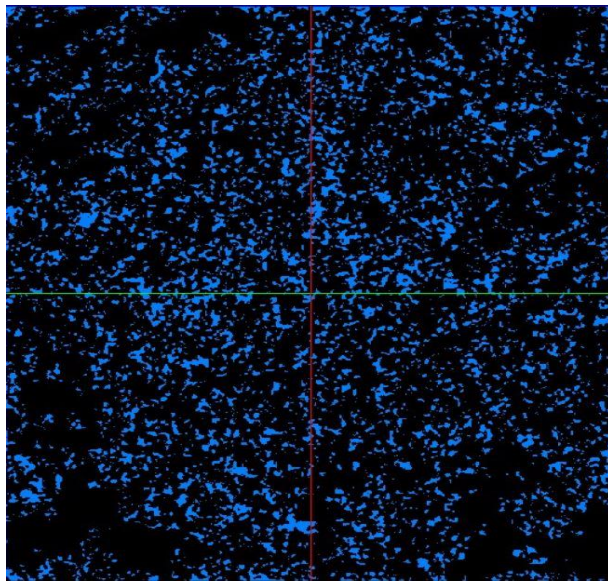


Figure 4-24: 9137-7 sub-plug after applying axis connectivity

Table 4-6 shows the porosity obtained using lab measurements and PerGeos software after applying axis connectivity for carbonate sub-plugs. Other carbonate sample micro-CT figures can be found in **Error! Reference source not found..**

Table 4-6: Porosity from laboratory measurement compared with the estimated porosity using PerGeos software for carbonates

Sample	Lab Porosity (%)	Estimated Porosity (%)
9137-1	13.25	10.35
9058-3	7.23	6.35
9135-5	13.68	12.46
9137-7	14.23	14.02
9136-8	10.41	9.27

4.5 QEMSCAN

Figure 4-25 and Figure 4-26 shows 2D QEMSCAN maps illustrating mineral identification, distribution on a polished embedded section within the miniplugs of two samples namely Bandera Brown and 9135-5 respectively. Table 4-7 shows the results obtained from QEMSCAN for the two samples. Result for Bandera Brown has a high percentage of Quartz, in addition, it contains Albite and Illite and Biotite with the same percentage 3%. 21% of the scanned sample has zero density which represents the void space. Cross validating QEMSCAN and XRD results show a good agreement. Sample 9135-5 has only Calcite and Dolomite which also agrees with XRD result as it also has the same minerals with comparable percentages.

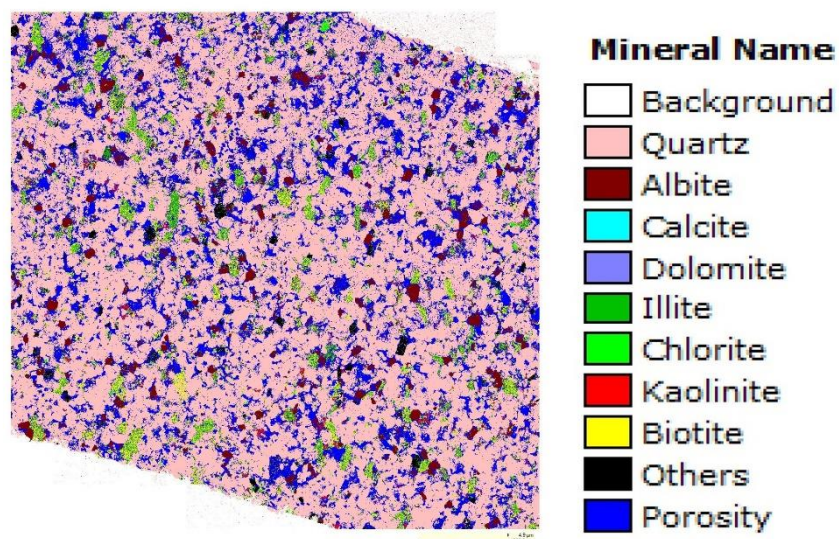


Figure 4-25: 2D QEMSCAN map for Bandera Brown sample

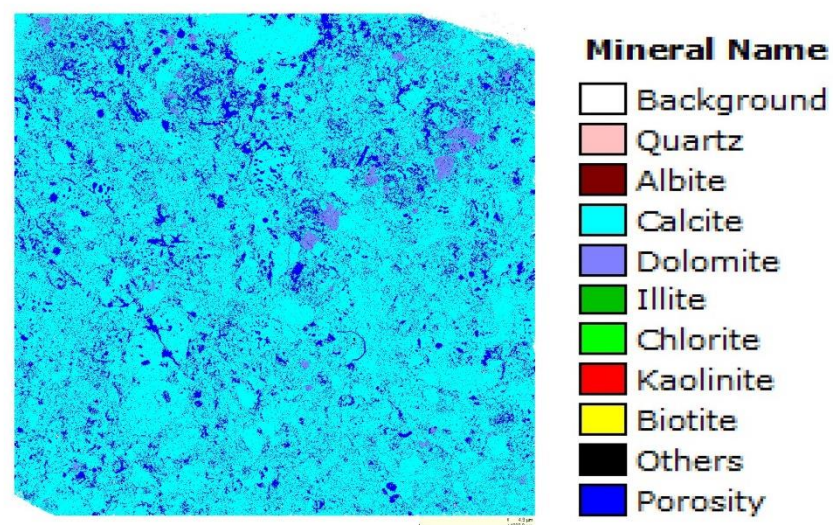


Figure 4-26: 2D QEMSCAN map for sample 9135-5

Table 4-7: QEMSCAN results

Sample	Bandera Brown	9135-5
Quartz	65	0
Albite	3	0
Calcite	0	80
Dolomite	0	1
Illite	3	0
Chlorite	1	0
Kaolinite	1	0
Biotite	3	0
Others	2	0
Porosity	21	19

4.6 Permeability Simulations

Numerical flow simulations were then completed using the standard lattice-Boltzmann method (LBM). Prior to running the flow simulation, the final segmented images were resampled to a uniform voxel resolution; the size of the sub-region is set as 600 x 600 x 600 for input as simulation geometry. The results from the fluid flow simulation single-phase permeability show a good agreement with the permeability obtained using helium-gas permeameter as shown in Table 4-8 for sandstones and Table 4-9 for carbonate.

Table 4-8: Permeability from laboratory measurement compared with the estimated porosity using LBM simulations for sandstones

Sample	Lab Permeability (mD)	Estimated Permeability (mD)
Berea Puff	182.87	507.74
Crab Orchid	13.51	24.79
Bandera Grey	210.07	250.44
Bandera Brown	5.03	6.76
Colton	0.28	0.11
Berea Grey	141.71	151.16

Table 4-9: Permeability from laboratory measurement compared with the estimated porosity using LBM simulations for carbonates

Sample	Lab Permeability (mD)	Estimated Permeability (mD)
9137-1	0.73	2.35
9058-3	0.68	1.69
9135-5	2.83	2.61
9137-7	0.80	5.84
9136-8	0.32	1.58

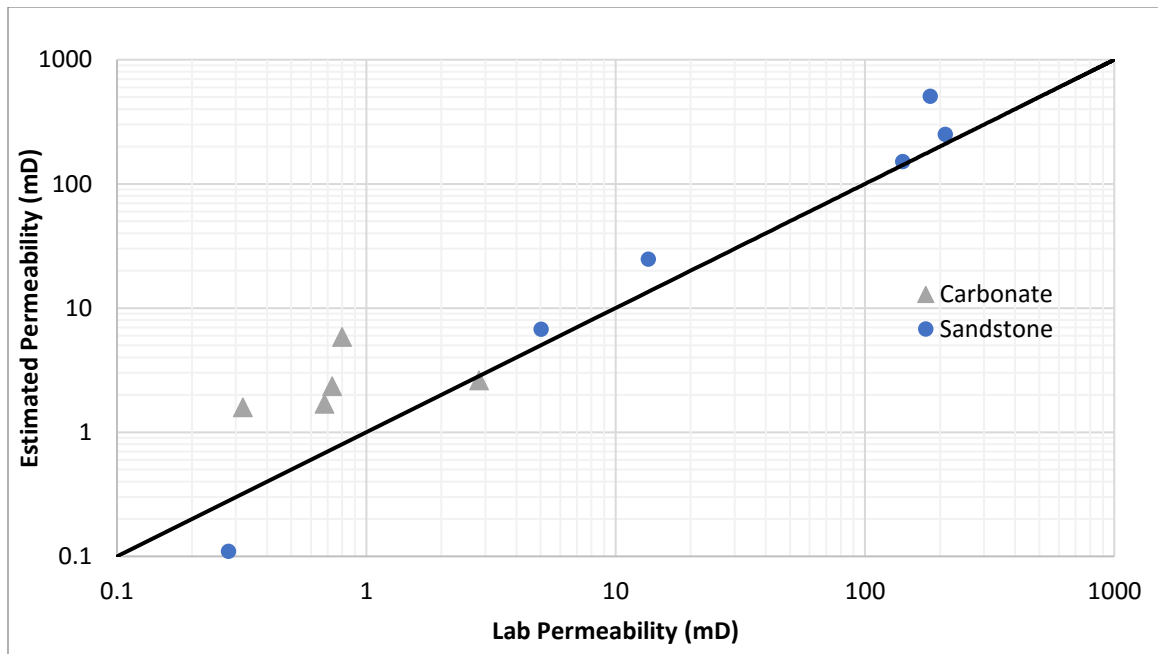


Figure 4-27: Calculated permeability vs lab permeability for all samples used in this study

Figure 4-27 shows a log-log plot of the estimated and lab permeability for all the samples used in this study. For the sandstones, the samples are mostly homogeneous which made it easier in selecting right areas to trim the core sample for micro CT scan. Results for the sandstone samples show a good agreement between the estimated and lab permeability.

For the carbonates, due to the heterogeneity of the samples it was difficult to select the sub-plug for scanning using micro CT. The difference between the estimated permeability and the measured one is mostly because the selected digital rock is not completely representative of the host relatively-larger sample used in the measurement. The measured

lab permeability of the samples are very low as compared to the estimated values from simulation, thus, it is difficult to compare both results. The deviation from 1:1 correlation line is higher at very low permeability < 1 mD. From the literature if the discrepancy is within factor 2 the agreement is good due to the reality of the carbonates.

Chapter 5

CONCLUSION

Digital rock physics is an emerging, non-destructive technology, which expands the conventional laboratory analysis of reservoir rocks, and can help to compute rock properties and fluid flow characteristics and thereby deepen our understanding of fluid flow through porous media. X-ray CT and X-ray micro CT high-resolution images of rocks are generated, which reveal the inner rock structure and allow visualization and analysis of connected pore-space, fluid distribution and mineral composition. PerGeos software is used to convert image stacks into 3D segmented images, which are then used as input models for computer simulations that will help to approximate rock transport properties.

In this thesis, a multiscale imaging approach is used to characterize sandstone and carbonate rock samples, using Digital Core Analysis. After accurate laboratory measurements of porosity and permeability, the same samples are used for imaging. Sub-plugs extracted from the whole core samples are scanned at 4 microns resolution. After processing and segmenting 3D acquired images using PerGeos software, the connected porosity is estimated. The results of porosity is comparable to experimental measurements. For estimating permeability, LBM is applied to simulate fluid flow in porous media.

Simulating fluid flow of a sub-plug image requires high memory and takes longer simulation time, whereas taking a micro-plug from the sub-plugs shows quicker simulation run with less computational resources. The permeability of the micro-plugs is estimated, which contains 600 x 600 x 600 voxels for all the samples. Results show good agreement between measured and simulated permeability. For accurate prediction of absolute permeability using LBM, several important modeling parameters had to be considered, e.g. the size of digital rock chosen as representative elementary volume (REV) and image resolution. It was shown that for all samples, the chosen size of models was enough to be REV. The effect of decreasing in image resolution showed a huge impact on the estimated permeability, making it overestimated significantly. As practice indicates, the typical limit of acceptable resolution should not exceed 10 $\mu\text{m}/\text{pixel}$ in order to get reasonable values of permeability. Image based simulation of petrophysical properties of samples shows good comparison to measured data. The presented simulation technique for fluid transport through porous media allows for better understanding and quantification of how microscopic properties affect macroscopic transport. It also has been demonstrated to be quite robust.

By using different samples with a wide range of porosity and permeability it was possible to prove that suggested digital core analysis techniques could be a reliable complement of routine laboratory experiments, at least, for widely used homogeneous sandstone samples. For carbonate sample, however, it had been challenging to estimate main reservoir

properties due to its complex heterogeneity. The most important factors, which had influence on the results, were image resolution, representative sample size and proper simulation set-up (i.e. different approaches for single and multi-phase flow, boundary conditions, etc.).

5.1 Future work

This work can be extended in the following areas:

- Further investigations are recommended for a better understanding of the impact of the clay micropores on permeability. Different clay minerals and various crystal morphologies need to be considered to make a more general conclusion.
- For the simulation of low and ultra-low permeability rock samples there are some limitations using the micro-CT methodology such as resolution of the image and segmentation techniques. SEM images will provide interesting results to be studied in more detail.
- Future extensions will include multiphase flow properties. These developments should lead to an improved understanding of traditional petrophysical correlations applied within the industry.
- It would be interesting to study the effect of clay distribution and anisotropy on the P-wave and S-wave velocities of the sandstones.

- Comparing pore size distributions of the rocks using Micro CT and NMR can provide and ensure the credibility of the characterized rock samples.

APPENDICES

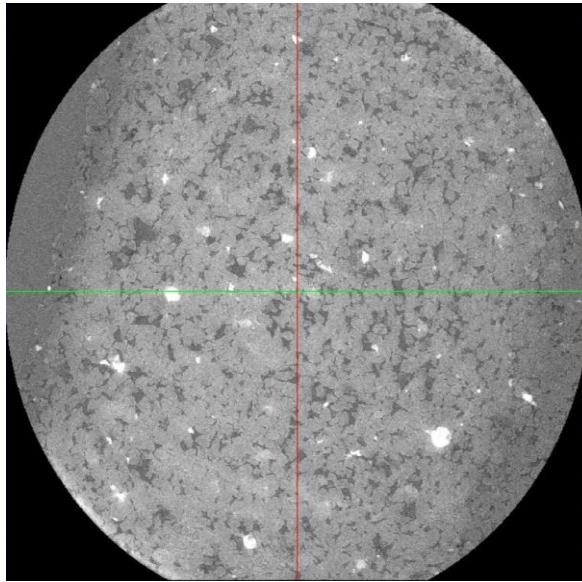


Figure A1: Berea Puff sub-plug image scanned at 4 microns resolution

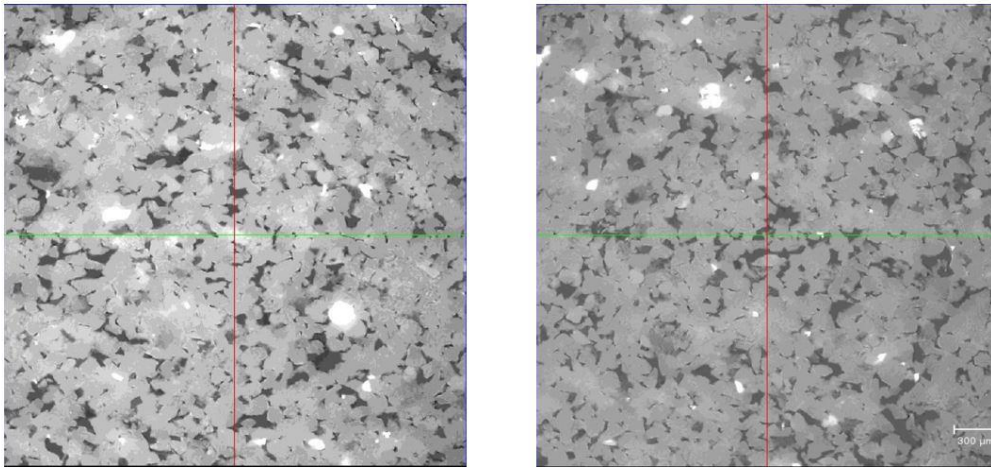


Figure A2: Berea Puff sub-plug before and after applying non-local means filter

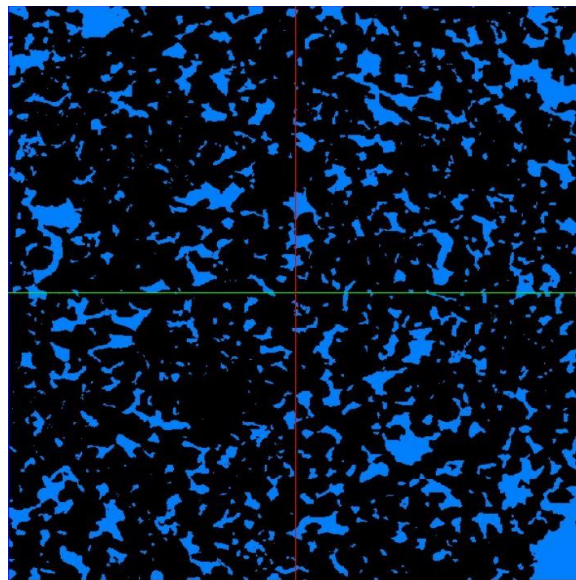


Figure A3: Berea Puff sub-plug after the segmentation process

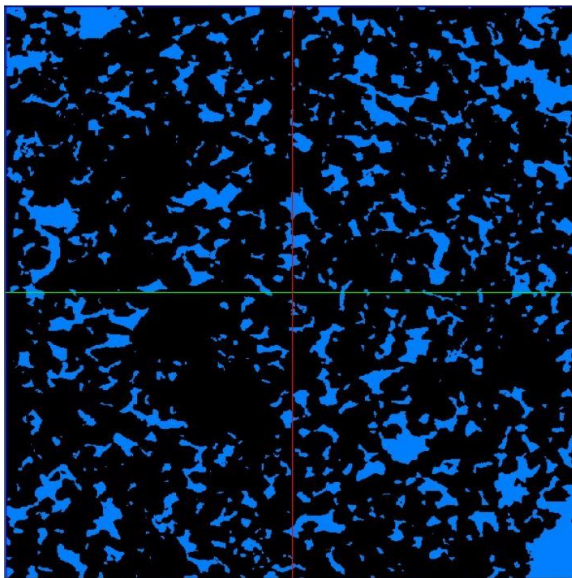


Figure A4: Berea Puff sub-plug after applying axis connectivity

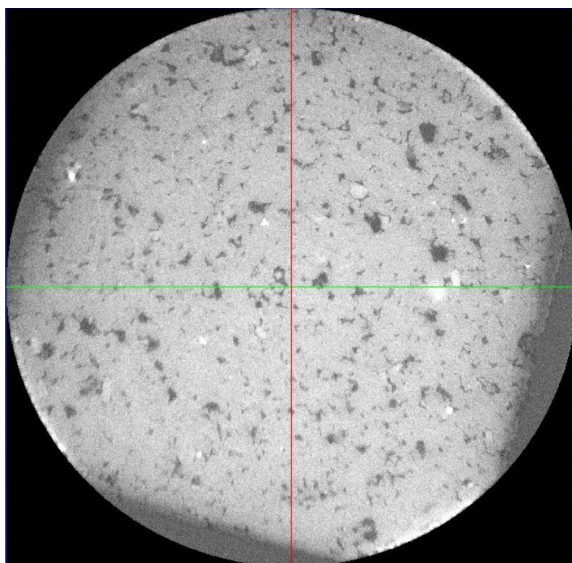


Figure A5: Crab Orchid sub-plug image scanned at 4 microns resolution

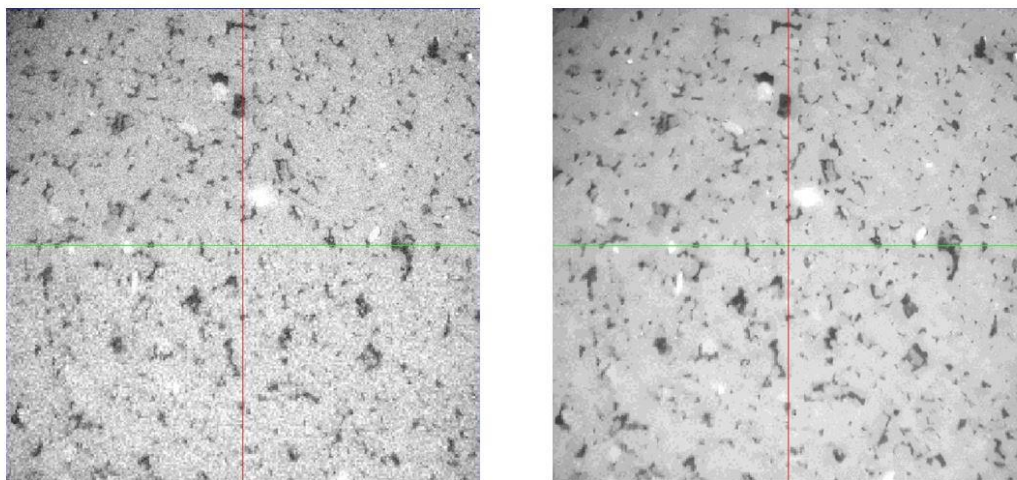


Figure A6: Crab Orchid sub-plug before and after applying non-local means filter

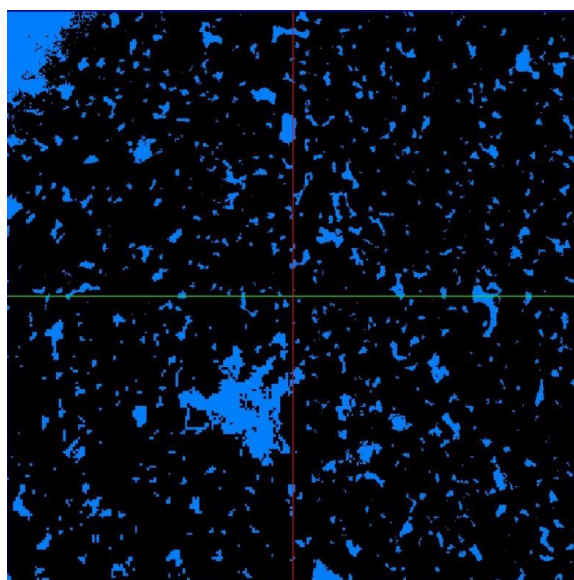


Figure A7: Crab Orchid sub-plug after the segmentation process

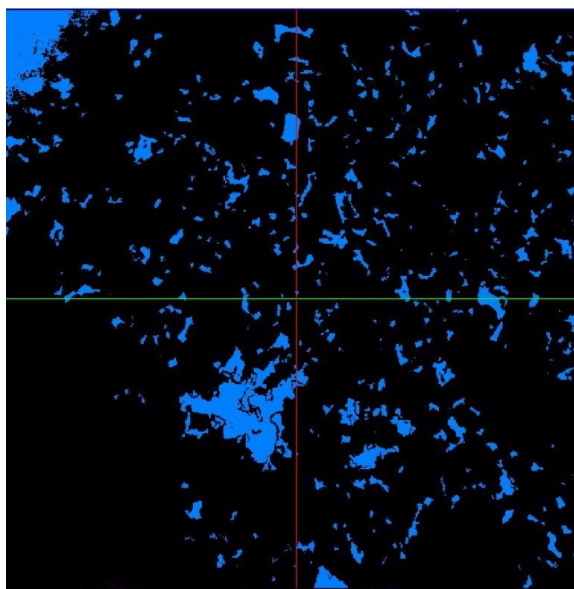


Figure A8: Crab Orchid sub-plug after applying axis connectivity

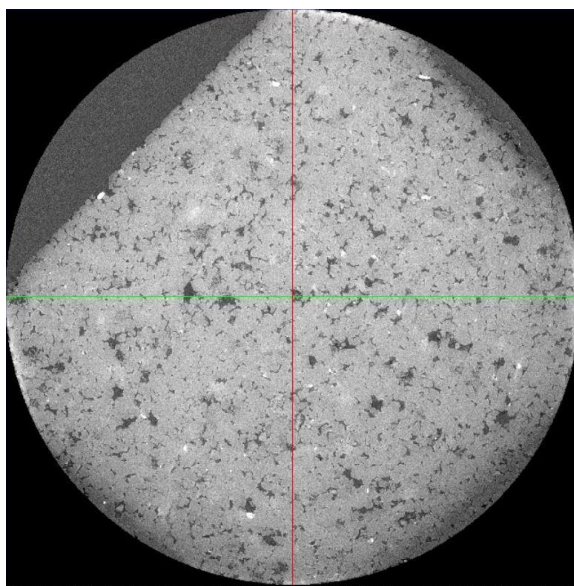


Figure A9: Bandera Brown sub-plug image scanned at 4 microns resolution

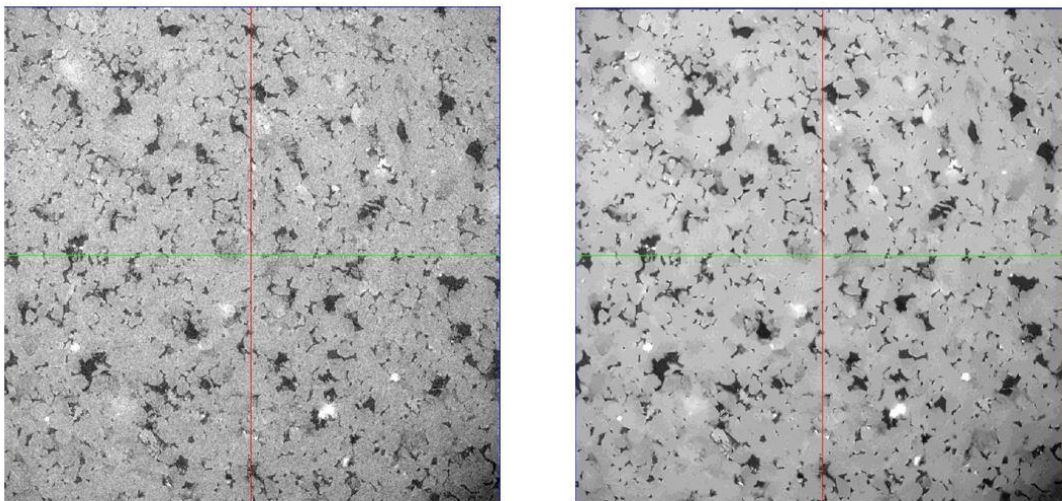


Figure A10: Bandera Brown sub-plug before and after applying non-local means filter

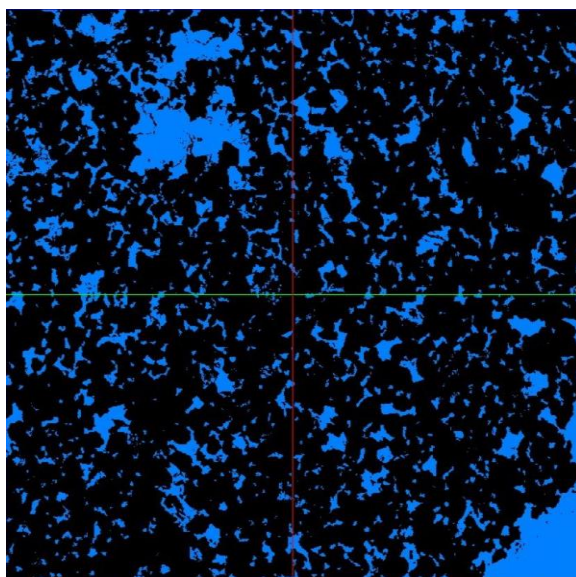


Figure A11: Bandera Brown sub-plug after the segmentation process

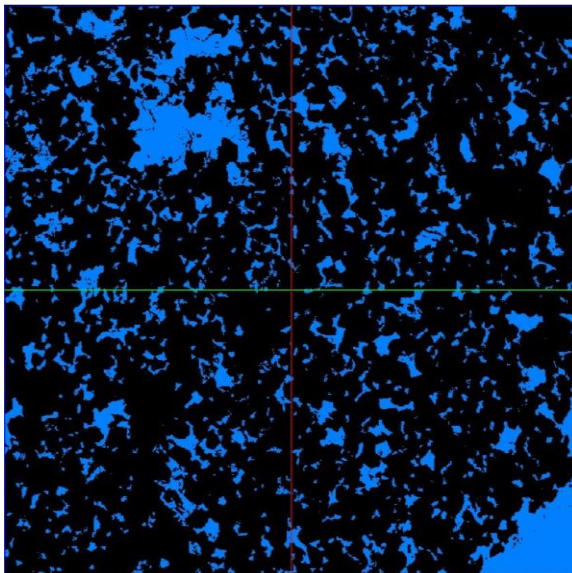


Figure A12: Bandera Brown sub-plug after applying axis connectivity

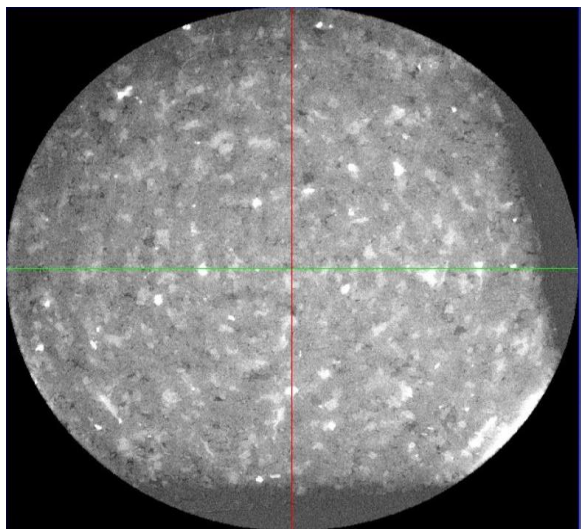


Figure A13: Colton sub-plug image scanned at 4 microns resolution

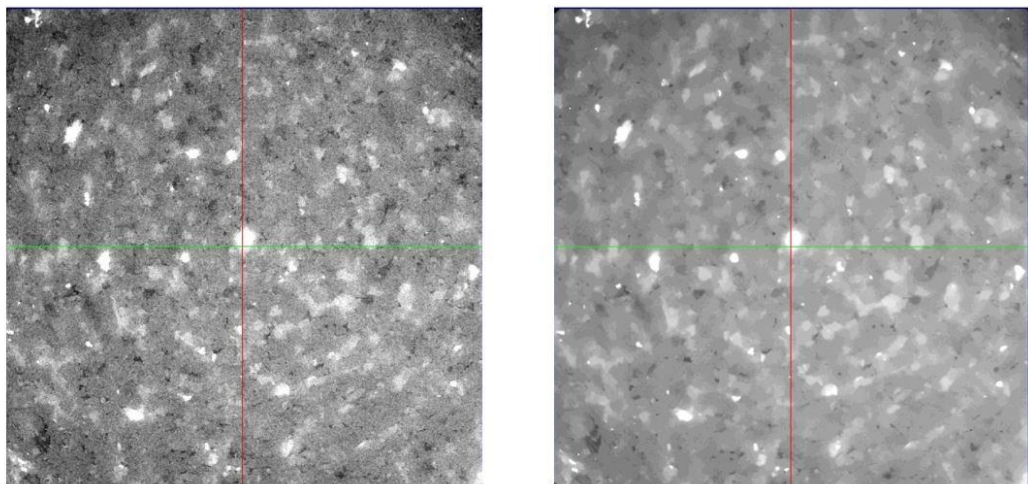


Figure A14: Colton sub-plug before and after applying non-local means filter

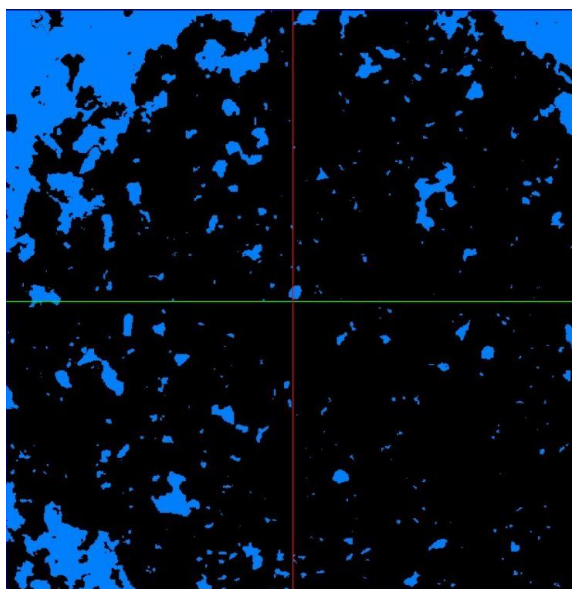


Figure A15: Colton sub-plug after the segmentation process

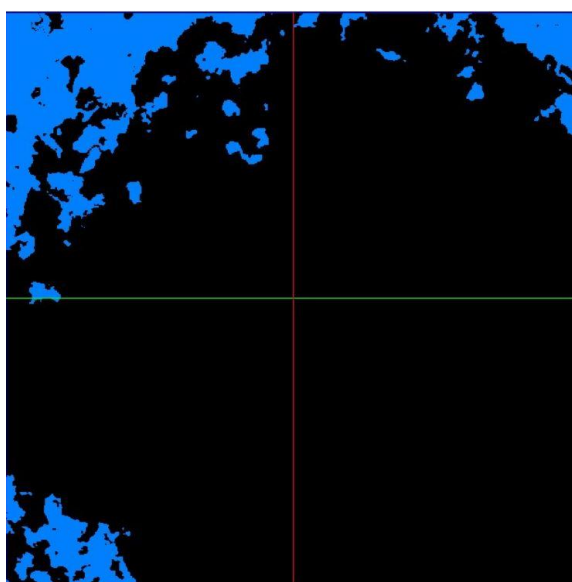


Figure A16: Colton sub-plug after applying axis connectivity

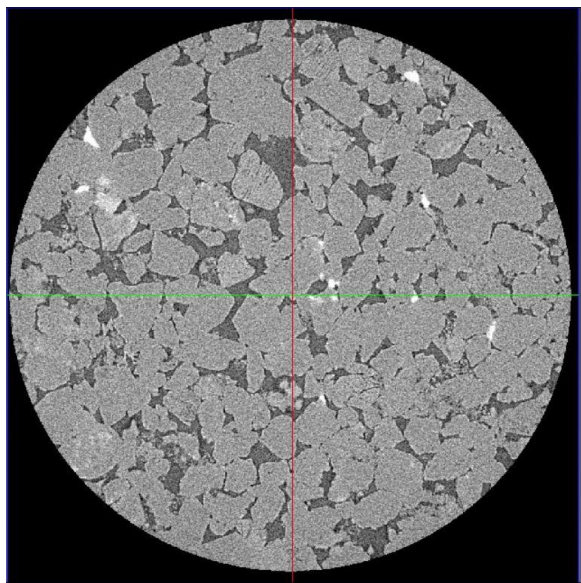


Figure A17: Berea Grey sub-plug image scanned at 4 microns resolution using Helical X-ray Micro-CT

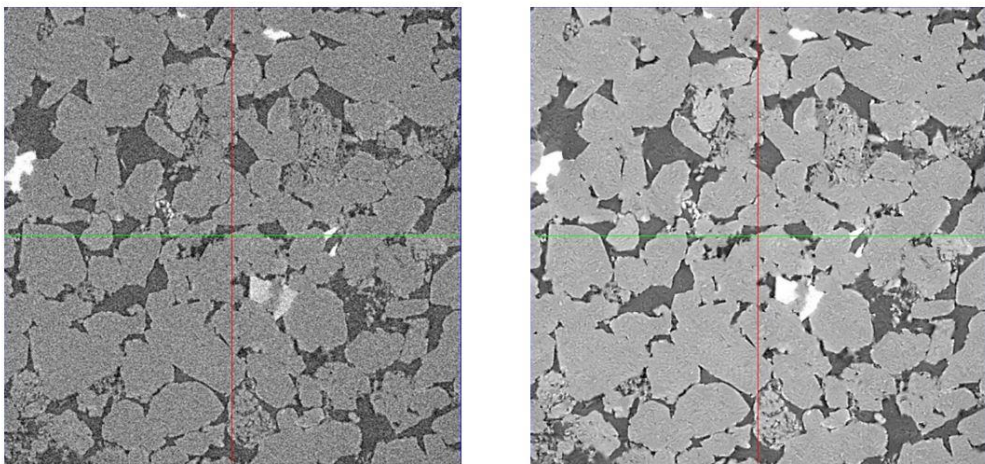


Figure A18: Berea Grey sub-plug before and after applying non-local means filter

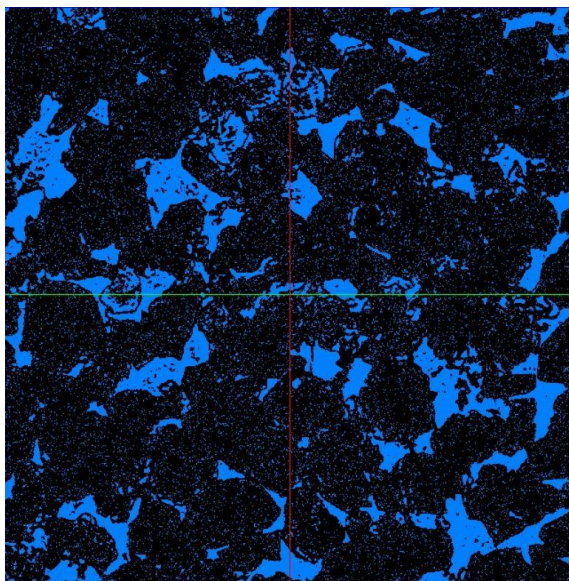


Figure A19: Berea Grey sub-plug after the segmentation process

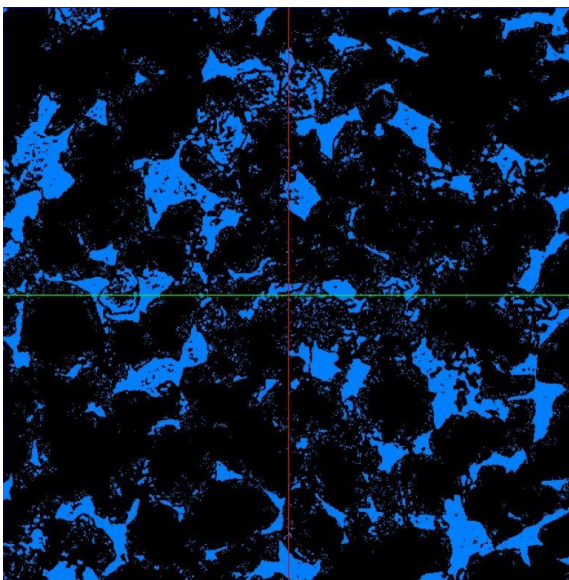


Figure A20: Berea Grey sub-plug after applying axis connectivity

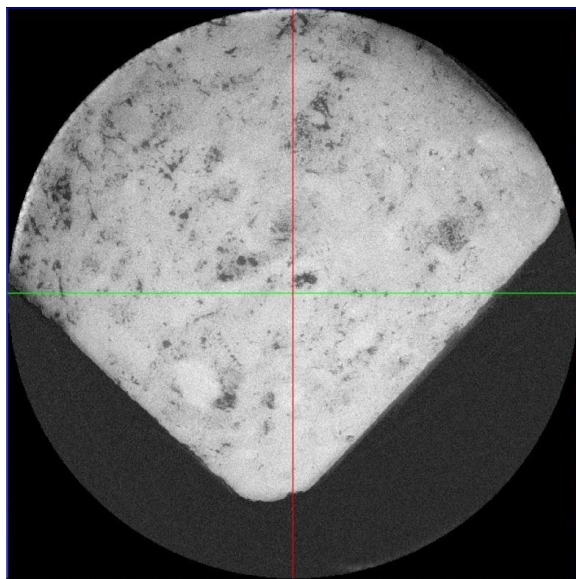


Figure B21: 9137-1 sub-plug image scanned at 4 microns resolution

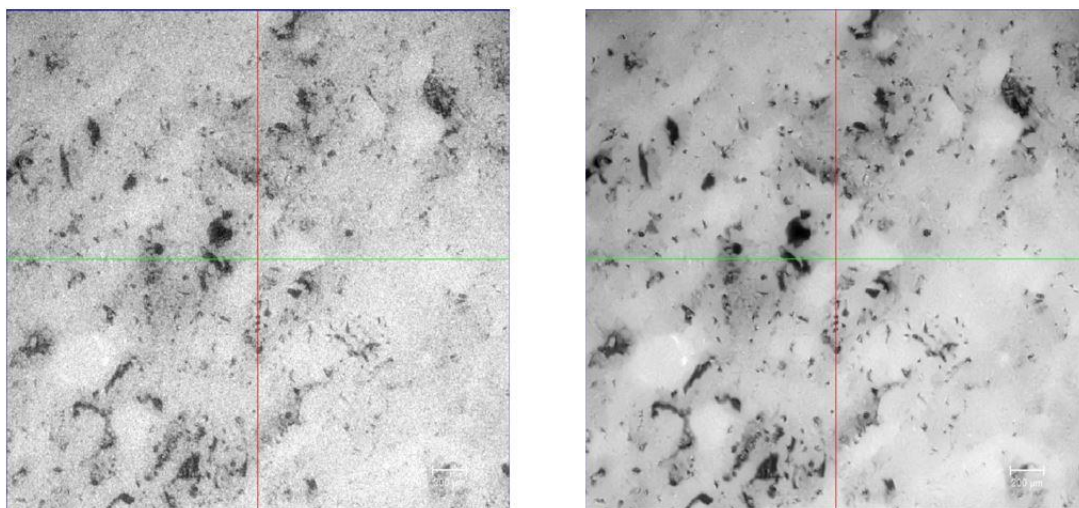


Figure B22: 9137-1 sub-plug before and after applying non-local means filter

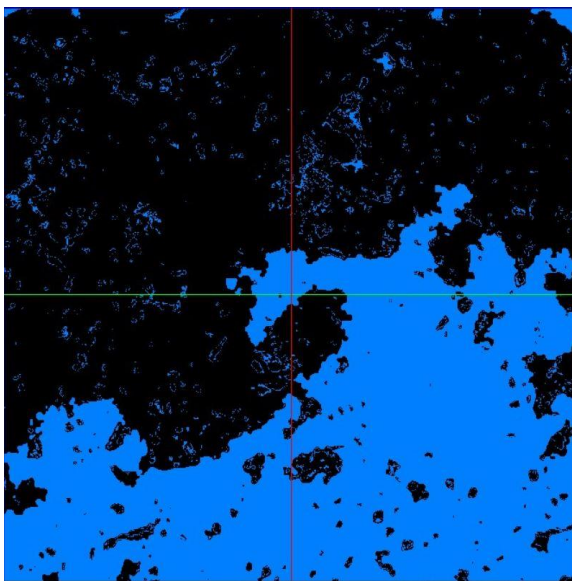


Figure B23: 9137-1 sub-plug after the segmentation process

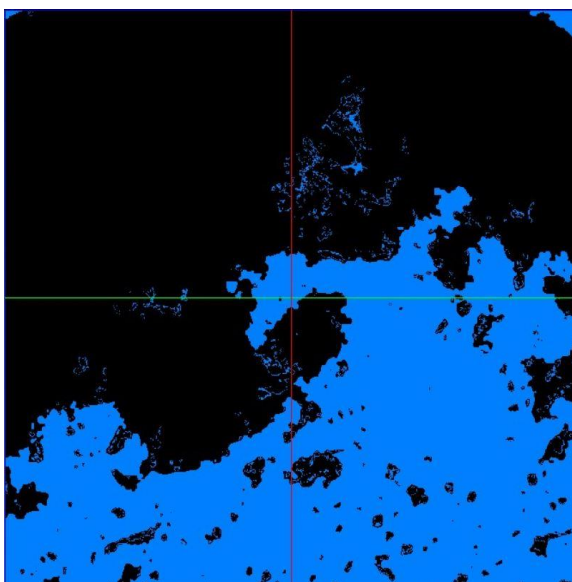


Figure B24: 9137-1 sub-plug after applying axis connectivity

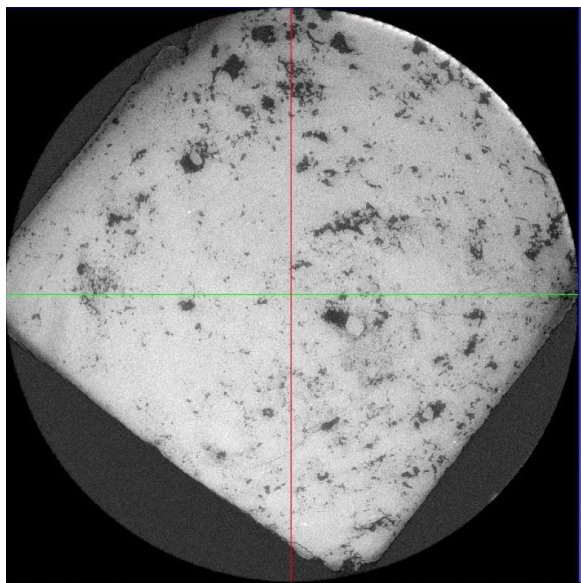


Figure B25: 9058-3 sub-plug image scanned at 4 microns resolution

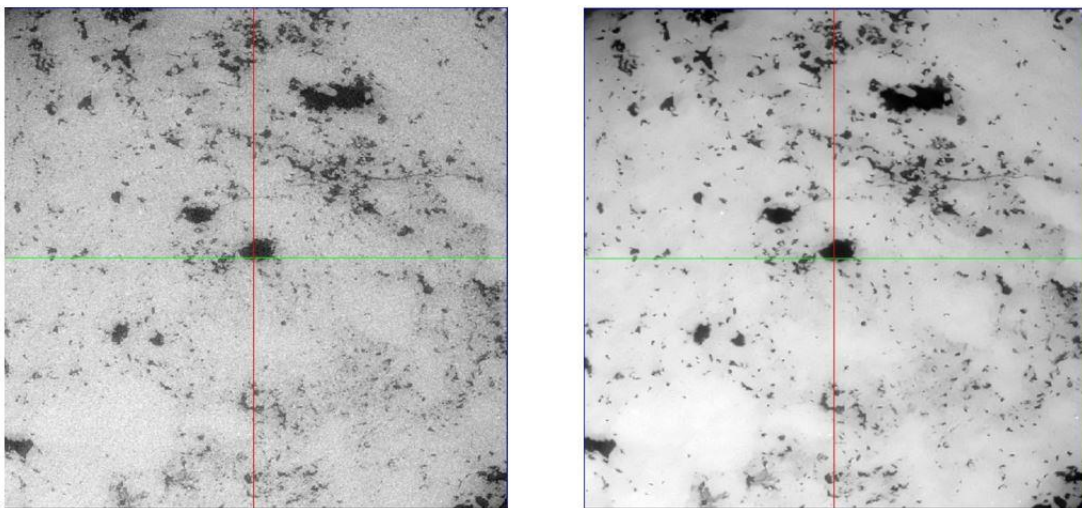


Figure B26: 9058-3 sub-plug before and after applying non-local means filter

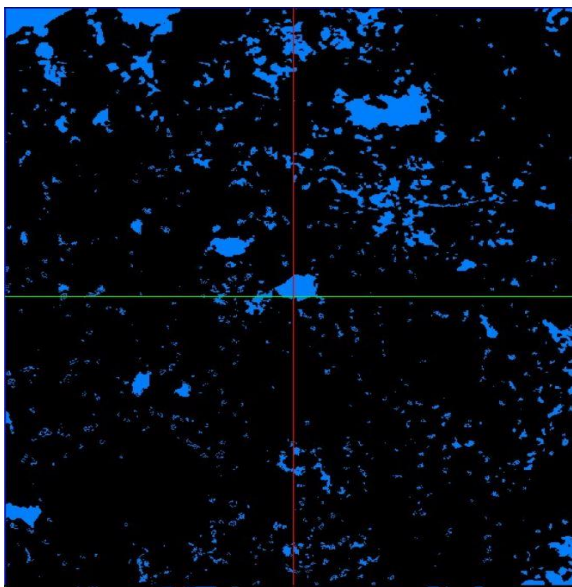


Figure B27: 9058-3 sub-plug after the segmentation process

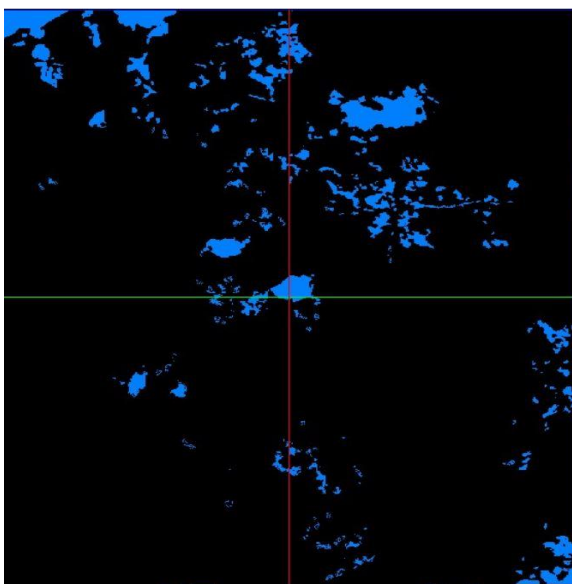


Figure B28: 9058-3 sub-plug after applying axis connectivity

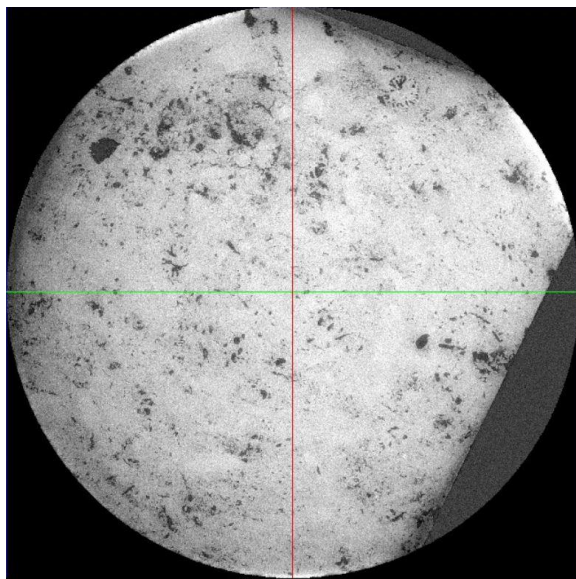


Figure B29: 9135-5 sub-plug image scanned at 4 microns resolution

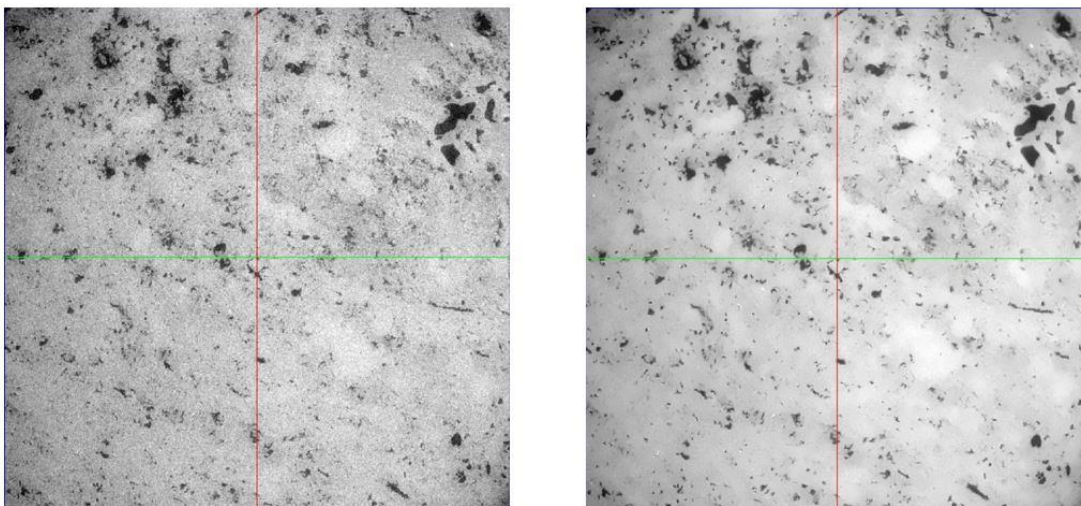


Figure B30: 9135-5 sub-plug before and after applying non-local means filter

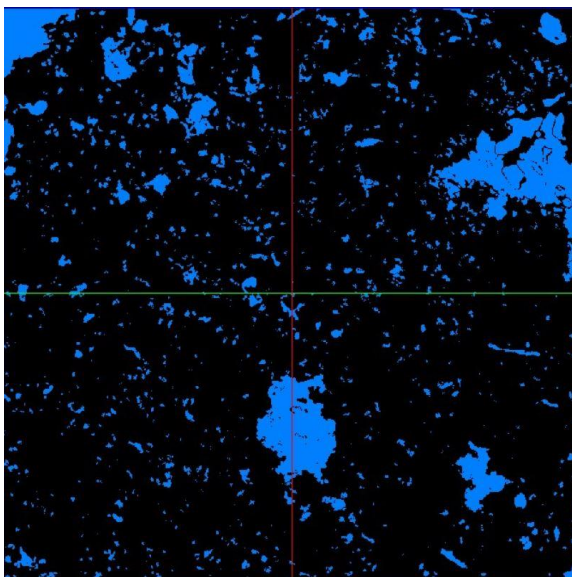


Figure B31: 9135-5 sub-plug after the segmentation process

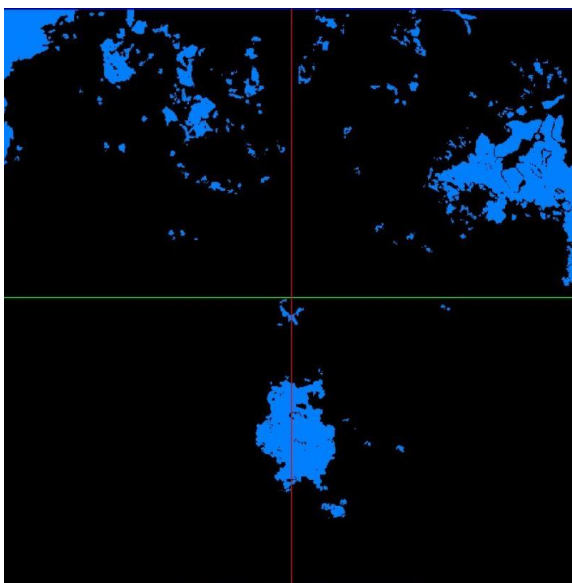


Figure B132: 9135-5 sub-plug after applying axis connectivity

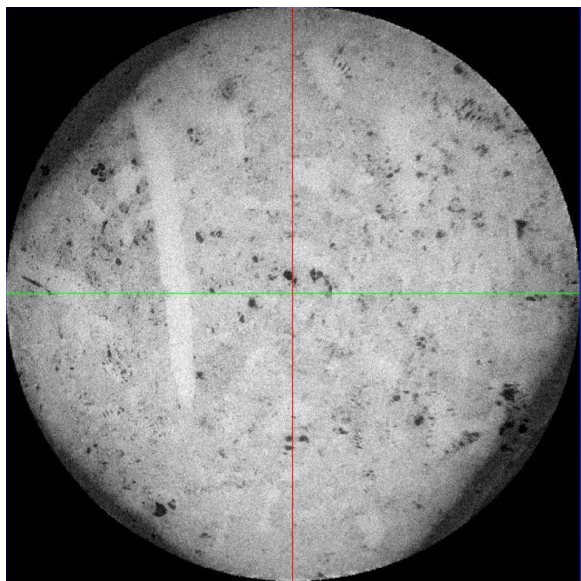


Figure B33: 9136-8 sub-plug image scanned at 4 microns resolution

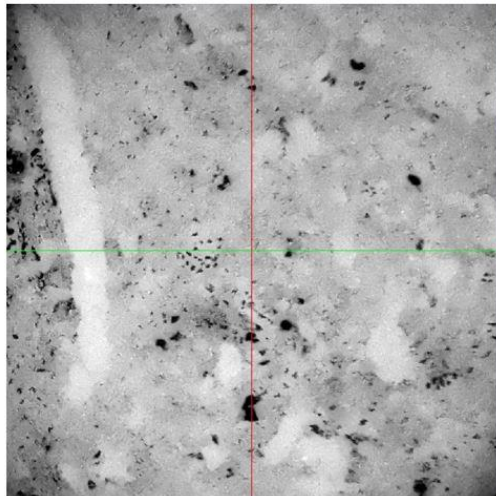
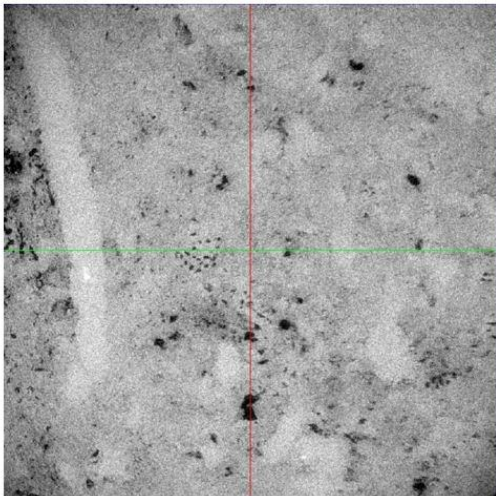


Figure B34: 9136-8 sub-plug before and after applying non-local means filter

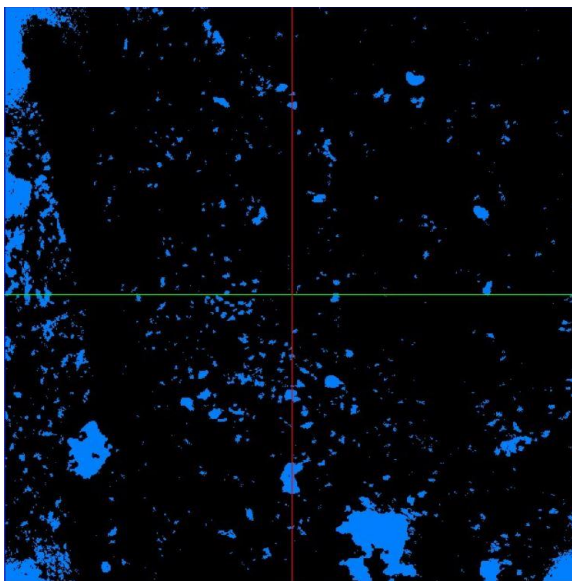


Figure B35: 9136-8 sub-plug after the segmentation process

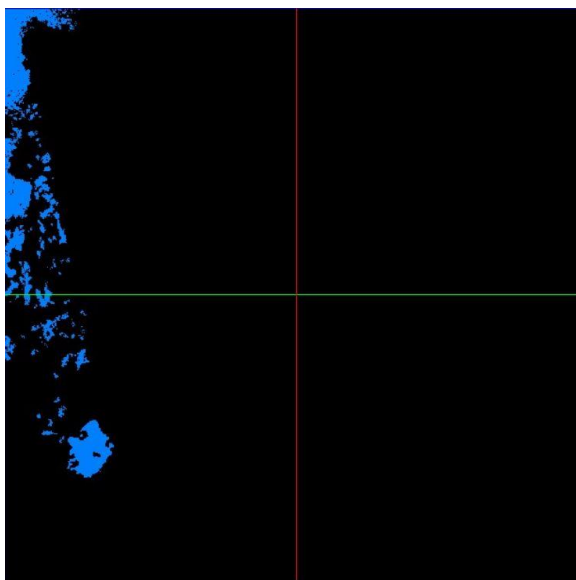


Figure B36: 9136-8 sub-plug after applying axis connectivity

REFERENCES

- [1] M. A. Gibrata *et al.*, “SPE 161187 Digital Rock Physics and Challenge in Formation Evaluation of Carbonate Reservoir , Case Study,” 2012.
- [2] M. O. Amabeoku, S. Aramco, T. M. Al-ghamdi, S. Aramco, and Y. Mu, “IPTC 17132 Evaluation and Application of Digital Rock Physics (DRP) for Special Core Analysis in Carbonate Formations,” 2013.
- [3] J. K. Jasti, G. Jesion, and L. Feldkamp, “Microscopic Imaging of Porous Media With X-Ray Computer Tomography,” *SPE Form. Eval.*, vol. 8, no. 3, pp. 189–193, 1993.
- [4] J. Arns, C. H. Arns, A. P. Sheppard, R. M. Sok, M. A. Knackstedt, and W. V. Pinczewski, “Relative permeability from tomographic images ; effect of correlated heterogeneity,” vol. 39, pp. 247–259, 2003.
- [5] P.-E. Oeren and S. Bakke, “Reconstruction of Berea sandstone and pore-scale modeling of wettability effects,” *J. Pet. Sci. Eng.*, vol. 39, pp. 177–199, Sep. 2003.
- [6] G. Jin, C. Torres-Verdin, F. Radaelli, and E. Rossi, “Experimental Validation of Pore-Level Calculations of Static and Dynamic Petrophysical Properties of Clastic Rocks,” *SPE Annual Technical Conference and Exhibition*. Society of Petroleum Engineers, Anaheim, California, U.S.A., p. 13, 2007.

- [7] A. Grader *et al.*, “A COMPARATIVE STUDY OF DIGITAL ROCK PHYSICS AND LABORATORY SCAL EVALUATIONS OF CARBONATE CORES,” pp. 1–12, 2010.
- [8] M. Z. Kalam, “Digital Rock Physics for Fast and Accurate Special Core Analysis in Carbonates,” 2012.
- [9] M. S. Jouini, S. Vega, and A. Al-ratrout, “Numerical estimation of carbonate rock properties using multiscale images,” pp. 405–421, 2015.
- [10] K. Rahimov, A. M. Alsumaiti, and M. S. Jouini, “QUANTITATIVE ANALYSIS OF ABSOLUTE PERMEABILITY AND POROSITY IN CARBONATE ROCKS USING DIGITAL ROCK PHYSICS,” pp. 1–8, 2016.
- [11] K. Ali *et al.*, “ELECTRICAL AND PETROPHYSICAL PROPERTIES OF SILICICLASTIC RESERVOIR ROCKS FROM PORE- SCALE MODELING,” pp. 1–12, 2011.
- [12] O. Lopez, A. Mock, J. Skretting, E. Boye, and P. Jr, “INVESTIGATION INTO THE RELIABILITY OF PREDICTIVE PORE-SCALE MODELING FOR SILICICLASTIC RESERVOIR ROCKS,” pp. 1–12, 2010.
- [13] M. Kalam, T. Al Dayyani, A. Grader, and C. Sisk, “Digital rock physics analysis in complex carbonates,” *World Oil*, vol. 232, pp. 85–90, May 2011.

- [14] Z. Kalam, S. Seraj, Z. Bhatti, A. Mock, P. E. Øren, and V. Ravlo, “Relative permeability assessment in a giant carbonate reservoir using Digital Rock Physics Laboratory test.”
- [15] M. A. Knackstedt, S. Latham, M. Madadi, A. Sheppard, T. Varslot, and C. Arns, “Digital rock physics: 3D imaging of core material and correlations to acoustic and flow properties,” *Lead. Edge*, vol. 28, no. 1, pp. 28–33, Jan. 2009.
- [16] A. Sakellariou *et al.*, “Micro?CT facility for imaging reservoir rocks at pore scales,” in *SEG Technical Program Expanded Abstracts 2003*, Society of Exploration Geophysicists, 2003, pp. 1664–1667.
- [17] P. Gouze and L. Luquot, “X-ray microtomography characterization of porosity, permeability and reactive surface changes during dissolution,” *J. Contam. Hydrol.*, vol. 120–121, pp. 45–55, Mar. 2011.
- [18] S. Galaup, Y. Liu, and A. Cerepi, “New integrated 2D–3D physical method to evaluate the porosity and microstructure of carbonate and dolomite porous system,” *Microporous Mesoporous Mater.*, vol. 154, pp. 175–186, 2012.
- [19] W. Zhu, P. Baud, and T. Wong, “Micromechanics of cataclastic pore collapse in limestone,” *J. Geophys. Res. Solid Earth*, vol. 115, no. B4, Apr. 2010.
- [20] S. Latham, T. Varslot, and A. Sheppard, “IMAGE REGISTRATION :

- ENHANCING AND CALIBRATING X-RAY MICRO-CT IMAGING,” pp. 1–12, 2008.
- [21] D. B. S. Youssef, M. F. S. Bekri, and E. R. O. Vizika, “Improving the Estimations of Petrophysical Transport Behavior of Carbonate Rocks Using a Dual Pore Network Approach Combined with Computed Microtomography,” pp. 505–524, 2012.
- [22] Y. Ji, P. Baud, V. Vajdova, and T. Wong, “Pore2Field - Flows and Mechanics in Natural Porous Media from Pore to Field Scale Pore2Field - Physique des écoulements en milieux poreux naturels : Characterization of Pore Geometry of Indiana Limestone in Relation to Mechanical Compaction,” vol. 67, no. 5, 2012.
- [23] J. Dvorkin, J. Walls, A. Tutuncu, M. Prasad, A. Nur, and A. Mese, “Rock Property Determination Using Digital Rock Physics,” pp. 1–4, 2001.
- [24] W. J. Bosl, J. Dvorkin, and A. Nur, “A study of porosity and permeability using a lattice Boltzmann simulation,” *Geophys. Res. Lett.*, vol. 25, no. 9, pp. 1475–1478, May 1998.
- [25] J. Dvorkin, N. Derzhi, E. Diaz, and Q. Fang, “Relevance of computational rock physics,” vol. 76, no. 5, 2011.
- [26] M. A. Knackstedt *et al.*, “Digital Core Laboratory: Properties of reservoir core

- derived from 3D images,” *SPE Asia Pacific Conference on Integrated Modelling for Asset Management*. Society of Petroleum Engineers, Kuala Lumpur, Malaysia, p. 14, 2004.
- [27] L. Xuefeng, S. Jianmeng, and W. Haitao, “Numerical simulation of rock electrical properties based on digital cores *,” vol. 6, no. 1, pp. 1–7, 2009.
- [28] H. Andrä *et al.*, “Digital rock physics benchmarks—Part I: Imaging and segmentation,” *Comput. Geosci.*, vol. 50, pp. 25–32, 2013.
- [29] H. Andrae *et al.*, “Digital rock physics benchmarks—Part II: Computing effective properties,” *Comput. Geosci.*, vol. 50, pp. 33–43, Jan. 2013.
- [30] N. Saxena, “Exact equations for fluid and solid substitution,” *Geophysics*, vol. 79, p. L21, May 2014.
- [31] Z. Wang, R. Wang, R. Weger, T. Li, and F. Wang, “Pore-scale modeling of elastic wave propagation in carbonate rocks,” *GEOPHYSICS*, vol. 80, pp. D51–D63, Jan. 2015.
- [32] S. Iglauer, C. H. Pentland, and A. Busch, “CO₂ wettability of seal and reservoir rocks and the implications for carbon geo-sequestration,” *Water Resour. Res.*, vol. 51, no. 1, pp. 729–774, Jan. 2015.
- [33] M. J. Oak, L. E. Baker, and D. C. Thomas, “Three-Phase Relative Permeability of

- Berea Sandstone,” *J. Pet. Technol.*, vol. 42, no. 8, pp. 1054–1061, 1990.
- [34] P. Valvatne and M. J. Blunt, “Predictive pore-scale modeling of two-phase flow in mixed wet media,” *Water Resour. Res.*, vol. 40, Jul. 2004.
- [35] R. Ehrlich, S. K. Kennedy, S. J. Crabtree, and R. L. Cannon, “Petrographic image analysis; I, Analysis of reservoir pore complexes,” *J. Sediment. Res.*, vol. 54, no. 4, pp. 1365–1378, Dec. 1984.
- [36] T. Bultreys, W. De Boever, and V. Cnudde, “Earth-Science Reviews Imaging and image-based fluid transport modeling at the pore scale in geological materials : A practical introduction to the current state-of-the-art,” *Earth Sci. Rev.*, vol. 155, pp. 93–128, 2016.
- [37] H. J. Vinegar, “X-Ray CT and NMR Imaging of Rocks,” *J. Pet. Technol.*, vol. 38, no. 3, pp. 257–259, 1986.
- [38] E. M. Withjack, “Computed tomography for rock-property determination and fluid-flow visualization,” *SPE Form. Eval.*, vol. 3, no. 4, pp. 696–704, 1988.
- [39] M. M. Honarpour, V. Cromwell, D. Hatton, and R. Satchwell, “Reservoir Rock Descriptions Using Computed Tomography (CT),” *SPE Annual Technical Conference and Exhibition*. Society of Petroleum Engineers, Las Vegas, Nevada, p. 8, 1985.

- [40] S. L. Wellington and H. J. Vinegar, "X-Ray Computerized Tomography," *J. Pet. Technol.*, vol. 39, no. 8, pp. 885–898, 1987.
- [41] P. K. Hunt, P. Engler, and C. Bajsarowicz, "Computed tomography as a core analysis tool: Applications, instrument evaluation, and image improvement techniques," *J. Pet. Technol.*, vol. 40, no. 9, pp. 1203–1210, 1988.
- [42] R. M. Moss and J. W. Russo, "Quantitative Determination Of Secondary Porosity Using X-Ray Computed Tomography And Wireline Logs," *SPWLA 32nd Annual Logging Symposium*. Society of Petrophysicists and Well-Log Analysts, Midland, Texas, p. 25, 1991.
- [43] F. Suzuki, "X-Ray Computed Tomography For Carbonate Acidizing Studies," *Annual Technical Meeting*. Petroleum Society of Canada, Calgary, Alberta, p. 12, 1990.
- [44] A. T. Watson and J. Mudra, "Characterization of Devonian Shales With X-Ray-Computed Tomography," *SPE Form. Eval.*, vol. 9, no. 3, pp. 209–212, 1994.
- [45] M. A. Vickerd, R. Thring, J. M. Arocena, J. B. Li, and R. Heck, "Changes in Porosity Due to Acid Gas Injection As Determined by X-Ray Computed Tomography," *J. Can. Pet. Technol. - J CAN Pet. TECHNOL*, vol. 45, Aug. 2006.
- [46] E. da S. Sales, L. C. B. Bianco, J. C. de Queiroz Neto, E. F. Campos, and R. T.

- Lopes, “Study of Skin Damage in Unconsolidated Sandstone by Computed Tomography,” *European Formation Damage Conference*. Society of Petroleum Engineers, Scheveningen, The Netherlands, p. 7, 2007.
- [47] E. M. Withjack and I. Akervoll, “Computed Tomography Studies of 3-D Miscible Displacement Behavior in a Laboratory Five-Spot Model,” *SPE Annual Technical Conference and Exhibition*. Society of Petroleum Engineers, Houston, Texas, p. 13, 1988.
- [48] H. Taud, R. Martinez-Angeles, J. F. Parrot, and L. Hernandez-Escobedo, “Porosity estimation method by X-ray computed tomography,” *J. Pet. Sci. Eng.*, vol. 47, no. 3, pp. 209–217, 2005.
- [49] Y. Géraud, F. Surma, and F. Mazerolle, “Porosity and fluid flow characterization of granite by capillary wetting using X-ray computed tomography,” *Geol. Soc. London, Spec. Publ.*, vol. 215, no. 1, p. 95 LP-105, Jan. 2003.
- [50] B. Vega, A. Dutta, and A. R. Kovscek, “CT Imaging of Low-Permeability, Dual-Porosity Systems Using High X-ray Contrast Gas,” *Transp. Porous Media*, vol. 101, no. 1, pp. 81–97, Sep. 2014.
- [51] S. C. M. Krevor, R. Pini, L. Zuo, and S. M. Benson, “Relative permeability and trapping of CO₂ and water in sandstone rocks at reservoir conditions,” *Water Resour. Res.*, vol. 48, no. 2, Feb. 2012.

- [52] J.-H. Choi, Y. Seol, R. Boswell, and R. Juanes, “X-ray computed-tomography imaging of gas migration in water-saturated sediments: From capillary invasion to conduit opening,” *Geophys. Res. Lett. - Geophys RES LETT*, vol. 38, Sep. 2011.
- [53] V. Cnudde and M. N. Boone, “Earth-Science Reviews High-resolution X-ray computed tomography in geosciences : A review of the current technology and applications,” *Earth Sci. Rev.*, vol. 123, pp. 1–17, 2013.
- [54] M. Van Geet, S. Rudy, and M. Wevers, “Towards 3-D petrography: Application of microfocus computer tomography in geological science,” *Comput. Geosci.*, vol. 27, pp. 1091–1099, Nov. 2001.
- [55] F. Thauvin and K. K. Mohanty, “Network Modeling of Non-Darcy Flow Through Porous Media,” *Transp. Porous Media*, vol. 31, no. 1, pp. 19–37, 1998.
- [56] L. Louis, T. Wong, P. Baud, and S. Tembe, “Imaging strain localization by X-ray computed tomography: Discrete compaction bands in Diemelstadt sandstone,” *J. Struct. Geol.*, vol. 28, pp. 762–775, May 2006.
- [57] D. Silin and G. Goloshubin, “An Asymptotic Model of Seismic Reflection from a Permeable Layer,” *Transp. Porous Media*, vol. 83, no. 1, pp. 233–256, 2010.
- [58] P. Bhattad, C. S. Willson, and K. E. Thompson, “Effect of Network Structure on Characterization and Flow Modeling Using X-ray Micro-Tomography Images of

Granular and Fibrous Porous Media,” pp. 363–391, 2011.

- [59] D. Lu, M. Zhou, J. H. Dunsmuir, and H. Thomann, “NMR T2 distributions and two phase flow simulations from x-ray micro-tomography images of sandstones,” *Magn. Reson. Imaging*, vol. 19, no. 3, pp. 443–448, 2001.
- [60] Z. Jiang, K. Wu, G. Couples, M. I. J. van Dijke, K. S. Sorbie, and J. Ma, “Efficient extraction of networks from three-dimensional porous media,” *Water Resour. Res.*, vol. 43, no. 12, Dec. 2007.
- [61] M. E. Coles, R. D. Hazlett, P. Spanne, W. E. Soll, E. L. Muegge, and K. W. Jones, “Pore level imaging of fluid transport using synchrotron X-ray microtomography,” *J. Pet. Sci. Eng.*, vol. 19, no. 1, pp. 55–63, 1998.
- [62] P. Bertels, D. A. Dicarlo, and J. Blunt, “Measurement of aperture distribution , capillary pressure , relative permeability , and in situ saturation in a rock fracture using computed tomography scanning,” vol. 37, no. 3, pp. 649–662, 2001.
- [63] J. Gelb, A. Gu, T. Fong, L. Hunter, S. H. Lau, and W. Yun, “A CLOSER LOOK AT SHALE : REPRESENTATIVE ELEMENTARY VOLUME ANALYSIS WITH LABORATORY 3D X-RAY COMPUTED MICROTOMOGRAPHY AND NANOTOMOGRAPHY,” pp. 1–8, 2011.
- [64] H. Dong, S. Fjeldstad, L. Alberts, S. Roth, S. Bakke, and P.-E. Oeren, “PORE

NETWORK MODELLING ON CARBONATE: A COMPARATIVE STUDY OF
DIFFERENT MICRO-CT NETWORK EXTRACTION METHODS,” Jan. 2008.

- [65] W. D. Carlson, T. Rowe, R. Ketcham, and M. Colbert, “Applications of high-resolution X-ray computed tomography in petrology, meteoritics and palaeontology,” *Geol. Soc. London, Spec. Publ.*, vol. 215, pp. 7–22, Jan. 2003.
- [66] H. Sun, S. Vega, and G. Tao, “Study on Permeability Anisotropy in Carbonate Reservoir Samples Using Digital Rock Physics,” no. 1, pp. 1–13, 2015.
- [67] H. Sun, S. Vega, G. Tao, H. Yong, and B. Li, “SPE-183114-MS Estimation of Petrophysical Parameters of Heterogeneous Carbonate Rock Sample with Multi-Scale CT Images,” pp. 1–12, 2016.
- [68] B. F. Bohor and R. E. Hughes, “Scanning electron microscopy of clays and clay minerals,” *Clays Clay Miner.*, vol. 19, no. 1, pp. 49–54, 1971.
- [69] S. Peng, J. Yang, X. Xiao, B. Loucks, S. Ruppel, and T. Zhang, “An Integrated Method for Upscaling Pore-Network Characterization and Permeability Estimation: Example from the Mississippian Barnett Shale,” *Transp. Porous Media*, vol. 109, Jun. 2015.
- [70] J. H. Hubbell *et al.*, “A Review, Bibliography, and Tabulation of K, L, and Higher Atomic Shell X-Ray Fluorescence Yields,” *J. Phys. Chem. Ref. Data*, vol. 23, no. 2,

pp. 339–364, Mar. 1994.

- [71] M. R. H. Sarker and S. S. Texas, “SPE 126039 Advances in Micro-CT Based Evaluation of Reservoir Rocks,” pp. 9–11, 2009.
- [72] D. C. Applications, R. Characterization, S. Siddiqui, A. A. Khamees, and S. A. R, “SPE 90520 Dual-Energy CT-Scanning Applications in Rock Characterization,” 2004.
- [73] S. M. Shah, J. Yang, J. P. Crawshaw, O. Gharbi, E. S. Boek, and I. C. London, “SPE 166252 Predicting Porosity And Permeability Of Carbonate Rocks From Pore- To Core-Scale Using Medical CT , Confocal Laser Scanning Microscopy And Micro CT,” 2013.
- [74] J. T. Skinner, F. D. Tovar, D. S. Schechter, and A. Texas, “Computed Tomography for Petrophysical Characterization of Highly Heterogeneous Reservoir Rock,” 2015.
- [75] H. Al-Owihan *et al.*, “Advanced Rock Characterization by Dual Energy CT Imaging: A Novel Method in Complex Reservoir Evaluation,” *International Petroleum Technology Conference*. International Petroleum Technology Conference, Doha, Qatar, p. 17, 2014.
- [76] M. R. Dernaika, M. A. Basoni, A. M. Dawoud, M. Z. Kalam, and S. M. Skjæveland, “Variations in Bounding and Scanning Relative Permeability Curves With Different

- Carbonate Rock Type,” *SPE Reserv. Eval. Eng.*, vol. 16, no. 3, pp. 265–280, 2013.
- [77] M. Al Mansoori *et al.*, “Application of Digital and Conventional Techniques to Study the Effects of Heterogeneity on Permeability Anisotropy in a Complex Middle East Carbonate Reservoir,” *SPWLA 55th Annual Logging Symposium*. Society of Petrophysicists and Well-Log Analysts, Abu Dhabi, United Arab Emirates, p. 24, 2014.
- [78] G. De Prisco, J. Toelke, and M. R. Dernaika, “COMPUTATION OF RELATIVE PERMEABILITY FUNCTIONS IN 3D DIGITAL ROCKS BY A FRACTIONAL FLOW APPROACH USING THE LATTICE BOLTZMANN,” pp. 1–12, 2012.
- [79] Y. mu and M. Dernaika, *DRAINAGE AND IMBIBITION CAPILLARY PRESSURE CURVES OF CARBONATE RESERVOIR ROCKS BY DIGITAL ROCK PHYSICS*. 2012.
- [80] A. Grader, Y. Mu, J. Toelke, C. Baldwin, and Q. Fang, “SPE 138591 Estimation of Relative Permeability using the Lattice Boltzmann Method for Fluid Flows in a Cretaceous Formation , Abu Dhabi,” no. Md, 2010.
- [81] R. M. Sok, M. A. Knackstedt, T. Varslot, A. Ghous, S. Latham, and A. P. Sheppard, “Pore Scale Characterization of Carbonates At Multiple Scales: Integration of Micro-CT, BSEM, And FIBSEM,” *Petrophysics*, vol. 51, no. 6, p. 9, 2010.

- [82] O. Lopez *et al.*, “VALIDATION OF FUNDAMENTAL CARBONATE RESERVOIR CORE PROPERTIES USING DIGITAL ROCK PHYSICS,” pp. 1–12, 2012.
- [83] W. B. Lindquist, S.-M. Lee, D. A. Coker, K. W. Jones, and P. Spanne, “Medial axis analysis of void structure in three-dimensional tomographic images of porous media,” *J. Geophys. Res. Solid Earth*, vol. 101, no. B4, pp. 8297–8310, Apr. 1996.
- [84] M. L. Porter and D. Wildenschild, “Image analysis algorithms for estimating porous media multiphase flow variables from computed microtomography data: a validation study,” *Comput. Geosci.*, vol. 14, no. 1, pp. 15–30, 2010.
- [85] D. B. Silin *et al.*, “SPE 84296 Robust Determination of the Pore Space Morphology in Sedimentary Rocks,” 2003.
- [86] C. H. Arns, F. Bauget, A. Limaye, A. Sakellariou, and T. J. Senden, “Pore-Scale Characterization of Carbonates Using X-Ray Microtomography,” no. December, pp. 475–484, 2005.
- [87] A. S. Al-kharusi and M. J. Blunt, “Network extraction from sandstone and carbonate pore space images,” vol. 56, pp. 219–231, 2007.
- [88] R. Ketcham and G. Iturrino, “Nondestructive high-resolution visualization and measurement of anisotropic effective porosity in complex lithologies using high-

- resolution X-ray computed tomography,” *J. Hydrol.*, vol. 302, pp. 92–106, Feb. 2005.
- [89] T. Varslot and R. M. Sok, “MULTI-SCALE IMAGING AND MODELING WORKFLOW TO CAPTURE AND CHARACTERIZE MICROPOROSITY IN SANDSTONE,” pp. 1–13, 2013.
- [90] E. H. Saenger, E. T. H. Zurich, C. Madonna, and E. T. H. Zurich, “Digital rock physics : Numerical vs . laboratory measurements,” vol. i, no. Figure 1, pp. 3693–3697, 2011.
- [91] T. S. Yun, Y. J. Jeong, K. Y. Kim, and K.-B. Min, “Evaluation of rock anisotropy using 3D X-ray computed tomography,” *Eng. Geol.*, vol. 163, pp. 11–19, 2013.
- [92] S. S. El Din, A. Dhabhi, O. Oil, O. Adco, M. R. Dernaika, and W. Laboratories, “SPE 137679 Whole Core Versus Plugs : Integrating Log and Core Data to Decrease Uncertainty in Petrophysical Interpretation and STOIP Calculations,” 2010.
- [93] M. Skalinski, R. Salazar, G. Latorraca, Z. Yang, and J. Urbach, “HETEROGENOUS CARBONATES – INTEGRATING PLUG AND WHOLE CORE DATA USING ROCK TYPES,” 2012.
- [94] A. Dehghan Khalili, J.-Y. Arns, F. Hussain, Y. Cinar, W. Pinczewski, and C. H. Arns, “Permeability Upscaling for Carbonates From the Pore Scale by Use of

- Multiscale X-Ray-CT Images,” *SPE Reserv. Eval. Eng.*, vol. 16, no. 4, pp. 353–368, 2013.
- [95] D. A. Coker and J. H. Dunsmuir, “Morphology and physical properties of Fontainebleau sandstone via a tomographic analysis,” vol. 101, 1996.
- [96] B. P. FLANNERY, H. W. DECKMAN, W. G. ROBERGE, and K. L. D'AMICO, “Three-Dimensional X-ray Microtomography,” *Science* (80-.), vol. 237, no. 4821, p. 1439 LP-1444, Sep. 1987.
- [97] R. D. Hazlett, “Simulation of capillary-dominated displacements in microtomographic images of reservoir rocks,” *Transp. Porous Media*, vol. 20, no. 1, pp. 21–35, 1995.
- [98] R. A. Ketcham and W. D. Carlson, “Acquisition , optimization and interpretation of X-ray computed tomographic imagery : applications to the geosciences,” vol. 27, pp. 381–400, 2001.
- [99] D. Wildenschild and A. P. Sheppard, “Advances in Water Resources X-ray imaging and analysis techniques for quantifying pore-scale structure and processes in subsurface porous medium systems,” *Adv. Water Resour.*, vol. 51, pp. 217–246, 2013.
- [100] S. Bryant and M. Blunt, “Prediction of relative permeability in simple porous

- media,” *Phys. Rev. A*, vol. 46, no. 4, pp. 2004–2011, Aug. 1992.
- [101] C. H. Arns *et al.*, “Computation of linear elastic properties from microtomographic images : Methodology and agreement between theory and experiment by This paper is a contribution of the National Institute of Standards and Computation of linear elastic properties from microt,” vol. 67, no. 5, pp. 1396–1405, 2002.
- [102] M. J. Blunt *et al.*, “Advances in Water Resources Pore-scale imaging and modelling,” *Adv. Water Resour.*, vol. 51, pp. 197–216, 2013.
- [103] E. De Boever *et al.*, “Quantification and Prediction of the 3D Pore Network Evolution in Carbonate Reservoir Rocks To cite this version : HAL Id : hal-00702951 Quantification and Prediction of the 3D Pore Network Evolution in Carbonate Reservoir Rocks,” 2012.
- [104] M. J. B. U, “Flow in porous media 76 pore-network models and multiphase flow,” 2001.
- [105] S. Chen and G. D. Doolen, “LATTICE BOLTZMANN METHOD,” no. Kadanoff 1986, 1998.
- [106] I. Fatt, “The Network Model of Porous Media.” Society of Petroleum Engineers, p. 38, 1956.
- [107] S. Bakke and P.-E. Oeren, “3-D Pore-scale modelling of sandstones and flow

- simulations in the pore networks,” *SPE J.*, vol. 2, pp. 136–149, Jan. 2013.
- [108] V. Mani and K. K. Mohanty, “Pore-Level Network Modeling of Three-Phase Capillary Pressure and Relative Permeability Curves,” *SPE J.*, vol. 3, no. 3, pp. 238–248, 1998.
- [109] P.-E. Oren, S. Bakke, and O. J. Arntzen, “Extending Predictive Capabilities to Network Models,” *SPE J.*, vol. 3, no. 4, pp. 324–336, 1998.
- [110] M. Piri and M. J Blunt, “Three-dimensional mixed-wet random pore-scale network modeling of two- And three-phase flow in porous media. I. Model description,” *Phys. Rev. E. Stat. Nonlin. Soft Matter Phys.*, vol. 71, p. 26301, Mar. 2005.
- [111] M. J. Blunt, M. D. Jackson, M. Piri, and P. H. Valvatne, “Detailed physics , predictive capabilities and macroscopic consequences for pore-network models of multiphase flow,” vol. 25, pp. 1069–1089, 2002.
- [112] V. Suicmez, M. Piri, and M. J. Blunt, “Effects of wettability on hydrocarbon trapping,” *Adv. Water Resour. - ADV WATER RESOUR*, vol. 31, pp. 503–512, Mar. 2008.
- [113] T. Ramstad, N. Idowu, C. Nardi, and P.-E. Øren, “Relative Permeability Calculations from Two-Phase Flow Simulations Directly on Digital Images of Porous Rocks,” *Transp. Porous Media*, vol. 94, no. 2, pp. 487–504, 2012.

- [114] M. Halisch, “Application and Assessment of the Lattice Boltzmann Method for Fluid Flow Modeling in Porous Rocks genehmigte Dissertation,” 2013.

Vitae

Name	Ali Adel Ali Mahmoud
Nationality	Egyptian
Date of Birth	September 20, 1991
Email	engaliadel1991@gmail.com
Address	Shubra, Cairo, Egypt
Postal Code	11631
Academic Background	Master of Science in Petroleum Engineering
Research Interests	Rock Characterization, Digital Rock Physics and Petrophysics
Educational Background	MSc. Petroleum Engineering – 2019 King Fahd University of Petroleum & Minerals, KSA B.E Petroleum Engineering – 2013 Suez University, Egypt